Dissertation

submitted to the

Combined Faculty of Natural Sciences

and Mathematics of the Ruperto

Carola University Heidelberg, Germany

for the degree of

Doctor of Natural Sciences

Presented by

M.Sc. Abaya Prakash

born in: Thanjavur, India

Oral examination: 3.8.2021

Molecular characterization of the recruitment machinery for amyloid aggregates to the Insoluble Protein Deposit (IPOD) in *Saccharomyces cerevisiae*

Referees: Prof. Dr. Bernd Bukau
Prof. Dr Matthias Mayer

I declare that I have written the submitted dissertation myself and in this process, have used no other sources or materials than those explicitly indicated. The work was carried out at the Department of Innere Medicine I, University Hospital of Heidelberg, Heidelberg in the group of Dr. Jens Tyedmers.

Heidelberg, June 2021 Abaya Prakash

Abstract

Increasing evidence suggests that the accumulation of misfolded protein species into specific spatially separated deposition sites is a cytoprotective response of the cell. Yeast has at least three different protein quality control sites for the deposition of aggregated proteins. The JUxtaNuclear Quality control (JUNQ)/IntraNuclear Quality control site (INQ) and the Cyto-Q harbours unstructured, amorphously misfolded proteins, while the perivacuolar Insoluble PrOtein Deposit (IPOD) is regarded as a specialized deposition site for highly ordered amyloid aggregates. Recently, it was found that targeting of amyloid aggregates to the IPOD depends on proteins that function either in actin cable-based transport processes (Myo2, Tpm1/2) or in vesicular transport and vesicle fusion events (Sec18, Sec14, Sec21, Vps1). Knockdown/deletion of either of the above-mentioned factors resulted reversibly in multiple small aggregates of the model amyloid PrD-GFP dispersed throughout the cytoplasm instead of its proper accumulation at the IPOD. These multiple aggregates, also interpreted as transport intermediates co-localized with the Atg9 vesicle marker, Atg9, and the CVT (Cytoplasm-to-Vacuole Targeting) pathway substrate preApe1. Based on these findings, it was hypothesized that the recruitment machinery for amyloid aggregates to the IPOD overlaps with that for preApe1 to the neighbouring PAS (Phagophore Assembly Site) and involved Atg9 or related vesicles that are transported along actin cables to the IPOD. In the current study, we falsified this hypothesis by evaluating the effects of *in vivo* gene knockout studies of ATG9 and other key components of this pathway on the recruitment machinery.

In order to identify the key molecular factors and narrow down the vesicular pathways involved in the recruitment machinery for amyloid aggregates to the IPOD, we performed an unbiased mass spectrometry approach to isolate the transport intermediates of PrD-GFP generated in a VPS1 null mutant or a SEC18 knockdown strain. Candidates tested in follow-up experiments using *in vivo* knockdown/knock-out, and co-localization techniques confirmed our initial hypothesis that vesicular transport is involved in amyloid recruitment to the IPOD. Furthermore, we found that proper recruitment of PrD-GFP to the IPOD is disrupted upon depletion/deletion of components involved in Golgi to endosome targeting and intra-

Golgi transport processes (Mon2, Dop1, Cop1) as well as candidates mediating homotypic membrane fusion events as well as endosome to vacuole transport (Vps33, Vps45). Using fluorescence microscopy, we observed that Vps33, a Sec1/Munc18 family (SM) protein and core component of HOPS/CORVET multisubunit tethering complexes co-localized with the multiple PrD-GFP aggregates generated in MON2 null mutants. Based on these findings, it was proposed that PrD-GFP aggregates are recruited to the IPOD via endosomes/MVB (Multivesicular bodies), which are known for their role in delivering substrates to the vacuole as a part of endosomal vacuolar transport.

Zusammenfassung

Immer mehr Hinweise deuten darauf hin, dass die Anhäufung von fehlgefalteten Proteinspezies in spezifischen, räumlich getrennten Ablagerungsstätten eine zytoprotektive Reaktion der Zelle ist. Hefe hat mindestens drei verschiedene Protein-Qualitätskontrollstellen für die Ablagerung von aggregierten Proteinen. Die JUxtaNuclear Quality control (JUNQ)/IntraNuclear Quality control site (INQ) und die Cyto-Q beherbergen unstrukturierte, amorph fehlgefaltete Proteine, während der perivacuoläre Insoluble PrOtein Deposit (IPOD) als spezialisierte Ablagerungsstelle für hochgeordnete Amyloid-Aggregate gilt. Kürzlich wurde festgestellt, dass das Targeting von Amyloid-Aggregaten zum IPOD von Proteinen abhängt, die entweder bei aktinkabelbasierten Transportprozessen (Myo2 , Tpm1/2) oder bei vesikulären Transport- und Fusionsereignissen (Sec18, Sec14, Sec21, Vps1) eine Rolle spielen. Knockdown/Deletion eines der oben genannten Faktoren führte reversibel zu multiplen kleinen Aggregaten des Modell-Amyloids PrD-GFP, die im gesamten Zytoplasma verteilt waren, anstatt der eigentlichen Akkumulation am IPOD. Diese multiplen Aggregate, die auch als Transportintermediate interpretiert wurden, kolokalisierten mit dem Atg9-Vesikelmarker und dem CVT (Cytoplasm-to-Vacuole Targeting) Pathway-Substrat preApe1. Basierend auf diesen Resultaten wurde die Hypothese aufgestellt, dass die Rekrutierungsmaschinerie für Amyloid-Aggregate zum IPOD sich mit der für preApe1 zum benachbarten PAS (Phagophore Assembly Site) überschneidet und Atg9 oder verwandte Vesikel involviert, die entlang von Aktin-Kabelen zum IPOD transportiert werden. In der aktuellen Studie falsifizierten wir diese Hypothese, indem wir die Auswirkungen von in vivo Gen-Knockout-Studien von ATG9 und anderen Schlüsselkomponenten dieses Weges auf die Rekrutierungsmaschinerie untersuchten.

Um die molekularen Schlüsselfaktoren zu identifizieren und die vesikulären Wege einzugrenzen, die an der Rekrutierungsmaschinerie für Amyloidaggregate zum IPOD beteiligt sind, führten wir einen unvoreingenommenen massenspektrometrischen Ansatz durch, um die Transportintermediate von PrD-GFP zu isolieren, die in einer VPS1-Null-Mutante oder

einem SEC18-Knockdown-Stamm erzeugt wurden. Kandidaten, die in Folgeexperimenten mit in vivo Knockdown/Knockout- und Kolokalisationstechniken getestet wurden, bestätigten unsere anfängliche Hypothese, dass vesikulärer Transport an der Amyloid-Rekrutierung zum IPOD beteiligt ist. Darüber hinaus fanden wir heraus, dass die korrekte Rekrutierung von PrD-GFP an den IPOD durch Deletion/Deletion von Komponenten gestört wird, die am Golgi-Endosomen-Targeting und an intra-Golgi-Transportprozessen beteiligt sind (Mon2, Dop1, Cop1), sowie von Kandidaten, die homotypische Membranfusionsereignisse sowie den Endosomen-Vakuolen-Transport vermitteln (Vps33, Vps45). Mittels Fluoreszenzmikroskopie beobachteten wir, dass Vps33, ein Protein der Sec1/Munc18-Familie (SM) und Kernkomponente der HOPS/CORVET Multisubunit-Tethering-Komplexe, mit den multiplen PrD-GFP-Aggregaten, die in MON2-Null-Mutanten gebildet werden, kolokalisiert. Basierend auf den oben genannten Ergebnissen wurde ein Modell vorgeschlagen, bei dem PrD-GFP-Aggregate über Endosomen/MVB (Multivesikuläre Körper), die für ihre Rolle beim Transport von Substraten an die Vakuole als Teil des endosomalen vakuolären Transports bekannt sind, zum IPOD rekrutiert werden.

Contents

1 Introduction

1.1 Protein misfolding and aggregation

Proteins perform a myriad of biological functions in an organism. Protein folding refers to the process by which nascent polypeptides attain a three-dimensional conformation with a low free energy state, also termed the native state. As there are multiple low energy minima states possible within the funnel-shaped energy landscape of a folding polypeptide chain, there is no one predetermined route set for protein folding, but rather a lot of routes are possible, complicating this process [1]–[4]. Even properly folded proteins in the cell are at constant risk of unfolding/refolding or misfolding due to environmental stress, genetic predisposition to misfold, and translational errors [5]. Only correctly folded proteins have biological activity, long-term stability and can correctly interact with their specific partners [6], [7].

Misfolding occurs when a protein attains a conformational state that results in the formation of a non-functional structure [8]. About 20% of the nascent polypeptides are degraded immediately upon synthesis due to misfolding. Misfolded or partially folded intermediates often have hydrophobic or “sticky” residues on their surface, which would normally be buried inside the core structure [8]. These hydrophobic residues tend to co-capture other proteins or molecules with exposed hydrophobic structures, resulting in protein aggregation [5], [6], [8].

Protein misfolding and aggregation has gained a lot of attention in recent years due to their association with a wide range of neurodegenerative disorders such as Alzheimer’s Disease (AD), Parkinson’s Disease (PD), Huntington’s Disease (HD), Transmissible Spongiform Encephalopathies (TSEs), and Amyotrophic Lateral Sclerosis (ALS) [8]–[12]. All these disorders are caused by the folding of particular proteins into an abnormal three-dimensional conformation, which makes these proteins more prone to aggregate and form β-sheet-rich

amyloid structures [13]. These aggregates are deposited in various parts of the brain, leading to dysfunctions in the Central Nervous System (CNS) [14]. Furthermore, these aggregates act as a seed to slowly sequester and convert other misfolded proteins into toxic insoluble aggregates [12], [14]. Currently, there is no cure known for these often fatal diseases.

1.1.1 Causes of protein aggregation/misfolding

Protein misfolding and aggregation can result from a single severe event or a cascade of different moderate events, which can be classified into four classes.

Genetic factors

Mutations in the underlying gene can alter the amino acid sequence, which in turn can increase the tendency of the protein to misfold and/or accumulate into aggregates. Some of the examples for this are amyloidogenic CAG repeat expansions within the exon 1 of the Huntington gene in Huntington's disease and the mutations of Aβ and alpha-synuclein in familial forms of Alzheimer's and Parkinson's, respectively [9]. Mutations in different components of the protein quality control compartments can also provoke protein aggregation. For instance, mutations in the E3 ubiquitin ligase Parkin result in an early-onset form of Parkinson's disease [15]–[17].

Translational errors

The polypeptide sequence of the native proteins can be altered not only by genetic mutations but also by erroneous protein synthesis, which can be due to translational errors, transcription errors, aberrant splicing, premature termination, faulty posttranslational modifications, and kinetic missteps during folding [18]. A protein that hasn't been synthesized correctly may be non-functional or toxic and can impose fitness costs on the organism. For instance, the substitution of a single amino acid in the editing domain of an alanyl-tRNA synthetase causes widespread translation errors and protein misfolding, leading to degeneration of Purkinje cells in the mouse cerebellum, ataxia, and death [19].

Stress

Heat and oxidative stress also contribute to protein aggregation. Heat treatment of the cells above the optimal temperature range can lead to the bulk unfolding of cellular proteins, although this change is often reversible [20]. On the other hand increase in oxidative stress in the cells leads to the generation of excess reactive oxygen species (ROS), which in turn induces fragmentation of the polypeptide backbone and irreversible replacement of side chains of specific amino acid residues by carbonyl groups [21]. These irreversible modifications then lead to protein misfolding and aggregation. Oxidatively damaged proteins can't revert to the native state due to altered primary amino acid sequence [21]–[23]. In addition, oxidative stress also leads to the accumulation of cellular products of oxidation [24], [25]. One such example is the deposition of Lipofuscin, a highly cross-linked, undegradable oxidation product in ageing cells [24]. Lipofuscin inhibits the proteasomal clearance of oxidatively damaged proteins by competitively binding to the proteolytic cores in the 20S proteasomes and rendering them non-functional [24].

Cellular ageing

Cellular ageing leads to a decline in the capacity of the protein quality control machinery. Aged cells undergo higher oxidative stress, display a reduced capacity to eliminate toxic and misfolded protein species but rather accumulate them [21], [22], [26]–[28]. In humans, the misfolded protein species leading to several neurodegenerative diseases such as Alzheimer's, Parkinson's, and Huntington's disease have a late-onset and appear more frequently in aged cells. The aggregation of mutant forms of human superoxide dismutase 1 (SOD1), which causes familial form of ALS (Amyotrophic lateral sclerosis), is exacerbated during ageing in mice [29].

1.1.2 Structure of Protein aggregates

Aggregates can be structurally very diverse; amorphous aggregates with a low degree of structured elements to insoluble aggregates with a high degree of structured elements [5], [30], [31].

Amorphous aggregates

Amorphous aggregates are generated under conditions of stress and are usually disordered. Inclusion bodies generated by the overexpression of proteins in bacteria are examples of amorphous aggregates [32]. However, recent studies have shown that ordered amyloid-like structures can also be formed in bacterial inclusion bodies during recombinant protein expression [33], [34]. Likewise, it is also possible for soluble aggregates formed initially in the cell to become insoluble when they exceed a certain size, which often happens upon the onset of pathological conditions [32].

Amyloid aggregates

Amyloid aggregates are examples of insoluble ordered aggregates, and their appearance marks the hallmark of a wide range of neurodegenerative diseases termed amyloidosis, e.g., Alzheimer's disease, Parkinson's, ALS, etc. [13], [32], [33]. Although the underlying amyloid-forming proteins of these diseases are structurally and functionally unrelated, they form morphologically similar amyloid fibers [32], [33]. Amyloid fibrils are typically 7–12 nm in diameter, protease-resistant, have a very high content of beta-strands, and can form even in the absence of stress [32].

1.2 Prions

Another group of diseases that accumulate amyloid fibres are Prion diseases. Prions are infectious proteins that can transmit a trait or a disease without the need for an accompanying nucleic acid. They were originally identified in the sheep disease Scrapie but have now been identified in a range of organisms (bovine spongiform encephalopathy in cows, Creutzfeldt-Jacob disease of man) [32], [35]. Prion diseases are caused by the conformational change of the PrP protein from a normal host-encoded protein (PrP^{C}) into its pathological form (PrP^{Sc})(PrP^{C} --------> PrP^{Sc}). This pathological form of the protein PrP^{Sc} is protease-resistant, insoluble, forms amyloid fibrils, and can further template the conversion of the soluble protein form into the aggregated form [36]–[38]. Hence prions can be

considered as transmissible amyloids. Although several unrelated proteins can form prions in yeast, PrP is the only known prion protein in mammals [39].

1.2.1 Yeast Prions

The Baker's yeast *Saccharomyces cerevisiae* harbours several proteins which can undergo prion-like conformational conversion. Currently, yeast has at least seven prions ([*MOT3*$^{+}$], [*OCT*$^{+}$], [*SWI*$^{+}$], [*URE3*], [*PSI*$^{+}$], [*ISP*$^{+}$], [*RNQ*$^{+}$]) with many more proteins being potentially capable of forming prions [40]–[42]. Yeast prions can be formed spontaneously or by overproduction of their cellular protein determinants [43]. Most prions are self-propagating amyloid forms of the protein; however, exceptions exist [39]. Yeast can propagate prions stably for many generations. Hsp104 is essential for the propagation of amyloid-based prions [39]. Most yeast prions have a prion domain (PrD) enriched in asparagine and glutamine residues, but exceptions do exist [44]. Although several prions share some features, there is no single common feature defining a prion. Unlike mammalian prions, yeast/fungal prions are not uniformly fatal but can rather be beneficial under certain conditions. One example of a beneficial prion is the fungal [Het-S] prion, which is necessary for normal function and heterokaryon incompatibility [45]. Yeast prions provide a good model to study amyloid biology [39].

1.2.1.1 The yeast [*PSI*$^{+}$] prion

Of the seven known yeast prions, [*PSI*$^{+}$] is the best-characterized one [46]. It is the amyloid form of the translation termination factor, Sup35 [47]–[50]. Cells harbouring the non-prion soluble, functional form of Sup35 are called [*psi*$^{-}$] cells. In the [*PSI*$^{+}$] form, Sup35 is insoluble and in a prion/aggregated form. As a result, the cells carrying [*PSI*$^{+}$] have impaired translation termination efficiency, and Sup35 is functionally inactive [47].

While spontaneous *de novo* formation of [*PSI*$^{+}$] is rare and not yet completely understood, overexpression of Sup35 or only the PrD of Sup35 leads to [*PSI*$^{+}$] induction. As Hsp104 is essential for [*PSI*$^{+}$] propagation, treatment of [*PSI*$^{+}$] strain with 3-5 mM Guanidine

Hydrochloride leads to the curing of the prion ([*PSI*$^{+}$] to [*psi*$^{-}$]) by inhibiting the ATPase activity of Hsp104 [39], [51]. The AAA ATPase Hsp104 shears amyloid fibres to generate prion seeds termed propagons that are inherited from mother to daughter cells to ensure the inheritance of the prion state to the progeny. Inhibition of the ATPase activity of Hsp104 inhibits the generation of these propagons as well as inheritance of prion state to the progeny. This results in loss of prion state after several cell divisions [51]–[53].

Both *de novo* formation as well as [*PSI*$^{+}$] induction by overexpression of Sup35 is possible only in the presence of another prion, [*PIN*$^{+}$]. This [*PIN*$^{+}$] prion is a self-propagating amyloid of the Rnq1 protein [54]. It depends on Hsp104 for propagation and can be cured by Guanidine Hydrochloride [55].

1.2.1.2 The model substrate PrD-GFP

[*PSI*$^{+}$] is the prion of the protein Sup35 [47]–[50]. There are three different regions of the Sup35 protein; The “N” terminal Q/N-rich domain, the highly charged K/E-rich middle domain “M” and the “C” terminal domain. While the N terminal domain is required for the formation and templating of amyloid, the M domain promotes solubility in the non-prion form and contains Hsp104 binding sites to initiate propagon formation, whereas the C terminal domain is sufficient and essential for translation termination [56], [57]. The N and M domains of Sup35 combined are termed as “NM” or “PrD.” The prion domain (PrD) of Sup35 is sufficient and necessary to cause [*PSI*$^{+}$] induction in [*PIN*$^{+}$] yeast cells [58]. A GFP fusion to this prion domain of Sup35 (PrD-GFP) confers prion properties to GFP, deposits at the IPOD (Refer section 1.4.3.4), and provides a visually tractable prion model to study the amyloid properties of [*PSI*$^{+}$] in yeast [59].

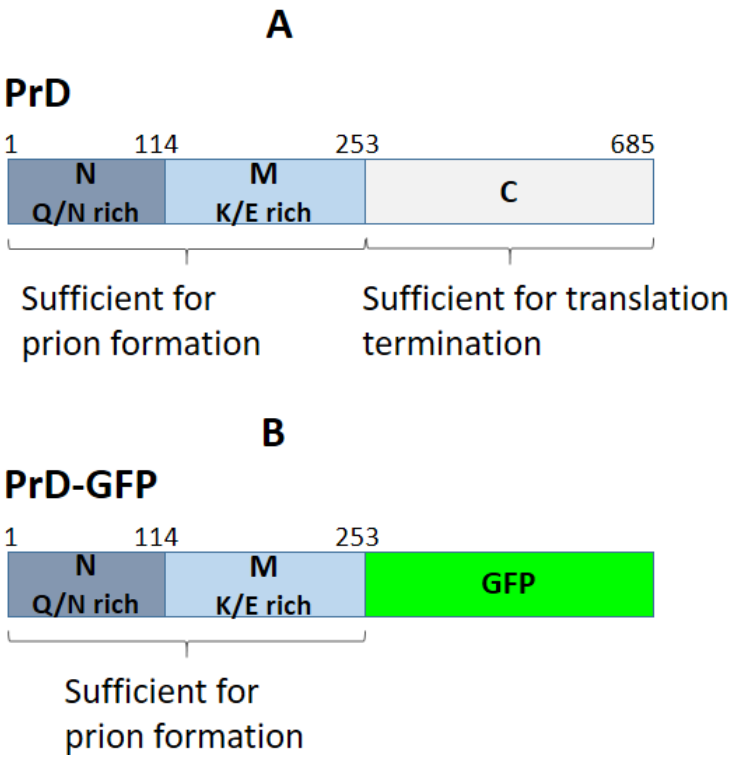

FIGURE 1: Domain Organization of the Sup35 protein. (A) The Sup35 protein contains three domains: the N-terminal domain (N), middle domain (M), and the C-terminal domain (C). The C-terminal domain is necessary and sufficient for translation termination, while the NM or PrD domain is sufficient for [*PSI*$^{+}$] formation. B) Replacement of C-terminal domain with GFP protein (PrD-GFP) serves as a visually tractable prion model to study the [*PSI*$^{+}$] amyloid-like properties in yeast [59].

1.3 Mechanisms for refolding or degradation of misfolded proteins

1.3.1 Chaperone mediated disaggregation

Different families of molecular chaperones assist in protein folding, refolding, and degradation. The Hsp70 family aids in aggregate disaggregation, prevention of aggregation, *de novo* protein folding, and refolding with the help of its two co-chaperones: Hsp40 and the nucleotide exchange factor (NEF) [60], [61]. Depending on the substrate type, different Hsp40 co-chaperones (Ydj1 for stress-induced aggregates, sis1 for amyloid aggregates) direct Hsp70 chaperones (Ssa1 to Ssa4) to bind to protein aggregates [62]. This initial Hsp40 directed Hsp70 substrate binding restricts the access of proteases to the aggregates and allows substrate

transfer to Hsp104. Hsp104 is the hexameric yeast disaggregase of the Hsp100 family (Clp in E.coli). Hsp70s act along with Hsp104 in the so-called Hsp70/Hsp100 bi-chaperone system to aid in the clearance of aggregated proteins [60], [63]. Hsp70 mediated substrate binding to Hsp104 (ClpB in E.coli) activates its ATPase activity, resulting in threading of the misfolded polypeptides one by one from the aggregates into the central pore of Hsp104/ClpB hexamer [64]–[66]. Substrate threading continues till Hsp104/ClpB encounters a tightly folded domain, leading to substrate dissociation (Figure 2). This ensures optimal refolding of the substrate by the bi chaperone system [5], [67].

A recent study by den Brave *et al.* in yeast reported that the Hsp40 chaperone, Apj1, promotes clearance of intra-nuclear aggregates in an Hsp70-dependent but Hsp104-independent manner [68]. Apj1 competes with Hsp104 for substrate binding in the nucleus and favours aggregate turnover over refolding to reduce the burden of accumulation of soluble substrates, which result from Hsp104 dependent disaggregation. Hence Apj1 mediated aggregate turnover serves as an alternative pathway to maintain proteostasis in nucleus [68].

Another recent study by Hjerpe *et al.* in mice showed that proteosome shuttle factor Ubiquilin 2 (UBQLN2) aids in the clearance of insoluble ubiquitinated protein aggregates by connecting the chaperone-mediated disaggregation pathway to proteasomal degradation. UBQLN2 binds to the Hsp70 bound ubiquitinated protein aggregates and targets them for degradation by the UPS (Ubiquitin Proteasome System) [69].

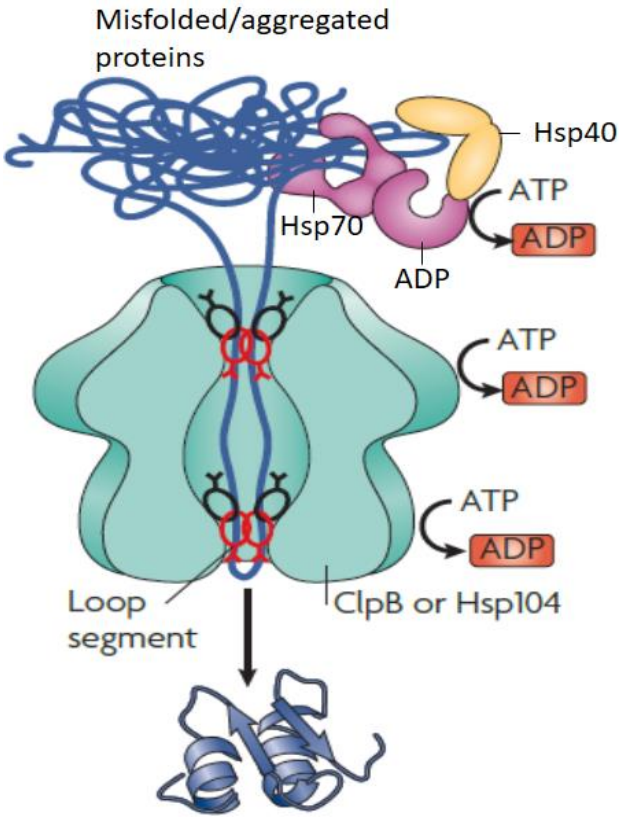

FIGURE 2: Protein disaggregation by the Hsp70-Hsp100 bi-chaperone system. The Hsp70, along with its co-chaperones, recognizes and binds to misfolded aggregated proteins before transferring them to the Hsp104 disaggregase. Substrate binding activates the ATPase activity of Hsp104/ClpB. This ATP hydrolysis provides energy for the threading of single polypeptide chains from the aggregates, one by one, through the central pore of the Hsp104/ClpB hexamer. This process proceeds until a tightly folded domain is encountered, leading to substrate dissociation. The unfolded polypeptide chains can be refolded to their native state by the Hsp70 system. The figure was adapted and modified from [5].

1.3.2 Proteasome mediated degradation of misfolded proteins

In eukaryotic cells, terminally misfolded soluble proteins which can no longer be refolded are targeted for proteolytic degradation by the 26S proteasome. The 26S proteasomal system is composed of one 20S core particle (CP) with catalytic activity and two 19S regulatory particles (RP) [70]. As substrates are usually polyubiquitinated before they are targeted for degradation by the proteasome, this pathway is also called as Ubiquitin Proteasome System (UPS), although ubiquitin independent proteasome degradation for some substrates has also been

reported [71]. Polyubiquitination of the substrates is dependent on the concerted action of three enzyme classes: E1, E2, and E3. There are different E3 enzymes that confer substrate specificity and play an important role in the ubiquitin-mediated proteolytic cascade. Ubr1 and San1 are examples of two E3 ligases in yeast that promote ubiquitination of misfolded cytosolic proteins [72], [73].

The UPS is important for the clearance of soluble misfolded proteins and helps in maintaining protein homeostasis in a cell. Studies by Kaganovich *et al.* showed that proteasome impairment in yeast cells inhibited clearance of misfolding prone proteins but rather resulted in their accumulation in specialized quality control compartments, now termed the JUNQ/INQ and Cyto Q [74]. Restoring proteasomal function in these experiments resulted in the clearance and dissolution of these protein quality control compartments indicating the important role played by UPS in deciding the fate of misfolded proteins [74].

Studies in mammalian cells also highlight the importance of UPS in the clearance of damaged proteins. Genetic disruption of 26S proteasomes in the primary neurons from the mouse brain leads to neurodegeneration as well as the formation of intraneuronal Lewy-like inclusions [75]. Another study in primary neuronal cultures of a mouse model of Huntington's disease (HD94 mice) observed defects in aggregate clearance upon inhibition of the proteasome [76]. Interestingly, the presence of protein aggregates can also impair the function of the UPS [77]. This was shown by Kopito and colleagues by using two aggregation sensitive proteins, a folding mutant (ΔF508) of CFTR (Cystic fibrosis transmembrane conductance regulator) that normally misfolds in the ER and is exported to the cytoplasm for clearance by UPS and the protein expressed from the exon1 of mutant Huntington gene (Htt103Q) [77]. Under physiological conditions, both these substrates are diffuse and are degraded by the UPS. But upon overexpression in HEK cells, they accumulate as aggregates that can no longer be cleared by the UPS and are sequestered into peripheral inclusions termed aggresomes [77]. These aggresomes are further cleared by autophagy [78]. Hence aggregated proteins are not degraded effectively by the UPS but rather directed to a specific autophagy pathway called aggrephagy [79]. The same is also true for proteins with long Poly-Q repeats, such as those of

the mutant Huntington protein, which causes Huntington's disease. Such proteins cause blocking/clogging of the proteasomes rendering them non-functional [80], [81]. Furthermore, these Poly-Q stretches can also sequester the proteasomes and trap them in these inclusions, making them unavailable for the clearance of other soluble misfolded proteins, thereby contributing to cellular toxicity and disease pathogenesis [77], [82].

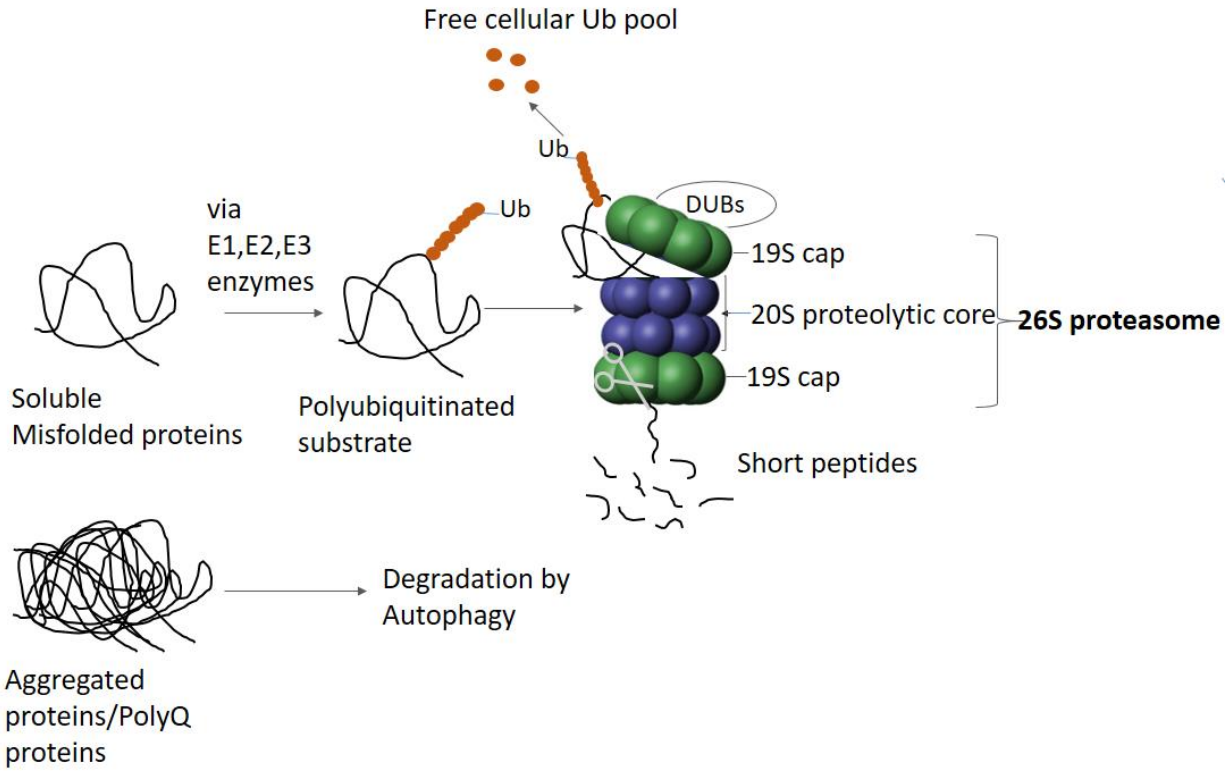

FIGURE 3: Degradation of soluble misfolded proteins by the 26S Proteasome system. Soluble misfolded proteins are ubiquitinated via the action of E1, E2, and E3 enzymes. Polyubiquitinated substrates are identified by the 19S regulatory subunit of the proteasome, which allows them to unfold and translocate into the narrow 20S proteolytic core chamber where the substrate is cleaved into short peptides. Deubiquitinating Enzymes (DUBs) will remove ubiquitin moieties from the polyubiquitinated substrates releasing free ubiquitin. Aggregated and PolyQ proteins inactivate the proteasome by sequestering them or by causing clogging/blockage of their narrow 20S proteolytic core and are degraded mostly by autophagy [77], [79].

1.3.3 Aggregate clearance by Autophagy

Autophagy/macroautophagy or self-eating is a process by which cells degrade or "eat" part of their own cytoplasmic content upon nutrient-deficient conditions such as starvation. In Macroautophagy, sequestration of cellular components takes place in specific double-membrane structures termed autophagosomes. In contrast to mammals, autophagosomes in yeast originate at a single small membranous organelle termed the Phagophore assembly site (PAS), located close to the vacuole [83]–[86]. Eventually, the outer membrane of the autophagosomes fuses with the lysosomal/vacuolar membrane to release its contents into the acidic vacuolar lumen for its degradation by vacuolar peptidases. Based on the cargo selection, autophagy can be either selective or non-selective [87]. Non-selective or bulk autophagy or macroautophagy involves non-specific degradation of bulk cytoplasmic contents. Although macroautophagy operates under basal conditions, it is strongly induced by starvation [88]. Selective autophagy, on the other hand, is a receptor-mediated degradation of specific cargoes and operates both in normal vegetative conditions (non-induced conditions) as well as in response to different stimuli (induced conditions) [87], [88]. An example of non-induced selective autophagy is the Cytoplasm-to-vacuole targeting (Cvt) pathway (Refer section 1.3.3.1). Studies show that there is evidence for cross talk between the autophagic and the proteasomal system, as inhibition of autophagy leads to the activation of proteasomes and vice versa [89].

In mammalian cells, a selective ubiquitin-dependent autophagic pathway called aggrephagy has been reported [79], [84]. Aggregated or tightly folded proteins that are resistant to proteasomal degradation often accumulate as ubiquitinated substrates in the cell. These ubiquitinated substrates are identified by specific adaptors such as p62/SQSTM1 and NBR1 that link the ubiquitin pathway to the autophagic pathway [90], [91]. These adaptors have a UBA domain for ubiquitin conjugate binding and a distinct binding site called AIM (Atg8 interacting motif) or LIR (LC3 interacting region) domain which mediates binding to the autophagosomal protein LC3 (Atg8 in yeast). LC3 (conjugated to the lipid Phosphatidylethanolamine) aids in the formation of autophagosomes and serves as a central docking site for the packaging of the cargoes into autophagosomes for their subsequent

degradation by autophagosome-lysosomal fusion [63], [79], [84]. It was unclear whether such a pathway also existed in yeast. Studies by the Jentsch lab confirmed the existence of a class of Ubiquitin/Atg8 adaptors also in yeast, termed CUET proteins that target ubiquitinated substrates for autophagic degradation [92]. CUET proteins such as Cue5 and its human homolog TOLLIP have a CUE binding domain instead of a UBA domain, which mediates Ubiquitin binding as well as an AIM domain that mediates binding to Atg8. Cue5 recruits the ubiquitin ligase Rsp5, and together they can promote the clearance of both PolyQ (Htt96Q) as well as starvation-induced aggregates. Hence, this study provided evidence that Cue5 and Rsp5 connect the UPS pathway to the autophagic pathway in yeast to mediate the degradation of aggregated proteins [92].

1.3.3.1 Cytoplasm to Vacuole (Cvt) targeting pathway

The cytoplasm-to-vacuole targeting (Cvt) pathway is a type of selective autophagy in which precursors of resident vacuolar hydrolases such as Ape1 and Ams1 are transported into the vacuolar lumen [93]–[96]. Ape1 is initially synthesized as a precursor in the cytosol (preApe1), which rapidly oligomerizes to form a homododecamer that further organizes into a higher-order structure termed the Ape1 complex [97]. The specific receptor protein, Atg19, binds to the Ape1 complex, and together they are now termed Cvt complex [98]–[100]. The adaptor protein Atg11 recognizes and binds to the Atg19 in the Cvt complex as well as to a group of cytoplasmic vesicles that contain the transmembrane protein Atg9 and are termed Atg9-vesicles [86], [101]. Atg9 vesicles arise from the Golgi and are localized to multiple peripheral sites in the cytoplasm, one of which is the Phagophore assembly site (PAS), where it plays a role in autophagosome formation [102]–[104]. These Atg9 vesicles associate with actin cables via unknown factors and transport the Cvt complex (now containing preApe1, Atg19, Atg11, and Atg9) to the PAS adjacent to the vacuole where preApe1 is sequestered into double-membrane Cvt vesicles [103], [105], [106]. At the PAS, Atg19 interacts with Atg8 that regulates the formation of double-membrane Cvt vesicles, and also tethers the Cvt complex to the phagophore [107]. Finally, the Cvt vesicles fuse with the vacuole to deliver preApe1, which is processed into a mature form (mApe1) lacking the pro-peptide. The delivery of preApe1 by Cvt vesicles to the vacuole takes place in nutrient-rich conditions in yeast.

However, during starvation, these Cvt vesicles, along with their content, are incorporated into autophagosomes and are delivered to the vacuole along with other bulk cytoplasmic content [108].

1.3.4 Aggregate release by Exophore production

Recently, a novel pathway for clearance of PolyQ aggregates via large membrane-bound vesicles (4µm) called exophores has been described in *Caenorhabditis elegans* [109]. Exophore production serves as an alternate pathway for cells to get rid of aggregated/toxic proteins or dysfunctional organelles under conditions of proteostasis. Higher aggregate load or inhibition of autophagic/proteasomal/mitochondrial quality control pathways correlate with an increase in exophore production [109].

1.4 Spatial Protein Quality Control Network

Various conditions in a cell can cause a protein to misfold. When protein misfolding exceeds the capacity of the protein quality control system to refold or degrade misfolded proteins, cell employs an additional strategy, i.e. sequestration of misfolded/aggregated proteins into different specialized quality control sites [74]. Such a spatial sequestration of aggregated proteins has many advantages such as 1) protection of the cellular environment from the accumulation of potentially toxic aggregated protein species, 2) possible reorganization of protein quality control factors/chaperones acting on these aggregates, 3) asymmetric inheritance of aggregated/misfolded proteins to generate aggregate free progeny [5], [63], [74], [110]–[112].

1.4.1 Deposition of aggregated proteins in bacteria

In bacteria, misfolded proteins accumulate in inclusion bodies, which often form at the periphery of the cell [113]–[116]. Usually there are 1-2 inclusions per cell. The exact reasons for the peripheral localization of aggregates is still unclear, but the mechanism by which the

aggregates are localized to the cell poles is thought to be either an active energy driven processes or a passive mechanism of nucleoid exclusion [5]. However, the localization of the aggregates at the cell poles aids in their asymmetric segregation during cell division [5], [117].

1.4.2 Deposition of aggregated proteins in mammals

In mammalian cells, misfolded and aggregated proteins accumulate in specialized inclusion bodies termed aggresomes. Aggresomes have a perinuclear localization at a site called MTOC (microtubule organizing center), where they are enclosed by a cage-like shell formed by vimentin filaments [78], [118], [119]. Previously, substrate ubiquitination mediated by Parkin/CHIP or other E3 ubiquitin ligases was thought to be a prerequisite for their targeting to aggresomes [16], [17], [78], [116]. In this case, the histone deacetylase HDAC6 acts as an adaptor and binds to both Lys63-linked polyubiquitin chains on the misfolded proteins as well as to the minus-end microtubule motor protein dynein to drive the transport of aggregated proteins to the MTOC in a microtubule-dependent manner [79], [119]. However, it is now known that some substrates can also be targeted to aggresomes in the absence of ubiquitination [116]. Disruption of either the microtubules/dynein motor function or inhibition of HDAC6 prevented aggresome formation and resulted in the accumulation of protein aggregates as dispersed foci in the cytoplasm [78], [119]. The formation of aggresomes initiates a type of specialized autophagy termed aggrephagy [79], [84]. At the MTOC, the aggresomes are recognized by the autophagic receptors p62/NBR1, which bind to both the ubiquitinated substrates in the aggresomes as well as to a key component of autophagic vesicles, Light Chain 3 (LC3) (yeast Atg8) to package the aggresomes into autophagosomes for their subsequent degradation by autophagosome-lysosomal fusion [79], [84], [90], [91].

1.4.3 Deposition of aggregated proteins in Yeast

Yeast has at least three different protein quality control sites for the deposition of aggregated proteins, the JUxtaNuclear Quality control (JUNQ)/IntraNuclear Quality control site (INQ), Q-bodies/Cyto-Q, and the perivacuolar Insoluble PrOtein Deposit (IPOD) [62], [74], [112].

Recently, another quality control compartment IMiQ (IntraMitochondrial protein Quality control), for the deposition of aggregated proteins in mitochondria has been described [120]. While JUNQ/INQ and Cyto-Q harbour more unstructured, amorphously misfolded proteins, the IPOD is often regarded as a specialized deposition site mainly for highly ordered amyloid aggregates [74] [112]. While it is known that Btn2 and Hsp42 act as sorting factors for misfolded proteins to the INQ/JUNQ and Cyto-Q, respectively, little is known about substrate targeting to the IPOD [53], [60], [62], [63], [121].

1.4.3.1 JUNQ/INQ

The "**JU**xta**N**uclear **Q**uality Control (JUNQ)" compartment was first described by Kaganovich *et al.* when following the fate of two cytosolic misfolded substrates Ubc9ts and VHL. Ubc9ts is a temperature-sensitive variant of the SUMO-conjugating enzyme ubc9, whereas VHL is the heterologously expressed „Von Hippel-Lindau tumor suppressor (VHL) " that misfolds in yeast due to the lack of its cofactor Elongin BC. Both Ubc9ts as well as VHL at 37°C and under conditions of proteasome inhibition accumulated in two distinct inclusions, one with juxtanuclear localization and the other with perivacuolar localization. The juxtanuclear inclusion and the peripheral inclusion were termed JUNQ and IPOD (**I**nsoluble **P**r**O**tein **D**eposit), respectively [74]. Initial studies revealed that JUNQ is cytosolic and located at an indentation to the nucleus [74]. Later studies involving electron microscopy and nuclear rim staining with fluorescently labeled nuclear pore components revealed an intranuclear localization of the JUNQ adjacent to nucleolus and chromatin and hence was renamed to INQ (IntraNuclear Quality control compartment) [63], [122], [123]. Additional experimental clarification may be required to reveal if the two sites are related/identical or rather independent structures [63], [124]. Hence the terms JUNQ/INQ are used here synonymously.

It is now known that JUNQ/INQ appears under conditions of heat shock and proteotoxic stress to sequester amorphous cytosolic and nuclear proteins. Initial evidence pointed to ubiquitination as a necessary sorting signal for substrate targeting to JUNQ/INQ. On the one hand, the yeast prion protein Rnq1, a bona fide IPOD substrate, sorts to JUNQ/INQ when

ubiquitinated. On the other hand, overexpression of Ubp4, a deubiquitinating enzyme, or deletion of two quality control E2 ubiquitin-conjugating enzymes Ubc4 and Ubc5, abolished JUNQ/INQ localization of the two misfolded model substrates VHL and Ubc9ts [63], [74], [112]. However, it has now been shown that ubiquitination is not a necessary sorting signal for all substrates to JUNQ/INQ [63]. For instance, the misfolded substrate tGnd1-GFP, which is ubiquitinated *in vivo* by San1 and Ubr1, can accumulate at JUNQ/INQ in a non-ubiquitinated state in cells lacking Ubr1 and San1. These findings further illustrate the absence of a single general signal for substrate targeting to JUNQ/INQ [63], [123].

Substrate targeting to JUNQ/INQ requires the action of the heat-shock protein Btn2 [53], [60], [125]. Btn2 interacts with the J domain protein Sis1 to facilitate the nuclear transport of misfolded proteins for proteasomal degradation [53], [63]. Furthermore, JUNQ/INQ formation also requires an intact actin cytoskeleton [123].

JUNQ/INQ like cytosolic compartments has also been described in various mammalian cell types [74], [126], [127]. Contrary to the observations in yeast, mammalian JUNQ has a perinuclear localization next to the microtubule-organizing center (MTOC) and Vimentin clusters and can also form in the absence of proteasome impairment [127].

1.4.3.2 CytoQ

Apart from JUNQ/INQ and IPOD yeast has an ensemble of multiple heat-stress-induced cytosolic aggregates collectively called as peripheral aggregates/ CytoQ/Q bodies/Stress foci [62], [74], [111], [121], [123], [125], [128]. To avoid confusion, they will be referred further in this thesis as CytoQ. Upon heat /stress conditions, multiple CytoQ foci are formed, which undergo fusion events to coalesce into a few foci or even only one single focus per cell [123]. Hence the formation of CytoQs is thought to be an early event in cellular protein quality control. CytoQs are located in the cytoplasm close to the ER and sequester amorphous aggregates in an Hsp42 dependent manner [62], [121]. The formation of CytoQ is an energy-dependent but cytoskeleton-independent process and requires an intact cortical ER. The Hsp104-dependent disaggregation machinery promotes CytoQ dissolution [62].

1.4.3.3 IMiQ (IntraMitochondrial protein Quality control)

Recently Bruderek *et al.* reported a novel site in the periphery of the mitochondrial nucleus, which accumulates aggregation-prone mitochondrial proteins and termed this site IMiQ [120]. IMiQ formation was observed in the presence of a fully functional mitochondrial protein quality control system and the substrates tested include destabilized reporter proteins in basal conditions as well as endogenous mitochondrial proteins under severe stress conditions. Substrate sequestration at IMiQ is dependent on intact microtubule and on the heat shock protein, Hsp78 [120]. Hence, apart from JUNQ/INQ, CytoQ and IPOD, IMiQ represents the fourth quality control compartment in yeast.

1.4.3.4 The Insoluble Protein Deposit (IPOD)

The Insoluble Protein Deposit (IPOD) located close to the vacuole is a specialized deposition site for amyloid aggregates, although non-amyloid substrates can also be targeted to it [63], [74], [112], [129], [130]. The IPOD is located close to the PAS, where the yeast cell initiates the formation of autophagosomes and Cvt vesicles and forms even in the absence of stress or proteasomal impairment. The IPOD was initially thought of as a deposition site for terminally aggregated proteins [59], [74]. Even amorphous substrates such as ubc9ts and VHL partitioned to the IPOD only when the JUNQ/INQ and Cyto-Q compartments were saturated. However, amyloid substrates such as yeast prions Rnq1, Ure2, and Sup35, Huntington exon1 with expanded polyglutamine and polyproline domains (Htt103Q), and proteins sensitive to oxidative modification of carbonylation preferentially localized to the IPOD [59], [74], [112], [131], [132].

Recently, it was observed that Proteosome Storage Granules (PSGs) transiently associated with the IPOD and damaged/inactive proteasomes were sorted from the PSGs to the IPOD where there were ubiquitinated and removed by a selective autophagic mechanism termed proteophagy. While the sorting of damaged proteasomes to the IPOD takes place in an Hsp42-dependent manner, proteophagic clearance of these ubiquitinated proteasomes from the IPOD requires the ubiquitin receptor Cue5 [133]–[135].

The yeast disaggregase, Hsp104, accumulates at the IPOD [74]. Its presence might reflect its role in the disaggregation of amyloid substrates deposited there. Time-lapse experiments with a GFP fusion of the prion domain of the amyloid-forming protein Sup35 (PrD-GFP) revealed that turnover of PrD-GFP aggregates deposited at the IPOD is dependent on Hsp104 based disaggregation as well as proteasomal function [136]. Although a role of autophagy in the clearance of IPOD substrates can't be eliminated and the IPOD also co-localizes with the autophagic marker Atg8 and the PAS, direct evidence for autophagic turnover of the IPOD is yet to be shown [59], [74], [112], [132], [136].

Substrate targeting to the IPOD

Substrate features

It is known that specific features of the substrates such as expression levels of aggregation-prone proteins as well as steric features such as N- or C-terminal orientation of a bulky GFP tag influence the targeting. For instance, overexpression of the non-amyloid construct, OPTN-GFP, resulted in the appearance of not only IPOD foci but also additional aggregate foci next to a major IPOD, indicating limitations of substrate sequestration at the IPOD [131]. Likewise, despite similar expression levels, an N-terminal GFP fusion of the non-amyloid construct GFP-FUS was more efficiently targeted to the IPOD as compared to a C-terminal (FUS-GFP) fusion [131], [137]. FUS (Fused in Sarcoma) is an RNA binding protein implicated in both sporadic and familial forms of ALS (Amyotrophic lateral sclerosis) [138]. GFP fusions of the human FUS protein in yeast serve as a valid model to study FUS mediated aggregation and toxicity [112], [137], [138].

Role of endosomal components/vesicle-mediated pathways in substrate targeting to the IPOD

Mounting evidence suggests that components of endomembrane trafficking and vesicular transport are involved in the targeting of different substrates to the IPOD [130], [136], [139], [140]. The finer details of the various experimental conditions, model substrates, and methods used to arrive at this conclusion are summarized below.

Recently, Hill *et al.* showed that the vacuole inheritance protein, Vac17 utilizes components of the actin-based cytoskeleton (Cmd1, Myo2) and endosomal pathway (Vps1 and Vps16) to sequester heat-induced aggregates at a perivacuolar deposition site, the IPOD [130]. The authors considered these perivacuolar inclusions as IPOD because of their co-staining with the vacuole upon FM464 staining. The main reporter used in this study was a GFP fusion of the heat shock protein Hsp104, which binds to aggregates and also co-localizes with the IPOD [74].

A genome-wide screen for genes involved in inclusion formation of heat-induced Hsp104-GFP aggregates clustered into four interrelated complexes; 1) the inositide-3,5-bisphosphate kinase complex, 2) the COG (conserved oligomeric Golgi) complex, 3) the HOPS/CORVET complex, and 4) the Mon2-Arl1 Golgi network [139]. All these complexes are involved in endocytosis and endomembrane trafficking pathways (Refer. Table 1). Furthermore, Sed5, the essential yeast cis-Golgi t-SNARE syntaxin, was identified to act in the sorting of misfolded and aggregated proteins to a site between the vacuole and mitochondria in an Hsp104 and COPII dependant manner. The authors considered this inclusion site as IPOD due to its perivacuolar localization and the rationale that Hsp104 mediated disaggregation of inclusions takes place at the IPOD [74][139]. This study shows evidence for vesicle-mediated transport and the involvement of the endosomal pathway in substrate targeting to the IPOD [139].

Huntington's disease is a neurological disease caused by PolyQ expansion in the Huntington protein (HTT). When there are more than 35 glutamine residues in the HTT protein, the protein is aggregation-prone and forms insoluble intracellular aggregates, also called Inclusion Bodies (IBs) [141]. Interestingly, studies show that the smaller soluble oligomers of HTT protein contribute toxicity more than the larger aggregation-prone ones, which might be rather protective [141][142]. This toxicity was also dependent on the proline-rich region flanking the C terminal of the polyglutamine stretch. Recent studies by Nyström and his co-workers showed that soluble Htt25QP (P for proline stretch) was more toxic than Htt25Q (no proline stretch), and the aggregated Htt103QP was more toxic in yeast cells deficient for actin-based polarization and clathrin-dependent endocytosis [142]. They attributed the observed toxicity to the physical interaction between the proline-rich region with the type 1 myosins (Myo3 and Myo5), leading to a reduction in actin patch polarization and endocytic defects.

Hence, this study highlighted the involvement of components of actin-based polarization and clathrin-dependent endocytosis in aggregate sorting and sequestration [142].

Song *et al.* reported that asymmetric segregation of heat-stress induced Hsp104 aggregates, as well as mutant Huntington protein (Htt103Q), depended not only on the ageing-related protein, Sir2 but also on actin-associated proteins Cmd1 and Myo2 as well as proteins involved in ER to Golgi trafficking and ER homeostasis [27], [143]–[145]. The authors even speculate that misfolded proteins might be transported to the IPOD in vesicles moving on actin cables via Myo2, and such a transport mechanism ensures mother cell-specific retention of damaged/aggregated proteins during cell division [144].

Vps1, the dynamin-like small GTPase and component of the late endosomal trafficking, was reported to be essential for the targeting of amyloid substrates to the IPOD [140]. Kumar *et al.* showed that loss of function mutants of VPS1 fail to recruit the model amyloid substrate, PrD-GFP, to the IPOD but rather accumulate them as multiple cytoplasmic foci, indicating targeting defects [140]. Another study reported a role of Vps1 in the recruitment of Wtf4 proteins to the Insoluble Protein Deposit (IPOD) [146]. Wtf4 gene is a meiotic driver in *Schizosaccharomyces pombe*. Meiotic drivers are genes that attempt to override the principles of inheritance and force their way into the next generation. If the gametes don't carry them, they eliminate the gametes by a poison-antidote mechanism. When expressed in *S.cerevisiae*, the $Wtf4^{poison}$ forms distributed toxic aggregates in the cytoplasm. $Wtf4^{antidote}$ promotes neutralization of $Wtf4^{poison}$ and together, the $Wtf4^{poison}$+$Wtf4^{antidote}$ are trafficked to the IPOD in a Vps1 dependent manner [146]. Recently, an unbiased screen for Hsp104 interactors in untreated, as well as in heat-shock treated yeast cells, identified Vps1 as a hit, and VPS1 null mutants showed mild defects in IPOD formation as well as in damage asymmetry [130].

Kumar *et al.* reported that knockdown/deletion of proteins that function either in actin cable-based transport processes, such as Myo2 and tropomyosin or in vesicular transport and vesicle fusion events, such as Sec18, Sec14, Sec21 prevented accumulation of model amyloids at the IPOD and resulted reversibly in multiple small aggregates dispersed throughout the cytoplasm [136], [140]. These multiple aggregates were interpreted as transport

intermediates; however, their detailed molecular composition remained unclear. Interestingly, the transport intermediates observed due to the depletion of Myo2 also co-localized with Atg9 and preApe1 [136]. The recruitment of vacuolar precursor aminopeptidase, preApe1 to the Phagophore Assemby site (PAS), adjacent to the IPOD, is dependent on small transport vesicles, termed Atg9 vesicles, that was suggested to move along actin cables (Refer section 1.3.3.1) [102]–[104]. Based on these findings, it was hypothesized that the recruitment machinery for amyloid aggregates to the IPOD overlaps with that for preApe1 to the neighbouring PAS and involves Atg9- or related vesicles that are transported along actin cables to the IPOD [112], [136], [140]. Further experiments are needed to evaluate the involvement of Atg9 vesicles/other vesicles in the recruitment of amyloids to the IPOD.

TABLE 1: Table summarizing the involvement of components of vesicle-mediated transport, actin cytoskeleton, and endosomal trafficking pathways in substrate targeting to the IPOD. The functions have been stated based on their description in Saccharomyces Genome Database (SGD).

Candidates	**Functions**	**Effects observed upon their deletion /depletion**	**Reporter used**
VAC17 VAC8	Vacuole Inheritance protein, forms a transport complex with Myo2 and Vac17(Myo2p-Vac17p-Vac8p)	Impaired asymmetric aggregate segregation. Impaired inclusion formation and clearance of heat-induced aggregates.	Hsp104-GFP Htt103Q
MYO2	Actin cytoskeleton	Impaired asymmetric aggregate segregation. Impaired aggregate clearance for heat-induced aggregates. Impaired targeting of amyloid substrates	Hsp104-GFP Htt103Q PrD-GFP
ACT1	Actin cytoskeleton	Impaired asymmetric aggregate segregation. Impaired aggregate clearance for heat-induced aggregates.	Hsp104-GFP Htt103Q
PIM1	Mitochondrial protease involved in the degradation of misfolded mitochondrial proteins	Impaired aggregate clearance for heat-induced aggregates.	Hsp104-GFP
VPS16 VPS41 VPS39	Subunit of HOPS/CORVET membrane tethering complexes. Vps39 additionally is also a component of vacuole-mitochondrion contacts (vCLAMPs), creates contact sites between Vacuole and Mitochondria	Impaired inclusion formation of heat-induced aggregates. Impaired aggregate clearance for heat-induced aggregates. Impaired asymmetric aggregate segregation.	Hsp104-GFP
VPS13 YPT7	Factor associated with vacuole-mitochondrial junctions, creates contact sites between Vacuole and Mitochondria	Impaired aggregate clearance for heat-induced aggregates.	Hsp104-GFP
FAB1 VAC14 FIG4	Inositide-3,5-bisphosphate kinase complex, involved in vacuolar sorting,	Impaired inclusion formation of heat-induced aggregates	Hsp104-GFP
COG8 COG7 COG2 COG3	Subunit of conserved oligomeric Golgi (COG) complex, mediates fusion of transport vesicles to Golgi compartments	Impaired inclusion formation of heat-induced aggregates	Hsp104-GFP Ubc9ts-mCherry
MON2	Mon2-Arl1 Golgi network, endosomal pathway	Impaired inclusion formation of heat-induced aggregates	Hsp104-GFP

VPS1	Dynamin like GTPase involved in late endosomal pathway	Impaired Inclusion formation of heat-induced aggregates. Impaired asymmetric aggregate segregation. Impaired targeting of amyloid substrates	Hsp104-GFP PrD-GFP
SED5	cis-Golgi t-SNARE syntaxin, vesicular transport between ER and Golgi	Impaired asymmetric aggregate segregation. Impaired inclusion formation of heat-induced aggregates. Impaired aggregate clearance of heat-induced aggregates.	Hsp104-GFP Ubc9ts Guk1-7 GFP
SEC13 SEC31	COPII vesicle component, ER to Golgi transport	Impaired inclusion formation of heat-induced aggregates.	Hsp104-GFP
USO1	Involved in vesicle-mediated ER to Golgi transport	Impaired inclusion formation of heat-induced aggregates	Hsp104-GFP
SIR2	NAD-dependent histone deacetylase	Impaired asymmetric aggregate segregation.	Htt103Q Hsp104
CMD1	Calmodulin, actin organization protein		
SEC53	Phosphomannomutase, folding and glycosylation of proteins in the ER lumen		
SEC18	SNARE disassembly chaperone, needed for vesicular transport between ER and Golgi	Impaired asymmetric aggregate segregation. Impaired targeting of amyloid substrates.	Htt103Q Hsp104 PrD-GFP
SEC14	Phosphatidylinositol/phosphatidylcholine transfer protein	Impaired targeting of amyloid substrates	PrD-GFP
SEC21	COPI vesicle component, Golgi to ER transport		

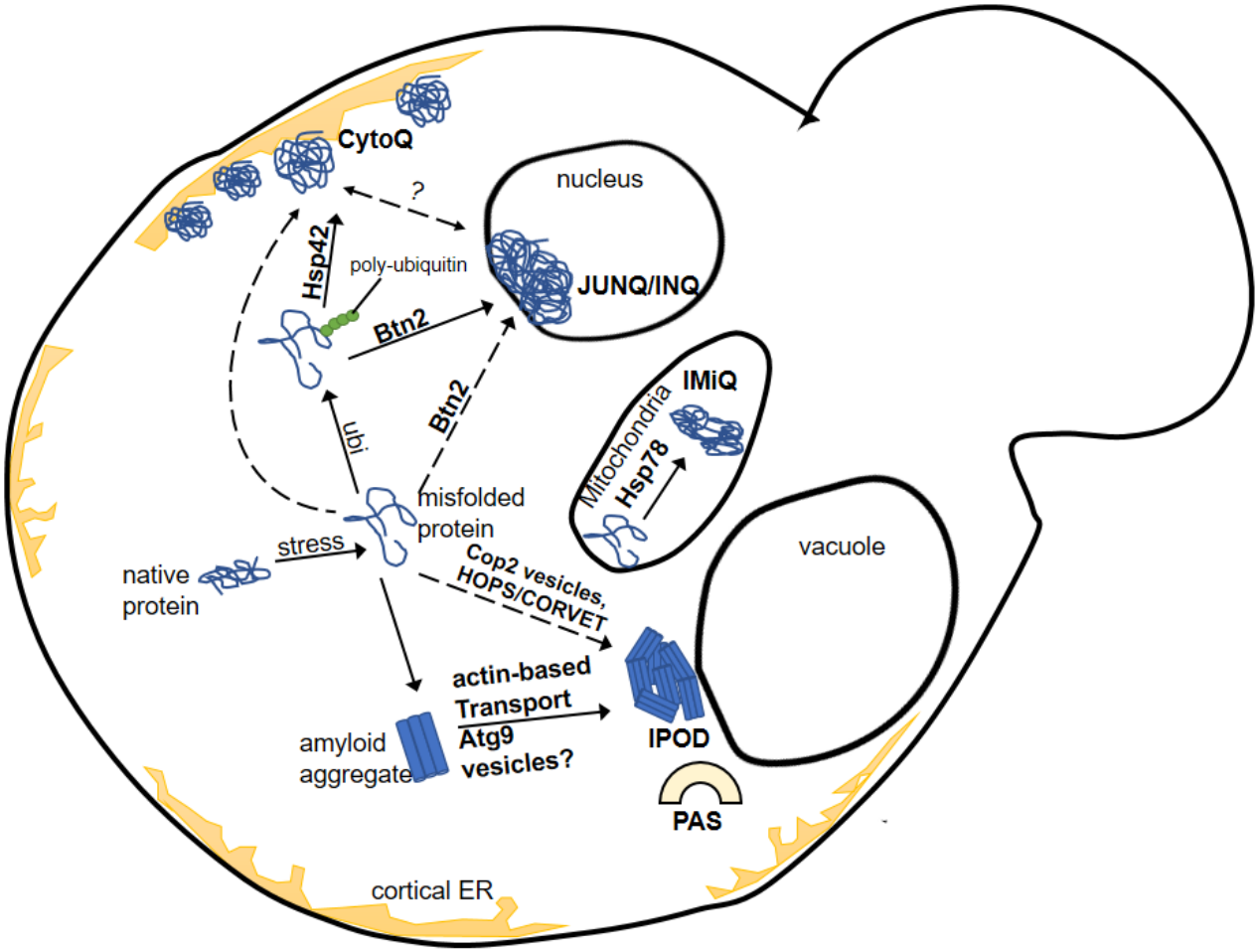

FIGURE 4: Overview of various spatial quality control compartments in yeast and their targeting factors for various substrate types. Soluble misfolded proteins are targeted to JUNQ/INQ and CytoQ with the nuclear sorting factor Btn2 and the cytosolic small heat shock protein Hsp42 respectively [62], [63], [121], [125]. Heat-induced aggregates interact with COPII anterograde trafficking pathway and components of the endomembrane trafficking system to be targeted to the IPOD [130], [139]. Amyloid aggregates are hypothesized to be targeted to the IPOD via Atg9 (or related) vesicles moving on actin cables [112], [136], [140]. The figure was modified from [112].

2 Aims

Deposition of misfolded proteins in spatially distinct quality control sites has been observed both in bacterial as well as eukaryotic cells [74], [111]. Initially, it was thought that these spatially distinct inclusions are formed in the cell only when the folding or degradation pathways are overwhelmed [53], [63], [74], [123]. But increasing evidence has shown that this is not always the case. Rather, inclusion formation is due to the cellular response to spatially and functionally sequester toxic misfolded species from the cellular environment [5], [74]. *Saccharomyces cerevisiae* has at least three distinct, well-characterized protein quality control compartments; JUNQ/INQ, CytoQ, and the IPOD [74]. The JUNQ/INQ and CytoQ sequester amorphously misfolded proteins in a Btn2 and Hsp42 dependent manner [53], [62], [63], [121], [123]. IPOD is located close to the vacuole and acts as a deposition site for mainly amyloid aggregates, although non-amyloid substrates can also be targeted to it [74]. Kumar *et al.* showed that targeting of amyloid substrates to the IPOD is dependent on the actin cytoskeleton, SNARE proteins, and involves vesicle-mediated transport [136], [140]. Furthermore, the delivery of PrD-GFP to the IPOD mimicked the faithful delivery of the resident vacuolar hydrolase preApe1 to the neighbouring PAS (Phagophore assembly site) [112], [136]. Transport of preApe1 to the PAS is dependent on the movement of Atg9 vesicles on the actin cables [102]–[104]. Based on all these observations, Atg9 was proposed as the probable vesicle type which transports PrD-GFP to the IPOD [112], [136], [140]. However, further tests to validate this hypothesis were not carried out in this study.

Hence, the main objectives of the current Ph.D. thesis were:

1) To test the involvement of Atg9 vesicles in the recruitment of PrD-GFP to the IPOD.

2) To set up and optimize a large-scale approach for the isolation of transport intermediates of PrD-GFP from yeast mutants that are defective for key hits of the recruitment pathway.

3) To identify and characterize cellular factors which are involved in the recognition, recruitment, and molecular arrangement of amyloid substrates at the IPOD.

3 Results

The recruitment of vacuolar precursor aminopeptidase, preApe1 to the Phagophore assembly site (PAS) via Cvt pathway is dependent on small transport vesicles, termed Atg9 vesicles, and requires intact cytoskeleton and SNARE proteins [102]–[104]. Previous findings from the lab hypothesized that both amyloid aggregates (PrD-GFP) as well as Cvt substrate, preApe1, are recruited to the IPOD and PAS, respectively, in a similar recruitment machinery involving the movement of Atg9 or related vesicles along actin cables [136]. This hypothesis was proposed due to the following lines of evidence:

1) Depletion of the actin cable-based motor protein, Myo2 prevented accumulation of model amyloids at the IPOD and resulted reversibly in multiple small aggregates dispersed throughout the cytoplasm [136]. These multiple aggregates were interpreted as transport intermediates. The transport intermediates of PrD-GFP formed under Myo2 depleting conditions co-accumulated with the Cvt substrate preApe1 and the marker protein of Atg9 vesicles, Atg9. [136].

2) Furthermore, the observed effects for the depletion of Sec18, Sec14, Vps1, Sec21 on the recruitment of amyloid aggregates to the IPOD also fall in line with the hypothesis of an Atg9 vesicle based transport machinery [112], [136], [140]. Atg9 vesicles require several SNARE proteins to transport their cargo to the PAS [87], [106]. It is plausible that depletion of Sec18, a SNARE disassembly chaperone, which is crucial for SNARE protein function, impairs Atg9 vesicle-based cargo transport to the PAS as well as to the IPOD [93], [112]. Sec14, a phosphatidylinositol /phosphatidylcholine (PI/PC), regulates the formation of phosphatidylinositol-4-phosphate (PI4P) along with Pik1, one of the two major yeast PtdIns 4-kinases. It has been shown that reduction of phosphatidylinositol-4-phosphate (PI4P) formation blocks anterograde transport of Atg9 vesicles from the Golgi to the PAS [147]. Sec14 mutants display a considerable reduction in the formation of phosphatidylinositol-4-phosphate (PI4P) and are defective in Atg9 vesicle cycling [112], [147]. Recently it was shown that Dnm2, the mammalian dynamin 2 is involved in the biogenesis of Atg9 containing vesicles

[148]. Though speculative, it is possible that Vps1, the yeast counterpart of mammalian Dnm2 might also be involved in the generation of Atg9 vesicles [112], [140]. A direct role of Sec21 with the function of Atg9 vesicles has not been confirmed so far. However, Sec21 being a component of both COPI and Vid (vacuole import and degradation) vesicles, is in line with the hypothesis that amyloid transport to the IPOD is mediated by vesicles [149]–[152].

It has to be noted that while several results hinted at the involvement of Atg9 vesicles, none of the tested positive candidates mentioned in Kumar *et al.* 2016, 2017 (Myo2, Sec18, Sec14, Sec21, Vps1) are unique for the Atg9 pathway but rather have key functions also in other vesicle-mediated pathways such as Vid (Vacuole import and degradation) pathway, COPI vesicle-mediated pathway or the general endosomal trafficking pathway. While Vid vesicles aid in the import of Fructose-1,6-bisphosphatase (FBPase), the key regulatory enzyme in gluconeogenesis in *S. cerevisiae,* into the vacuole, COPI vesicles mediate retrograde transport of proteins from the Golgi to ER and acts in the early secretory pathway while the endosomal trafficking pathway transports cargo from the Golgi to the vacuole via endosomes and Multivesicular bodies (MVBs) [149], [150], [153], [154]. Therefore, it was decided to test the involvement of these vesicular pathways one after another.

3.1 Testing the involvement of Atg9 vesicles in the recruitment of PrD-GFP to the IPOD

Proteomic analysis of Atg9 vesicles revealed Atg9, Atg27, Trs85, and Ypt1 as the major proteins present on its surface [104], [155]. Furthermore, additional candidates such as Atg11, Atg19, and Atg23 were also reported to be involved in the recruitment of preApe1 to the PAS [104], [156]. Atg27 and Atg23 are peripheral proteins that play a role in the biogenesis of Atg9 vesicles as well as aid in their correct targeting to the PAS [104], [156]. Trs85, a component of the transport protein particle III (TRAPPIII) complex, resides on Atg9 vesicles and recruits Ypt1, a Rab GTPase that has a role in vesicle tethering functions [104]. The adaptor protein Atg11 is an effector of Ypt1, binds to it as well as to the preApe1 receptor Atg19, and directs the movement of cargo bound Atg9 vesicles to the PAS [100], [104], [157].

Kumar *et al.* previously reported that null mutants of *ATG9, ATG11 and ATG19* showed no obvious recruitment defects of model amyloids (PrD-GFP) to the IPOD [136]. However, the effects of deletion of other key components of the Atg9 pathway in PrD-GFP targeting to the IPOD were not tested in this study. Hence, in the current study, the role of some of the key Atg9 pathway components in the recruitment of PrD-GFP to the IPOD was investigated in a [*PSI*$^{+}$] yeast strain, expressing PrD-GFP under control of a galactose inducible promoter and having a deletion in either of the following genes: *ATG9, ATG11, ATG23, ATG27, TRS85.*

If Atg9 vesicles are required for the recruitment of PrD-GFP to the IPOD, then deletion of the Atg9 protein or other crucial components of this pathway should impair proper recruitment. Surprisingly, none of the tested mutant strains (*atg9Δ, atg11Δ, atg23Δ, atg27Δ, trs85Δ*) showed obvious recruitment defects of PrD-GFP to the IPOD compared to the wild type (wt) control (FIGURE 5A). PrD-GFP in these mutant strains formed one focus in the majority of cells (FIGURE 5A,B). However, this was also the case for another established Cvt substrate, preApe1, which utilizes Atg9 vesicles to reach their target destination, the PAS. preApe1 formed one focus in the majority of the cells, similar to wt, in the null mutants of *ATG9* and *ATG11* strains [100]. However,~ 25% of these foci in *atg9Δ* and ~35% of foci in *atg11Δ* strains were not located at the PAS anymore, as revealed by FM464 vacuolar staining [100]. As the PAS site is located close to the vacuole, overlapping of GFP and FM464 fluorescence signals were considered as an indication of proper preApe1 PAS targeting. To test if the single foci of PrD-GFP observed in *atg9Δ* and *atg11Δ* strains are still targeted to the IPODs located close to the vacuolar rim, an FM464 staining was performed in these strains to visualize the vacuolar membrane. FM464 staining revealed comparable PAS targeting between the wild type (wt) and *atg9Δ* and *atg11Δ* strains (FIGURE 5C). Surprisingly, even the wild type (wt) strain displayed mislocalization of IPODs in the range of 10-15% compared to the mislocalization in *atg9Δ* (15-20%) and *atg11Δ* (10-15%) strains (FIGURE 5C,E). As the literature reported mislocalization of 25 – 35 % of GFP-Ape1 upon deletion of *ATG9* and *ATG11* but never clearly displayed the data of their wild type (wt) strain to our knowledge, these mutants and a corresponding wt strain were also tested for mistargeting of GFP-Ape1 (FIGURE 5D). Under conditions of the tested experimental setup, GFP-Ape1 showed a similar mislocalization in the wt strain (25-30%) as compared to an *atg9Δ* (25-30%) strain, both of which were in the range of the previously reported data (FIGURE 5F). Thus, taken together, these experiments

were inconclusive about the role of Atg9 vesicles not only in the recruitment of PrD-GFP to the IPOD but also for preApe1 recruitment to the PAS. Other approaches have to be employed to further validate or falsify the involvement of Atg9 vesicles in transporting amyloids to the PAS.

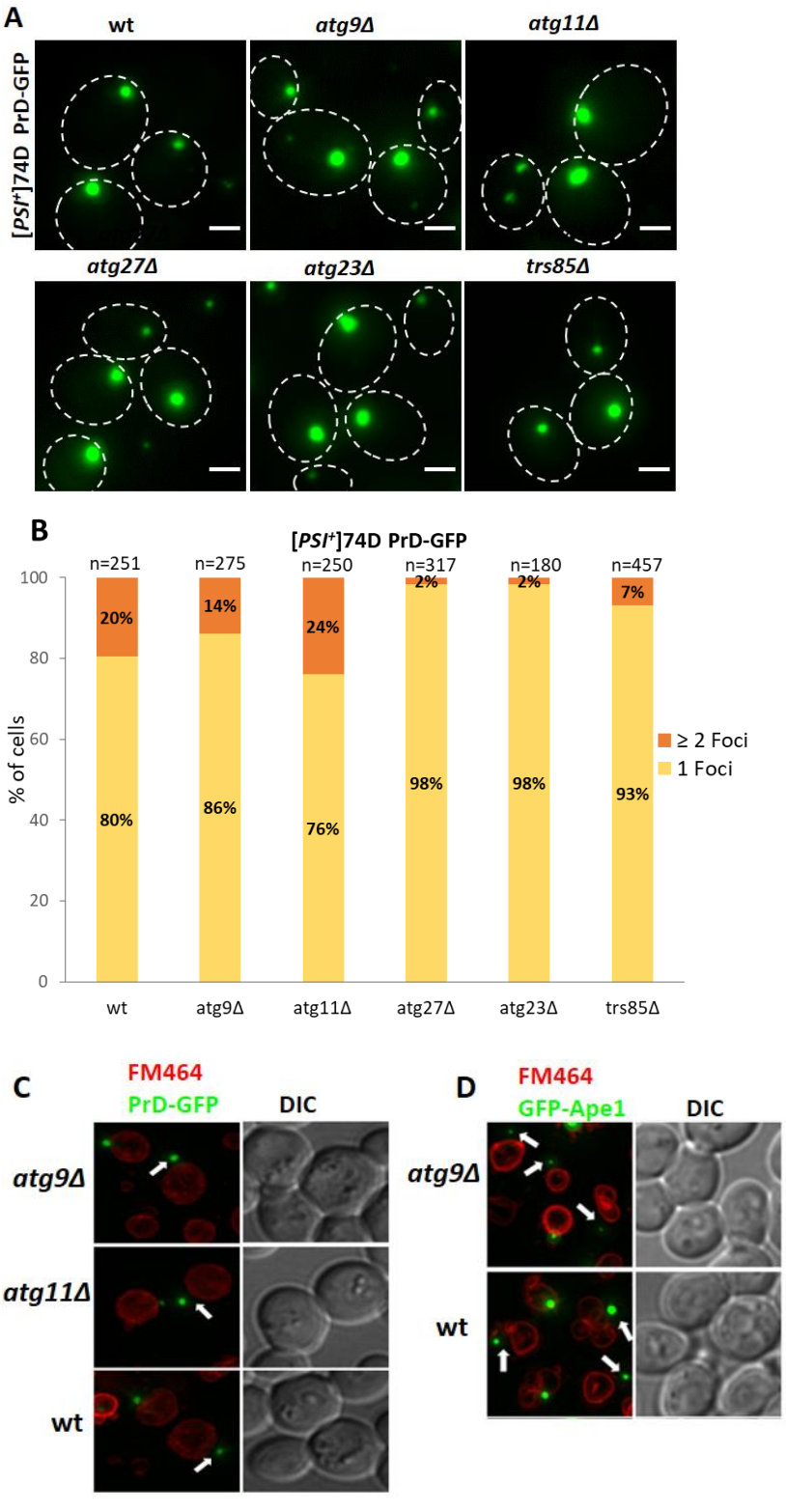

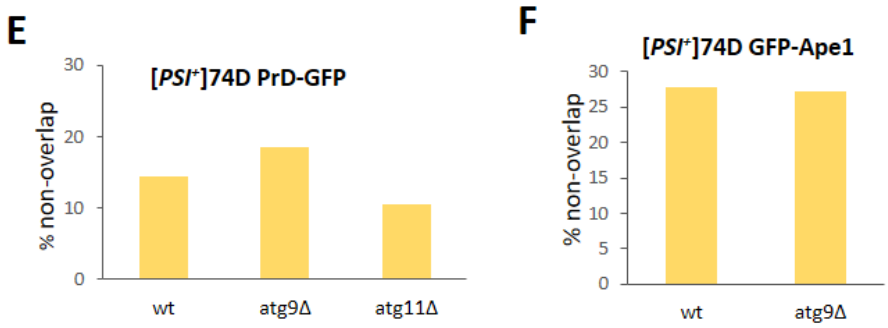

FIGURE 5: Neither ATG9 nor other components of the Atg9 pathway (ATG11, ATG23, ATG27, TRS85) are crucial for PrD-GFP sorting to the IPOD A) PrD-GFP was integrated into the genome (under control of the Gal1 promoter) and induced with galactose for 6 hours in a [*PSI*$^{+}$] wild-type (wt) strain or strains with the indicated deletions in Atg9 pathway components. Cultures were fixed with 4 % PFA and subjected to microscopy analysis. Images were acquired with a 100X objective and Z stacks with a step width of 0.2µm, overlayed as maximum intensity projection and processed using Image J software B) Quantification of PrD-GFP foci upon deletion of Atg9 pathway components compared to wild-type(wt) control. Frequencies of cells with 1 single IPOD focus or ≥2 foci are given in %. The total number of cells counted is denoted by n. C) FM464 Vacuolar rim-staining in corresponding yeast strains. Yeast strains grown to mid-log phase and induced with galactose for 5 hours for the induction of PrD-GFP and were pulsed with FM464 dye for 30 minutes, chased in YPD for 60 minutes and subjected to microscopy analysis. The FM464 signals are shown in red and the GFP signals in green. D) Same as C except that the expression of GFP-Ape1 was driven by a plasmid. E) Quantification of IPODs that are not localized at the vacuolar rim in *atg9Δ* and *atg11Δ* strains as compared to wt; n > 200 cells for each strain. (F) Quantification of GFP-Ape1 that are not localized at the vacuolar rim in GFP-Ape1+ *atg9Δ* strain as compared to its wt control (GFP-Ape1); n > 200 cells for each strain. Scale bar, 2 µm

3.2 Testing the involvement of Vid vesicles in the recruitment of PrD-GFP to the IPOD

The recruitment of PrD-GFP to the IPOD was hypothesized to require vesicle-based transport of amyloid aggregates along actin cables [136]. The results from Atg9 experiments were inconclusive about its involvement in the recruitment pathway (FIGURE 5). Hence, it was decided to test the involvement of Vid vesicles in PrD-GFP targeting to the IPOD as initial results from Kumar *et al.* 2016 were also in line with possible involvement of the Vid (Vacuole import and degradation) vesicles in the recruitment pathway. Vid pathway is a type of selective autophagy in which gluconeogenic enzymes induced under conditions of glucose starvation are inactivated and degraded by the vacuole upon glucose replenishment [149],

[158]. These gluconeogenic enzymes are transported to the vacuole for degradation via specialized vesicles called Vid vesicles [149], [152], [158]. FBPase (Fructose 1,6-bisphosphatase), the key regulatory enzyme for gluconeogenesis in yeast is a well-characterized substrate for this pathway [152]. Similar to Atg9 vesicles, Vid vesicle-based transport depends on the actin cytoskeleton and requires components of the SNARE membrane fusion machinery for its targeting to the vacuole [151], [152]. Although the current knowledge about the origin of these vesicles is limited, some of the major components of this pathway are revealed [151], [158].

Ubc1 (Ubiquitin-conjugating enzyme 1) aids in the biogenesis of Vid vesicles, and *ubc1Δ* strain exhibits defective FBPase import [152]. Vid24 and coatomer subunits of the COPI vesicles, including Sec21 and Sec28, are present on the surface of Vid vesicles and aid them in forming clusters with actin patches to merge with the endocytic pathway prior to substrate delivery into the vacuolar lumen [151], [152], [158]. This process is mediated by the interaction of Sec28 and Vid24 with two other Vid proteins; Vid28 and Vid30 [151]. Furthermore, the v-SNARE Nyv1, the two t-SNAREs (Vam3, Vam7), and the small GTPase Ypt7 aid in the trafficking of Vid vesicles to the vacuole, and their null mutants accumulate Vid vesicles in the cytoplasm [151].

Among the candidates tested for the Vid vesicle pathway, only deletion of *UBC1* impaired the targeting of PrD-GFP to the IPOD, resulting in around 30-35% of the cells showing two or more PrD-GFP aggregates per cell compared to the wild-type (wt) control (FIGURE 6A,B). All other mutant strains tested for this pathway (*vid30Δ*, *sec28Δ*, *nyv1Δ*, *vam3Δ*, *vam7Δ*, *ypt7Δ*) showed no obvious recruitment defects of PrD-GFP to the IPOD compared to the wild type (wt) control (FIGURE 6A). Hence, these results are inconclusive about the involvement of Vid vesicles and warrant further experiments.

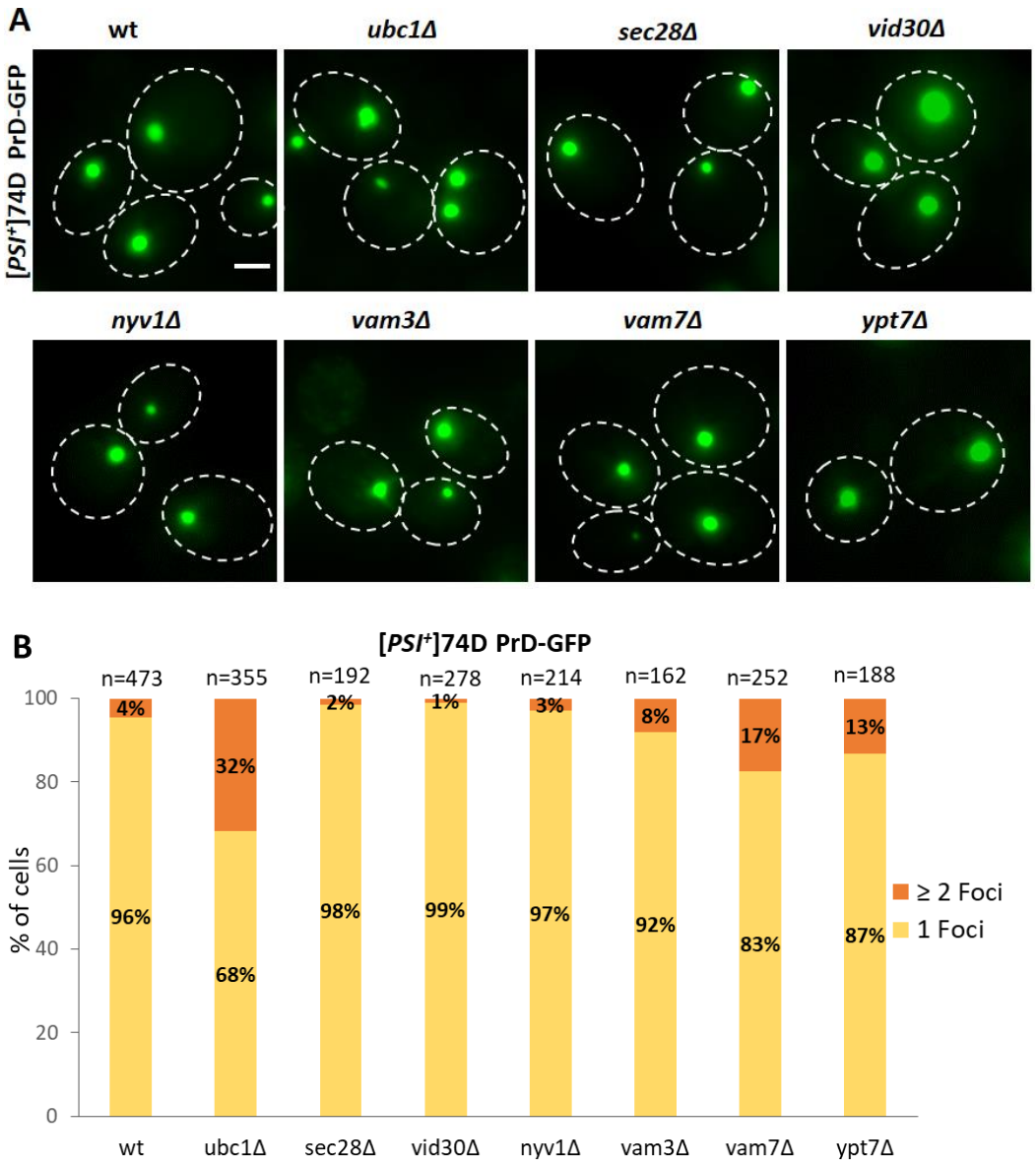

FIGURE 6: Ubc1 is required for the recruitment of PrD-GFP to the IPOD. A) PrD-GFP was integrated into the genome (under control of the Gal1 promoter) and induced with galactose for 6 hours in a [*PSI*$^{+}$] wild-type (wt) strain or strains with the indicated deletions in Vid vesicle pathway components. Cultures were fixed with 4 % PFA and subjected to microscopy analysis. Images were acquired with a 100X objective and Z stacks with a step width of 0.2µm, overlayed as maximum intensity projection and processed using Image J software B) Quantification of PrD-GFP foci upon deletion of Vid vesicle pathway components compared to wt control. Frequencies of cells with 1 single IPOD focus or ≥2 foci are given in %. The total number of cells counted is denoted by n. Scale bar, 2 µm

3.3 Unbiased large scale approach to identify additional factors of the recruitment machinery for amyloid aggregates to the IPOD

The experimental evidence collected so far could not confirm Atg9 vesicles nor Vid vesicles as the type of vesicles that recruit amyloid / PrD-GFP aggregates to the IPOD (Refer FIGURES 5,6). However, the hypothesis that the transport of aggregates to the IPOD is vesicle-mediated still holds true as the recruitment was affected by the depletion/deletion of components of the actin cytoskeleton (Myo2, Tpm1/2), SNARE protein (Sec18), endocytosis (Vps1), and vesicle fission and fusion events (Sec18, Sec21, Vps1) [112], [136], [140]. This vesicle-mediated recruitment hypothesis is further supported by several studies from other laboratories (Refer Table 1 in Introduction) that were able to link aggregate sorting to vesicular transport processes, endosomal structures, actin cytoskeleton, and vacuole biogenesis events [130], [139], [142], [144], [146]. To get more conclusive evidence on the identity of the vesicles involved and to characterize the molecular composition of the recruitment machinery for amyloid aggregates to the IPOD, an additional approach is needed.

3.3.1 Characterization of transport intermediates generated in *vps1Δ* strain by a large scale approach

Depletion/deletion of several previously confirmed recruitment factors (Myo2, Sec18, Sec21, Sec14, Vps1) resulted in the accumulation of several small PrD-GFP aggregates dispersed throughout the cytoplasm instead of its proper accumulation at the IPOD [136], [140]. These multiple aggregates were interpreted as transport intermediates, and it was rationalized that they should be strongly enriched for factors of the recruitment machinery [112], [136]. Therefore, the identification of these factors should aid in unraveling the molecular pathway involved in amyloid recruitment to the IPOD. Hence, it was decided to isolate the transport intermediates of PrD-GFP generated in a VPS1 null mutant yeast strain with an antibody against GFP followed by the identification of co-precipitating factors by mass spectrometry.

Vps1 is a previously confirmed positive hit of the recruitment pathway, and its deletion results in the accumulation of multiple aggregates of PrD-GFP (FIGURE 7A left panel) [140].

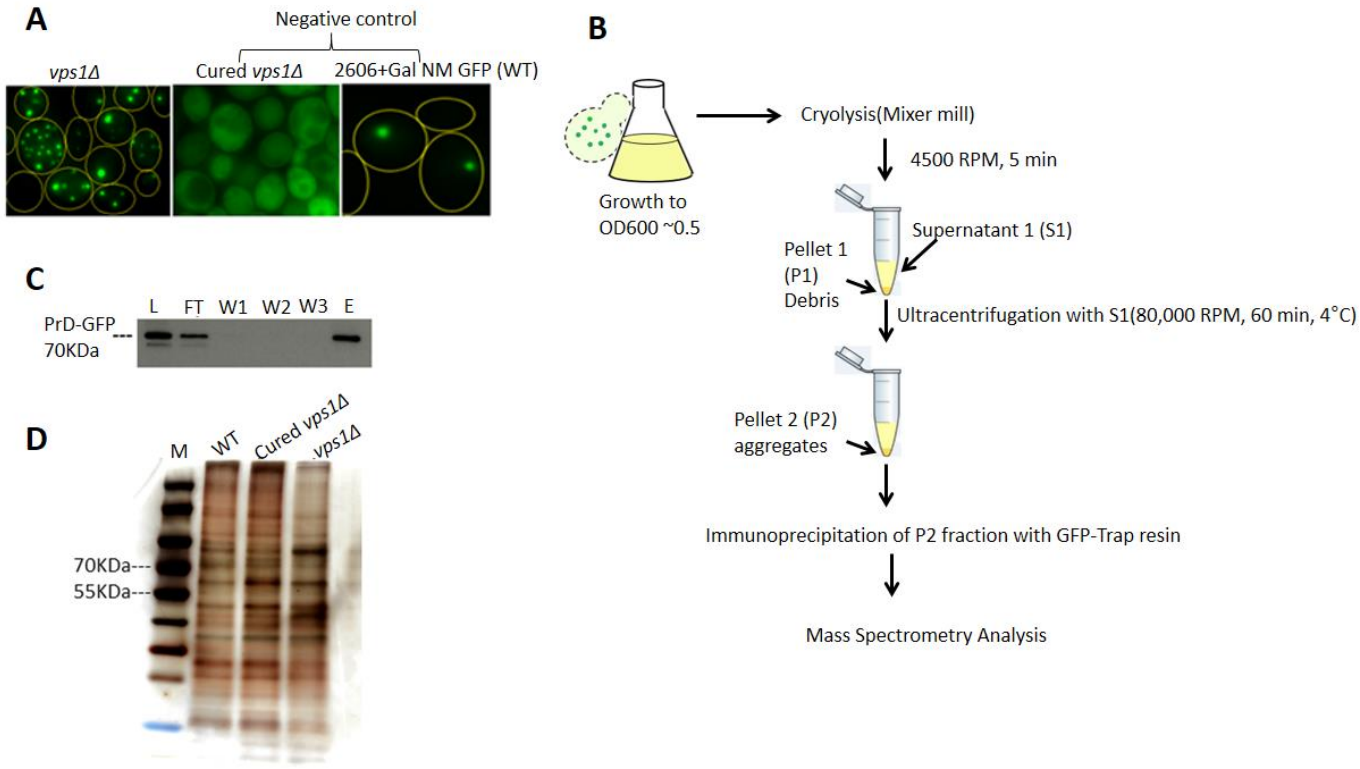

FIGURE 7: Overview of sample preparation steps for Large scale approach. A) Representative images depicting the phenotype of PrD-GFP aggregates in *vps1Δ*, cured *vps1Δ,* and WT (2606+Gal NM GFP) strain after induction of PrD-GFP (under control of the Gal1 promoter) with galactose for 6 hours. B) Flowchart of the sample preparation steps for Immunoprecipitation (IP) and mass spectrometry analysis. C) Western blotting with mouse monoclonal anti-GFP antibodies (1:1000) in yeast lysates from a *vps1Δ* strain, depicting eluate post IP with GFP trap beads. D) Silver staining with the eluates obtained post IP from *vps1Δ*, Cured *vps1Δ,* and WT (2606+Gal NM GFP) strain. L-Load, FT-Flowthrough, W1-Wash 1, W2-Wash 2, W3-Wash 3, E-Eluate.

Prions can be cured to soluble, non-aggregated form by treatment with low concentrations of Guanidine hydrochloride, which inhibits the activity of the yeast disaggregase Hsp104 (Refer section 1.2.1.1). A *vps1Δ* strain which expressed PrD-GFP in the soluble, non-prion form, also called cured *vps1 Δ* strain served as negative control for unspecific binding to the resin or the GFP binder (FIGURE 7A, middle panel). The WT (2606+Gal PrD-GFP) strain with no VPS1 deletion and a phenotype of one PrD-GFP focus representing the IPOD served as another negative control to differentiate between proteins co-accumulating with the IPOD in general, from those of the recruitment machinery to the IPOD (FIGURE 7A, right panel). The entire flow chart for sample preparation for Mass Spectrometry analysis is shown in FIGURE

7B. In brief, lysates from the three yeast strains (FIGURE 7A) were initially cleared of debris (P1, FIGURE 7B), and PrD-GFP aggregates were then pelleted by high-speed ultracentrifugation (P2, FIGURE 7B). The P2 fraction was used further for Immunoprecipitation with magnetic GFP Trap resin (Chromotek). Eluted samples post Immunoprecipitation were separated on an SDS gel (FIGURE 7C) and subjected to Mass Spectrometry analysis at the Core Facility for Mass Spectrometry & Proteomics/ZMBH, Heidelberg to identify proteins associated with the PrD-GFP transport intermediates.

The Mass Spectrometry analysis gave a total of 698 candidates out of which only 499 met the criteria for analysis (peptide count ≥2). These 499 candidates were further filtered quantitatively based on LFQ enrichment ratio (≥4.5 times enrichment in the *vps1Δ* strain compared to both the negative controls; cured *vps1Δ* and WT strain) to give a list of 111 candidates which were considered as top hits and analyzed further (FIGURE 8A). Gene Ontology analysis (GO term analysis) using DAVID (Database for Annotation, Visualization and Integrated Discovery) revealed that the top hits clustered into various functional groups such as; metabolic enzymes, proteasomal subunits, ribosomal, mitochondrial and nuclear Proteins, actin cytoskeleton-modulating proteins, proteins involved in the endocytic secretory pathway/autophagy, vacuolar processes and chaperones (FIGURE 8A). The candidates highlighted in green are either those that were already implicated/related in the recruitment pathway of PrD-GFP to the IPOD (Myo2, Ape1, Ams1) or previously known interactors of the prion domain (PrD) of Sup35 (Sse2) [59], [132], [159], [160]. Myo2 is a previously confirmed positive hit of this pathway [136]. Myo2 depletion shows recruitment defects and accumulates multiple small dispersed cytoplasmic PrD-GFP aggregates, which also co-localize with the Cvt pathway substrate, preApe1 [136]. Ams1 is another substrate of the Cvt pathway and is transported to the PAS along with preApe1 in the Cvt complex in an Atg9 and actin cytoskeleton-dependent manner [108]. Although not proven, it's plausible that the PrD-GFP transport intermediates observed in a Myo2 depletion strain also harbors Ams1 in addition to preApe1 and Atg9.

Contrary to what was expected, the top 111 hits revealed abundant enrichment of metabolic enzymes and proteins related to other processes such as transcription/translation/nuclear transport/mitochondrial function, but only traces of candidates involved in actin cytoskeleton and vesicle-mediated transport (FIGURE 8A,B). Furthermore, extending the analysis from the

top 111 hits to the entire spectrum of 499 candidates, which passed the basic criteria for evaluation (peptide count ≥2), revealed many more candidates with roles in endocytosis and vesicle-mediated processes. However, such candidates co-purified only in traces in *vps1* Δ strain compared to its controls and appeared at the bottom of the list (not shown here). Examples of some of the candidates which co-purified in traces include 1) previously confirmed positive hits of the recruitment machinery (Sec18, Sec21) [136], 2) 4 of the7 subunits of COPI coatomer which coats COPI vesicles (only the alpha subunit Cop1 appeared in the top 111 list (FIGURE 8A)) and, 3) previously shown interactors of Sup35 or its PrD (Pub1, Pab1, Sla2, Sis1, Ydj1, Ssa1/2) [59], [132], [159], [160]. The reason for the observed lower enrichment of these candidates compared to the abundant enrichment of their counterpart, metabolic enzymes, is unknown and warrants further investigation. Nonetheless, the identification of previously known/related components of the recruitment pathway, as well as established Sup35/PrD interactors, indicated that the large scale approach worked in principle and allowed for two different interpretations; 1) The hypothesis that PrD-GFP recruitment to the IPOD required vesicular structures was wrong and need re-evaluation, or, 2) The experimental conditions applied in the above-stated experiments did not preserve putative interactions between PrD-GFP and vesicular structures and need optimization.

To differentiate between these two possibilities, a candidate from the hit list (FIGURE 8A) involved in endosomal /vesicular transport (Cop1) was chosen, and the effect of its depletion on the recruitment of PrD-GFP to the IPOD was evaluated. Cop1 is the alpha subunit of the coatomer complex that coats COPI vesicles [150]. Cop1 vesicles mediate retrograde transport of proteins from Golgi to the endoplasmic reticulum (ER) and between intra-Golgi compartments [150], [161]. Depletion of Cop1 in yeast cells expressing PrD-GFP under the control of galactose promoter resulted in mislocalization of PrD-GFP from the IPOD and their accumulation as multiple aggregates in the cytoplasm (Refer FIGURE 19A,B). This experiment provided proof of concept that when candidates from the current list (FIGURE 8A) involved in vesicular transport and endosomal processes are depleted, then the recruitment of amyloids to the IPOD is impaired. However, the observation that the vast majority of such candidates co-purified only in traces indicated that the putative interactions between PrD-GFP aggregates and vesicular structures were not conserved during the initial experimental

conditions and required further optimization. The samples were optimized in three different ways, which are described in detail below.

A

Metabolic Enzymes		Proteosomal subunits	Mitochondrial Proteins	Endosomal/ Vesicular Transport	Ribosomal Proteins
ICL1	OYE2	RPT6	ATP2	CHC1	RPP0
TDH1	ACS1	RPT4	QCR2	DOP1	RPS14A
TDH2	ADE5	RPT5	YKR01C	COP1	RPS11B
ERG20	GPM1	RPT1	ATP1	GDI1	RPS3
IDP2	AAP1	RPT2	PIM1		RPS1A
LYS20	ACH1	RPT3			RPL9A
FBA1	PDC1			**Vacuolar processes**	RPL5
ENO1	ILV5	**CVT pathway/ autophagy**	**Chaperones**		
CAR2	ZWF1				**Transcription/ Translation**
TDH3	GPD1		HSP42	VMA5	
ADH2	LYS2	AMS1	SSE2	VMA13	
GFA1	ADE4	APE1		VMA2	WTM1
FAA1	IDP1			PMC1	POB3
FAA4	PDI1		**Nuclear Transport**		RTG2
URA2	ADE17	**Actin/Cytoskeleton**		**Others**	SUB2
SHM2	ASN1				STO1
TRM3	ADE2	ARP2	CSE1	SLT2	TMA108
PSA1	ADE13	ACT1	KAP95	RNR2	YDR341C
MIS1	ADH1	SAC6	NMD5	APE2	ILS1
CPA2	ARO8	ARP3	KAP120	ARB1	IKI3
GND1	ARG1	MYO5	CRM1	CDC12	
IDH1	TSL1	TUB3	MSN5	SKI3	**Cell wall Protein**
		MYO2	NOP58	RKR1	YJL171C
			PSE1	CDC53	
			KAP123	SRP68	
			SXM1	NAT1	

B

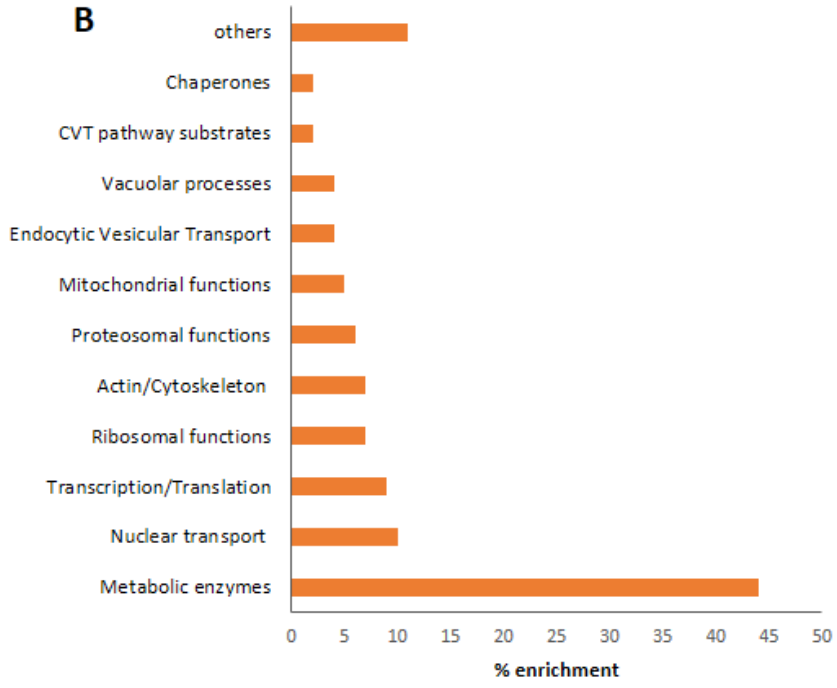

FIGURE 8: Functional grouping of candidates that co-purified with PrD-GFP aggregates and were identified by Mass Spectrometry. A) The top 111 hits that were highly enriched (≥4.5 times) in the *vps1Δ* strain compared to both the negative controls (cured *vps1Δ* and WT strain) were grouped according to their biological process using DAVID (Database for Annotation, Visualization and Integrated Discovery) database. B) Graphical representation of the enrichment of various functional groups in the top hit list of candidates obtained post Mass Spectrometry analysis.

3.3.2 Optimization of sample preparation steps for Immunoprecipitation and Mass Spectrometry analysis

3.3.2.1 Avoiding the use of detergent in sample preparation steps

The presence of detergent (NP40, 0.1%) in the buffer used for co-immunoprecipitation experiments might interfere with the integrity of vesicular structures or their interactions with PrD-GFP. Hence, it was tested if it can be omitted. Isolation of Atg9 vesicles in the literature has been reported to be done in the absence of detergents [104], [155]. As shown in Coomassie staining (FIGURE 9), lane 1 and lane 2 (from left) are lysates from a 2606 (74D) strain that does not express any GFP and served just as a negative control for non-specific binding to the GFP binder. Lane 2 (2606 N.D) (treatment in the absence of detergent) showed more non-specific binding than lane1 (2606 D) (with detergent). The same pattern is also observed for *vps1Δ* lysates in lane 3 (*vps1Δ* D) and lane 4 (*vps1Δ* N.D), where lane 4 (absence of detergent) showed a higher number of non-specific bands than lane3 (with detergent). Hence, it was impossible to eliminate detergent due to massive unspecific binding to the beads.

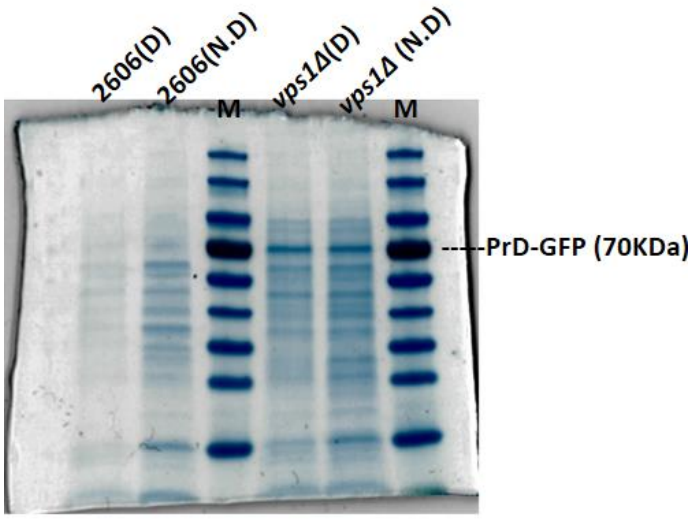

FIGURE 9: Coomassie staining of the eluates obtained post IP, from yeast lysates with a *vps1Δ* strain compared to 2606 (74D) strain. 2606 (74D) strain (control) has the same background as *vps1Δ* strain except that it expresses no GFP and is a negative control. D indicates detergent treatment, N.D indicates no detergent treatment. M stands for marker (Pageruler prestained protein ladder).

3.3.2.2 Immunoprecipitation using the entire soluble S1 fraction instead of the P2 pellet fraction

For Mass spectrometry analysis, the yeast strains were grown to an OD600 ~0.5 and cryolyzed by a mixer mill. The lysates obtained were cleared of debris (P1, FIGURE 10) by low speed centrifugation (4500 RPM, 5min), and the Supernatant (S1) was further subjected to ultracentrifugation (80,000 rpm, 60 min, 4°C) to pellet the PrD-GFP aggregates along with its interaction partners (P2, FIGURE 10). The P2 fraction was used further for Immunoprecipitation (IP) and Mass Spectrometry analysis. As shown in FIGURE 10, it's possible that the tight P2 pellet not only captured PrD-GFP along with its interaction partners but also captured unspecific interactions of sticky PrD-GFP aggregates with other macromolecular structures and aggregates of glycolytic and metabolic enzymes. This might explain their abundant enrichment in the Mass Spectrometry results (FIGURE 8A). To avoid this, it was decided to use the entire soluble S1 fraction for further experiments.

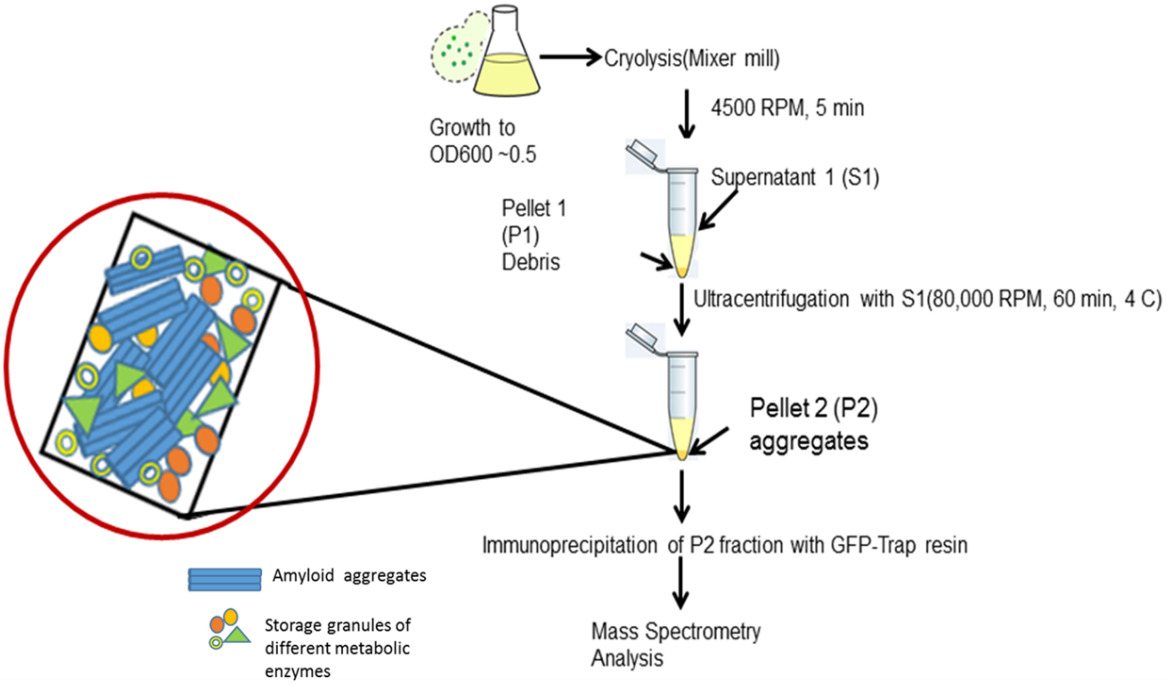

FIGURE 10: Flowchart highlighting the possibility of non-specific interactions of sticky PrD-GFP aggregates with other macromolecular structures and metabolic enzymes in the tight P2 pellet. To avoid this, the entire soluble S1 fraction can be used for IP and Mass spectrometry analysis.

3.3.2.3 Molecular crosslinking to preserve the putative interactions between PrD-GFP and vesicular structures

The Next attempt to preserve the putative interactions was to employ molecular crosslinking. This was achieved by a cleavable DSP (dithiobis (succinimidyl propionate)) cross-linker, which has an amine-reactive N-hydroxysuccinimide (NHS) ester at each end of an 8-atom spacer arm. N-hydroxysuccinimide (NHS) esters react with primary amines to form stable amide bonds at pH 7-9. Yeast lysates were crosslinked with DSP prior to detergent treatment (FIGURE 11C). It was decided to determine the efficiency of cross-linking from Mass Spectrometry results.

In conclusion, the mass spectrometry results from *vps1*Δ strain were successful in isolating components of recruitment machinery, although the bulk of them co-purified only in traces.

Hence, as a solution, it was decided to optimize the sample preparation steps as stated above but also to repeat the IP / Mass spectrometry approach again, not in *vps1Δ* strain, but rather using yeast strains having a knockdown in SEC18 gene, which results in the accumulation of reversible transport intermediates of PrD-GFP [136]. Knockdown of SEC18 gene was achieved by the auxin-based method for depleting an essential protein [162]. The same strain in the absence of auxin served as a negative control. In short, lysates obtained from yeast strains either having a knockdown in SEC18 (+Auxin) or no knockdown (-Auxin) were incubated with the DSP crosslinker for two hours before they were quenched with 40mM Tris (pH 7.5) (FIGURE 11C). After this, the lysates were treated with detergent before collecting the soluble supernatant S1 that was used further for IP (FIGURE 11A,C). Two sets of eluates (+/- crosslinker) were given for Mass Spectrometry analysis at the proteomics facility at the DKFZ.

1. Sec18 (+/- Auxin) treated with DSP

2. Sec18 (+/- Auxin) No DSP treatment

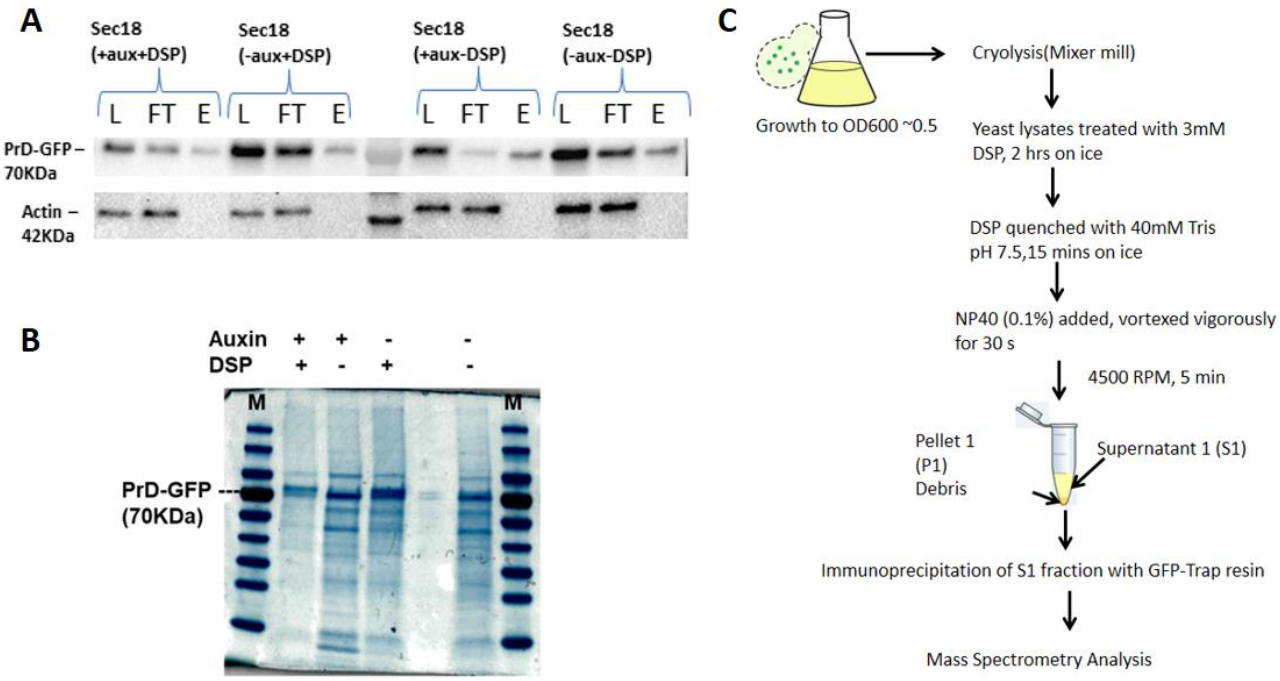

FIGURE 11: Comparable eluate was obtained post IP in DSP cross-linked S1 fraction of yeast lysates from a SEC18 knockdown strain. A) Western Blotting with mouse monoclonal anti-GFP antibodies (1:1000) in yeast lysates from a SEC18 knockdown strain. SEC18 knockdown was achieved with the auxin aid method [162]. 'aux' stands for Auxin and DSP is the crosslinker used. Mouse anti-actin antibody served as a loading control (42KDa). B) Coomassie staining with the eluates obtained post IP, from yeast lysates with and without SEC18 knockdown(+/-Auxin), treated with or without DSP. C) Overview of optimized sample preparation steps for IP

and mass spectrometry analysis. Yeast lysates were treated with the crosslinker before detergent treatment, and the entire soluble fraction (S1) was used for IP and Mass Spectrometry analysis. L- Load for IP; FT- flowthrough after incubation with GFP trap beads, E- eluate obtained post IP.

3.3.3 Identification of transport intermediates generated in SEC18 knockdown (+/-crosslinker) strain by Mass Spectrometry analysis

A total of 3529 proteins were detected in each of two sets of eluates (Sec18 (+/- Auxin) treated with and without DSP). The initial cut-off parameters (Enrichment ratio >=2; $p<0.05$; Enrichment ratio= LFQ Intensity Sec18 (+Auxin) / LFQ Intensity Sec18 (-Auxin) gave a list of 124 proteins enriched in Sec18 (+Auxin/+DSP) lysates compared to its control (Sec18 (-Auxin/+DSP) and 173 proteins enriched in Sec18 (+Auxin/-DSP) lysates compared to its control (Sec18(-Auxin/-DSP). To filter for top highly enriched candidates in both categories, the cut off parameters were further increased (enrichment ratio >=2; $p<0.001$), resulting in a list of 40 and 43 proteins for cross-linked and non cross-linked samples, respectively. They were considered as top hits and analyzed further (FIGURE 12A, B). Gene Ontology analysis using DAVID (Database for Annotation, Visualization and Integrated Discovery) revealed that the top hits for both cross-linked and non cross-linked samples, in general, clustered into various functional groups such as metabolic enzymes, ribosomal proteins, mitochondrial proteins, ATPases, proteins involved in transcription/translation, ubiquitin-ligase complex, actin cytoskeleton-modulating proteins as well as proteins involved in the endocytic/vesicular mediated pathway (FIGURE 12).

As seen in FIGURE 12 metabolic enzymes were no longer the most abundant functional group identified as in the first mass spectrometry run with *vps1Δ* samples (FIGURE 8A), indicating that the sample optimization steps were successful. However, the use of cross-linker did not improve the results, rather the opposite was achieved (Compare FIGURE 12A vs 12B). The top hits from cross-linker treated samples (FIGURE 12A) had lower enrichment (7.5%) of candidates involved in endocytic/vesicular pathway and actin cytoskeleton compared to non cross-linked treated samples (16%) (FIGURE 12B). The candidates highlighted in blue are those that were identified in both the cross-linked and non cross-linked treated samples. 79

candidates were common between the two categories. These candidates belonged to a wide range of various functional groups and not any one particular pathway.

A

Metabolic Enzymes	Transcription /Translation	Mitochondrial Functions	Others
AAT2			PBY1
	GAL11	COX9	REE1
ATPases	SEF1	MNP1	ABZ1
		MST1	YBR053C
MDL1	**Ubiquitin ligase complex**	IFM1	CNB1
		FUN14	SHO1
DNA replication		SOV1	YGR122W
	MOT2	MRPL51	MOB2
TOP2	GRR1		DRE2
	UFO1	**Vacuolar processes**	GCG1
Ribosomal Functions			PBP4
	Serine/Threonine phosphatase		YKR078W
		COT1	SDD3
NSA2		VBA4	
RRP15	FCP1	FAB1	**Protein Transport**
	SDS22		
Actin/Cytoskeleton			
SDA1	**Endosomal /Vesicular Transport**		NPC2
			ENB1
	GDI1		
	LTV1		

B

Metabolic Enzymes	Actin/Cytoskeleton	Mitochondrial functions	Endosomal/ Vesicular Transport
	RGD1		
GLO2	LAS17	RSM23	
IMD4		MHR1	VPS29
FAD1	**Transcription/ Translation**	TOM7	RAV1
STR3		SCO2	VPS45
		MIX23	COS3
ATPases	RLF2	RSM10	UFE1
	CAT8		
STE6		**Chaperones**	**Others**
RDH54	**Ubiquitin ligase complex**		
		HSP30	BNA1
Ribosomal functions		ERJ5	PDR16
	RAD18		YLR460C
		Oxidative Stress Response	BNI5
BUD21	**Serine/Threonine Kinase**		BUD4
RPS13			NTH2
RRS1		OCA1	
POL5	KIN1	GRX6	**Cell Wall Proteins**
NOP4	DUN1		
	YPK3	**Proteasomal functions**	
			YGP1
			CIS3
		PBA1	

FIGURE 12: Functional grouping of candidates that co-purified with PrD-GFP aggregates in a SEC18 knockdown strain and were identified by the Mass Spectrometry. A) The top 40 hits that were highly enriched (enrichment ratio >=2; p<0.001) in the Sec18 (+Auxin/+DSP) lysates compared to its control, Sec18 (-Auxin/+DSP). B) The top 43 hits that were highly enriched (enrichment ratio >=2; p<0.001) in the Sec18 (+Auxin/-DSP) lysates compared to its control, Sec18(-Auxin/-DSP). Candidates were grouped according to their molecular function using DAVID (Database for Annotation, Visualization and Integrated Discovery) database.

Furthermore, extending the analysis from the top hits to the entire spectrum of candidates for both cross-linked and non-cross-linked samples revealed that previously known positive hits of the recruitment pathway (DSP treated-Cop1; non DSP treated-preApe1, Ams1) as well as known interactors of Sup35 or its PrD (DSP treated-Hsp104, Ydj1 ; non DSP treated-Sla2, Sse1/2), and many more candidates involved in vesicle-mediated transport processes co-purified with SEC18 knockdown strains (both +/-DSP , not shown in FIGURE 12), although again only in traces. These results were similar to the one observed for *vps1Δ* strain (FIGURE 8). Various rounds of optimization of sample preparation steps (Refer section 3.3.2), use of cross-linker, or repeating the experiment in a yeast strain with proven reversible transport intermediates (such as SEC18 knockdown strain [136]) did not solve this problem either (FIGURE 12). However, the current results (Cop1 depletion, see FIGURE 19A,B), as well as previous results from the lab, have revealed the possibility to characterize the recruitment process of PrD-GFP to the IPOD through in vivo depletion of the candidates of interest and co-localization studies to visualize interactions [136], [140]. Therefore, it was decided not to repeat the large-scale approach but rather to test the interesting candidates through *in vivo* knockdown/knock-out and co-localization techniques.

The candidates to be analyzed were chosen based on the following parameters:

1) Candidates involved in vesicle-mediated transport, fission/fusion reactions (even if co-purified in traces with PrD-GFP in the mass spectrometry runs).
2) Top candidates identified by mass spectrometry analysis from lysates of both *vps1Δ* as well SEC18 knockdown strain.
3) Candidates that bound to the immobilized PrD-GFP resin in the previous experiments from the lab [136].

The candidates tested so far in knock-out / knock-down experiments are listed in FIGURE 13. The appearance of multiple aggregates or diffused background of PrD-GFP in fluorescence microscopy instead of one focus of PrD-GFP at the IPOD were considered a phenotype and validated further. The candidates in green represent those that tested positive and are described in more detail in the remaining sections. The candidates in pink/red are those that tested negative and showed no visible recruitment defects.

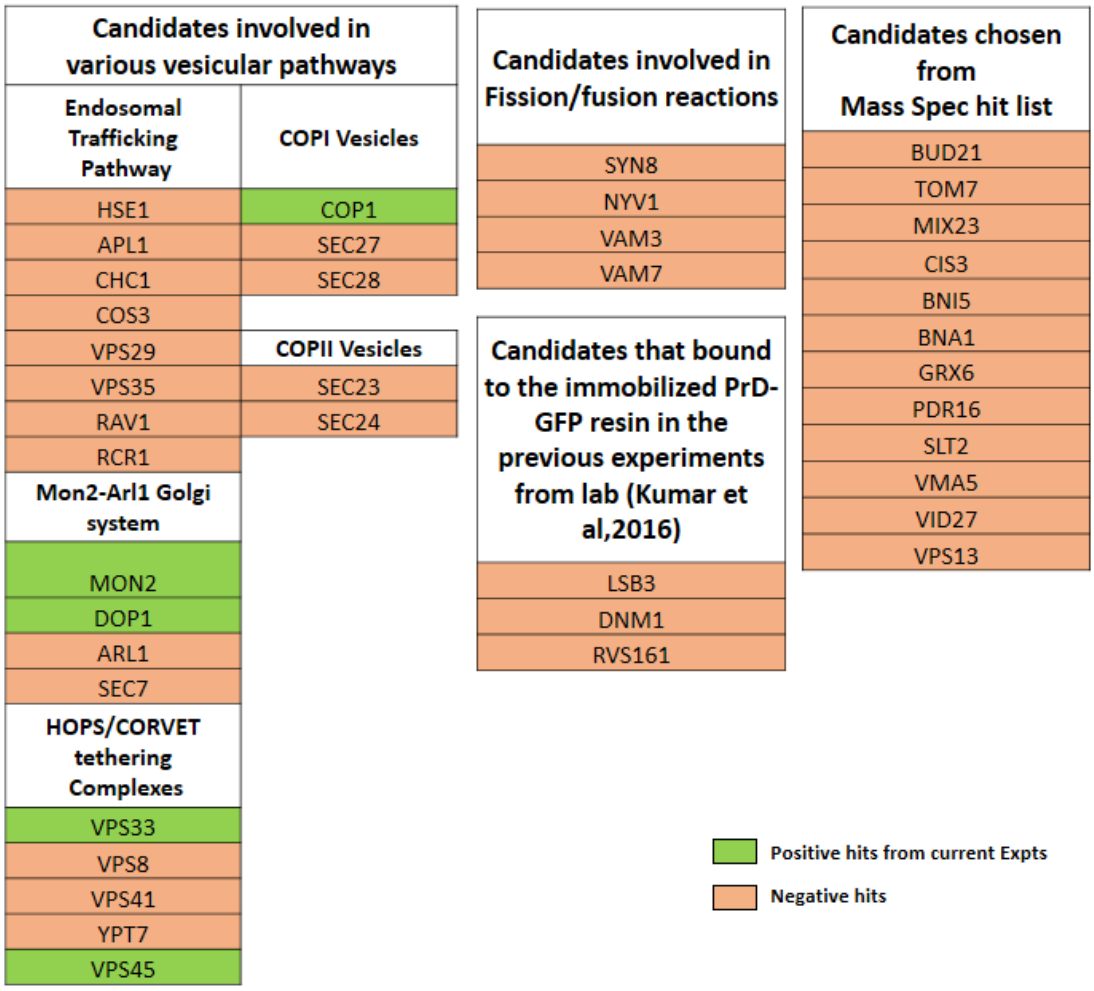

FIGURE 13: The table summarizes the candidates chosen to evaluate further by *in vivo* knockdown/knock-out experiments for their effect on PrD-GFP recruitment to the IPOD.

3.4 Mon2 and Dop1 are required for the proper recruitment of PrD-GFP to the IPOD

Recently, it was reported that the Mon2-Dop1 Golgi complex is required for the targeting of heat-induced aggregates to the IPOD [139]. When PrD-GFP transport intermediates in a *vps1Δ* strain (Refer FIGURE 8) was pulled down, both Mon2 (not shown in FIGURE 8) and Dop1 co-purified with the transport intermediates and were identified by mass spectrometry. Mon2 co-purified exclusively in *vps1Δ* strain but not in the other two negative controls (cured *vps1Δ,* WT), while Dop1 was highly enriched in *vps1Δ* strain compared to both the negative controls (FIGURE 8A). Mon2 is a peripheral membrane protein and localizes to both the trans-Golgi network as well as to the endosomes. Mon2 physically interacts with Dop1, recruits Dop1 to the Golgi, and together they function in the sorting of substrates between the Golgi and the endosomal system [163]–[165].

To test if Mon2 is also involved in sequestering amyloid aggregates at the IPOD, a [*PSI*$^{+}$] strain expressing PrD-GFP under control of a galactose inducible promoter and having a deletion in the *MON2* gene was created. This strain was induced with galactose for 6 hours along with its wild-type control (wt) (no *MON2* deletion), after which cells were fixed with PFA, and the aggregation pattern of PrD-GFP was visualized under the fluorescence microscope (FIGURE 14A). In the control, more than 95% of the cells showed one single large PrD-GFP dot/IPOD (FIGURE 14A left panel and 14C) as formerly described [59]. In contrast, 58 % of the cells showed multiple PrD-GFP foci upon deletion of *MON2* (FIGURE 14A right panel and 14C).

As Dop1 physically interacts with Mon2 and functions in the same pathway, it was evaluated next. Unlike Mon2, Dop1 is an essential gene, and its depletion was achieved by the auxin-based method for depleting an essential protein [162]. For this, a [*PSI*$^{+}$] strain carrying a C-terminal aid tag (degron-tag) in the endogenous DOP1 gene and expressing the plant E3 ligase SCF-TIR1 was generated. The addition of the plant hormone auxin promoted the interaction between SCF-TIR1 and the “aid” tagged protein, as a result of which the target protein was polyubiquitinated and degraded by the 26S proteasome. Hence, PrD-GFP was induced with galactose for 6 hours in the absence or presence of auxin, post which cells were fixed with PFA and visualized under fluorescence microscopy. Similar to *MON2* deletion, 57% of the cells showed multiple PrD-GFP foci phenotype upon depletion of Dop1 (FIGURE 14B, D). Depletion

of Dop1 was confirmed by Western Blot analysis with an antibody against an HA tag attached to the "aid" degron tag (FIGURE 14E). These results suggested that the presence of Mon2 and Dop1 is crucial for the successful recruitment of PrD-GFP to the IPOD.

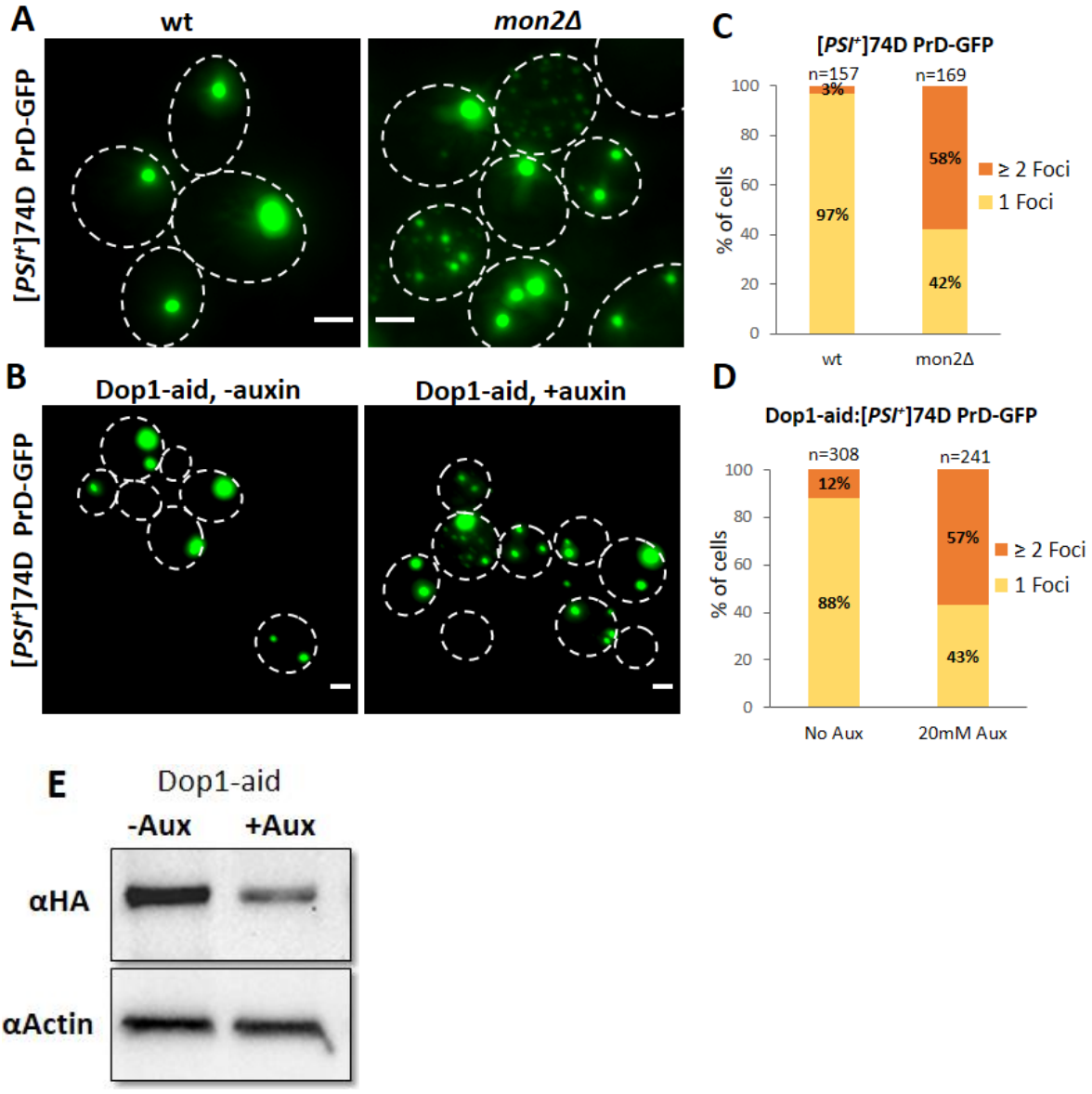

FIGURE 14: Mon2 and Dop1 are required for the proper recruitment of PrD-GFP to the IPOD. A) PrD-GFP was integrated into the genome (under control of the Gal1 promoter) and induced with galactose for 6 hours in a [*PSI*$^+$] wild-type (wt) strain (left panel) or strains having a deletion of MON2 (right panel). Cultures were fixed with 4 % PFA and subjected to microscopy analysis. Images were acquired with a 100X objective and Z stacks with a step width of 0.2µm, overlayed as maximum intensity projection and processed using Image J software. B) PrD-GFP was induced with galactose for 6 hours in a [*PSI*$^+$] wild-type strain with a C-terminal aid tag in DOP1 in the absence or presence of 20 mM of auxin as indicated. Cells were fixed with 4 % PFA and subjected to microscopy analysis. Images were obtained with a 63X objective and Z stacks with a step width of 0.2µm,

overlayed as maximum intensity projection and processed using Image J software. C) Quantification of PrD-GFP foci upon deletion of MON2 compared to wt control. D) Quantification of PrD-GFP foci upon depletion of Dop1 with 20mM auxin compared to the control, without auxin. E) Western blot analysis of the Dop1-aid strain treated with/without auxin (+/-Aux) with an antibody against an HA-tag present in the aid-tag. An anti-actin antibody served as loading control. Frequencies of cells with 1 single IPOD focus or ≥ 2 foci are given in %. The total number of cells counted is denoted by n. Scale bar, 2 µm.

3.5 Washout of auxin partially restores Dop1 function and causes re-localization of PrD-GFP aggregates to the IPOD

Depletion/deletion of Dop1 and Mon2 functions led to the accumulation of multiple PrD-GFP foci in the cytoplasm rather than recruiting these aggregates to one single IPOD site (FIGURE 14). If these multiple foci represented transport intermediates that accumulated upon depletion of Dop1 or Mon2 function, replenishment of the depleted proteins should reverse the observed recruitment defects. To test if the defect in PrD-GFP localization could be restored, auxin was washed out from Dop1-depleted cells that expressed PrD-GFP under control of a galactose-inducible promoter, and the cells were incubated in glucose-based media without auxin to monitor the fate of the pre-existing multiple PrD-GFP foci (FIGURE 15A,B). In the case of Dop1 strain, washout of auxin only partially reversed the multiple foci phenotype and formed one IPOD-like inclusion in 55% cells again (FIGURE 15A, left panel and 15B). The fact that the restoration of the Dop1 function caused the fusion of the multiple aggregates into one central IPOD focus was only found in a subset of cells could be explained by Western blotting results. As Dop1 levels were not fully replenished compared to the control (No auxin treated) (FIGURE 15E), longer auxin washout times might be needed to replenish the protein fully and to observe full recovery. However, this was not tested within the current dissertation due to time constraints. In addition, for further confirmation that some of the multiple fluorescence foci really refused again to one central IPOD rather than being degraded and leaving only one focus remaining, a time-lapse microscopy experiment was performed (FIGURE 15G). In brief, post-induction of PrD-GFP with galactose and auxin addition, cells were pelleted and placed onto an agarose pad on a microscope slide without auxin, but with glucose-based media instead of galactose. The shift from galactose to glucose media resulted in suppression of expression of PrD-GFP and allowed, therefore, to observe the fate of the pre-existing multiple PrD-GFP foci. Z-stack images were acquired every 5

minutes over a period of 1 hour. Within 1 hour of auxin removal in glucose-based media, some of the pre-existing multiple PrD-GFP foci directly refused to one central IPOD deposition site (FIGURE 15G). Although only a partial rescue of phenotype was observed by replenishing Dop1 protein, the above results from time-lapse microscopy clearly indicate that the observed multiple foci of PrD-GFP upon Dop1 depletion represent transport intermediates that are trapped on the way to the IPOD deposition site.

In order to test if the multiple foci that accumulated in a *mon2Δ* strain also represent transport intermediates which can refuse to one central IPOD upon replenishment of the protein, a [*PSI*$^{+}$] strain carrying a C-terminal aid tag (degron-tag) in the endogenous MON2 gene and expressing the plant E3 ligase SCF-TIR1 was generated. Depletion of protein was achieved by the addition of auxin. This was done because the recruitment defects observed for Mon2 in above-stated experiments (FIGURE 14) was achieved by a complete knock-out of this non-essential protein. Therefore, testing the reversibility of MON2 deletion was technically not possible in the same KO strain. Hence, like Dop1, the auxin aid-based method was used for the depletion of Mon2 protein levels [162]. However, auxin-based depletion of Mon2 resulted only in milder phenotype with only about 20% of the cells expressing multiple PrD-GFP foci compared to multiple dot phenotype seen in about 58% of the cells with the full knock-out (compare FIGURE 14C and 15D). This could be because the depletion of Mon2 by this method was too incomplete to induce the strong phenotype seen with the full knock-out, as revealed by Western blot analysis (Figure 15F).

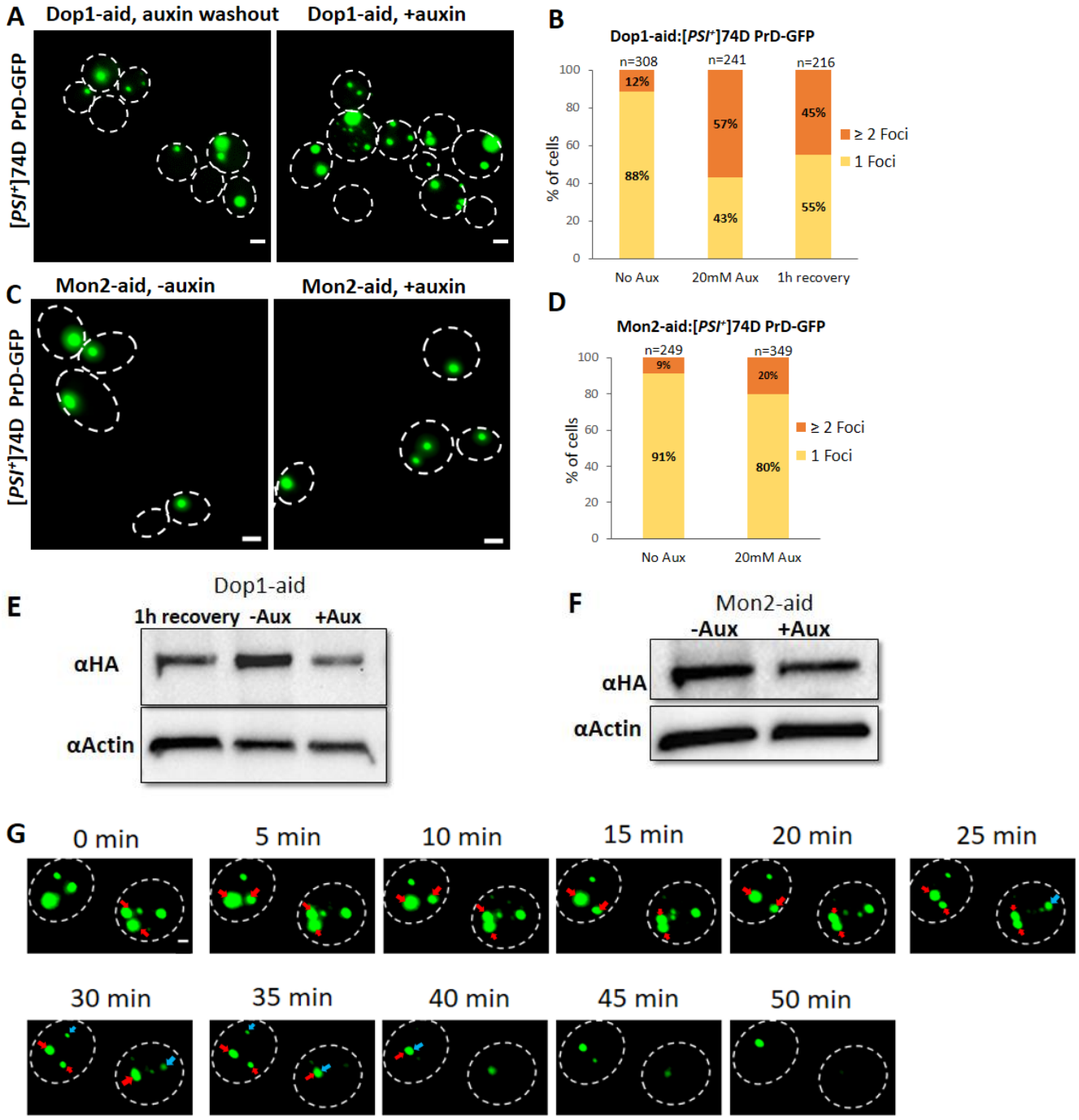

FIGURE 15: Washout of auxin restores Dop1 function and causes partial relocalization of PrD-GFP aggregates to the IPOD A) PrD-GFP was integrated into the genome (under control of the Gal1 promoter) and induced with galactose for 6 hours in a [*PSI*$^+$] wild-type strain with a C-terminal aid tag in DOP1 in the presence of 20 mM of auxin as indicated (right panel). Subsequently, cells were pelleted and resuspended in YPD in the absence of auxin to rescue Dop1 function, and further incubated for 1 hour prior to fixation with 4 % PFA and subjected to microscopy analysis (left panel). Images were obtained with a 63X objective and Z stacks with a step width of 0.2µm, overlayed as maximum intensity projection and processed using Image J software B) Quantification of PrD-GFP foci upon depletion of Dop1 with 20mM auxin compared to the control, no auxin or after auxin washout (1 hour recovery). C) PrD-GFP was induced with galactose for 6 hours in a [*PSI*$^+$] wild-type strain carrying PrD-GFP (under control of the Gal1 promoter) with a C-terminal aid tag in MON2 in the absence or presence of 20

mM of auxin as indicated. D) Quantification of PrD-GFP foci upon depletion of Mon2 with 20mM auxin compared to the control, without auxin. E,F) Western blot of the Dop1-aid strain (E), Mon2-aid strain (F) after auxin treatment compared to the negative control, without auxin or after auxin washout (1 hour recovery) with an antibody against an HA-tag present in the aid tag. An anti-actin antibody served as loading control. G) Microscopy images from a time-lapse microscopy experiment as in (A), but after removal of auxin. In brief, after induction of PrD-GFP and auxin addition for 6 hours, cells were pelleted, placed onto an agarose pad containing glucose-based media instead of galactose and covered with a microscopic slide. A z-stack with a step width of 0.3 µm was obtained every 5 min. Frequencies of cells with 1 single IPOD focus or ≥2 foci are given in %. The total number of cells counted is denoted by n. Scale bar, 2 µm.

3.6 Mon2 is also essential for the proper accumulation of different amyloid substrates (Rnq1 and Ure2) at the IPOD

In order to check if Mon2 is also required for targeting of additional bona fide IPOD substrates such as Ure2 and Rnq1 amyloids, a similar experiment was conducted as compared to PrD-GFP by introducing *mon2Δ* into yeast cells expressing either galactose-inducible Rnq1-YFP or Ure2-YFP constructs instead of PrD-GFP. In brief, the corresponding IPOD substrates were induced with galactose for 6 hours in a [*PSI*$^{+}$] *mon2Δ* strain or a wild-type (wt) strain. Subsequently, these cultures were fixed with 4% PFA and subjected to microscopy analysis. All corresponding *mon2Δ* strains expressing these IPOD substrates displayed one single IPOD in the control strain (no Mon2 depletion), but a multiple foci phenotype upon *MON2* deletion (FIGURE 16 A,C) similar to the effects observed with PrD-GFP strain with *MON2* deletion (FIGURE 14A). This shows that deletion of *MON2* affects the recruitment of not just the PrD-GFP substrate, but also other amyloid substrates (Rnq1, Ure2) to the IPOD.

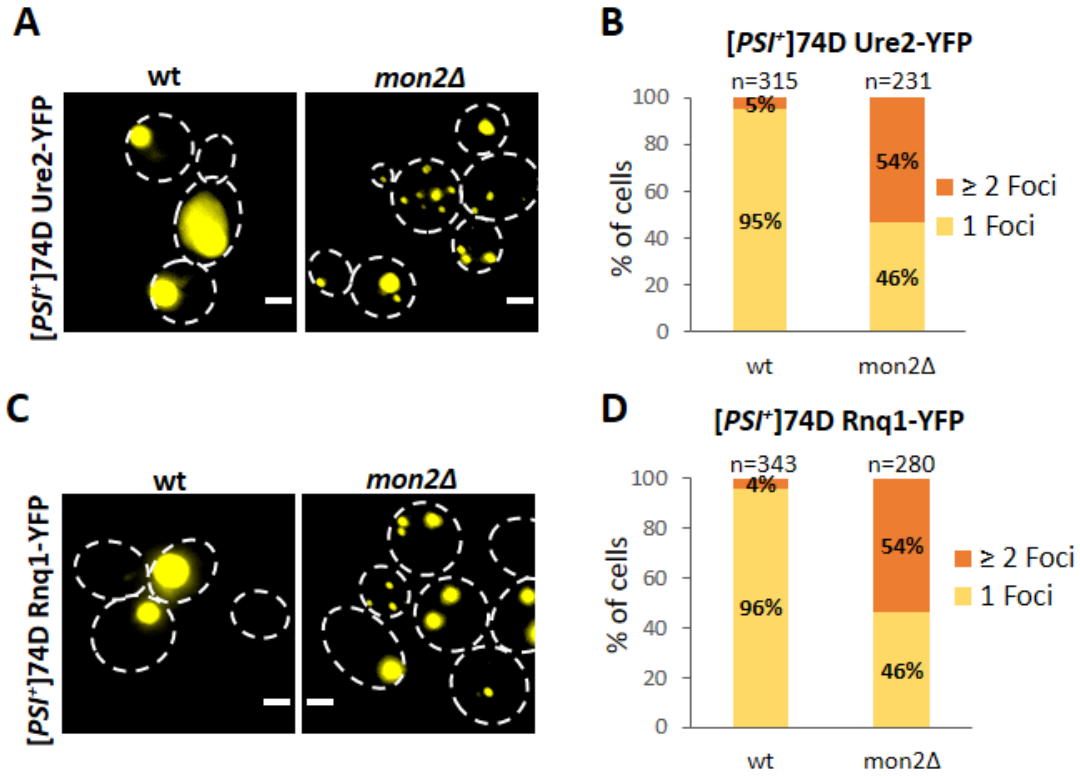

FIGURE 16: Mon2 is also essential for proper recruitment of different amyloid substrates (Rnq1, Ure2) at the IPOD. A) Deletion of MON2 in a yeast strain expressing Ure2-YFP (integrated into genome under control of the Gal1 promoter) and induced with galactose for 6 hours (right panel) compared to a corresponding wild-type (wt) control strain (left panel). Cultures were fixed with 4 % PFA and subjected to microscopy analysis. Images were obtained with a 63X objective and Z stacks with a step width of 0.2µm, overlayed as maximum intensity projection and processed using Image J software. B) Quantification of Ure2-YFP foci upon deletion of MON2 compared to wild-type (wt) control. C) Deletion of MON2 in a yeast strain expressing Rnq1-YFP (integrated into genome under control of the Gal1 promoter) and induced with galactose for 6 hours (right panel) compared to the corresponding wild-type (wt) control strain (left panel). D) Quantification of Rnq1-YFP foci upon deletion of MON2 compared to wild-type (wt) control. Frequencies of cells with 1 single IPOD focus or ≥2 foci are given in %. The total number of cells counted is denoted by n. Scale bar, 2 µm.

3.7 Deletion of Vps33 and Vps45 also impairs the recruitment of PrD-GFP to the IPOD

The Sec1/Munc18 (SM) family of proteins (Sec1, Sly1, Vps45, Vps33) play a key role in vesicle trafficking and protein transport events [166]–[168]. Sec1 and Sly1 are involved in the fusion of secretory vesicles with the plasma membrane, and fusion of ER-derived vesicles with the Golgi, respectively [166], [168], [169]. Vps45 and Vps33 aid in the fusion of Golgi-derived vesicles with the endosomes and transport of late endosomes to the vacuole [168], [169]. Additionally, Vps33 is one of the four core subunits (Vps33, Vps11, Vps16, Vps18) of two membrane tethering complexes, HOPS (homotypic fusion and vacuole protein sorting) and CORVET (class C core vacuole/endosome tethering) [153], [170]. These four subunits are shared between both complexes. Additionally, CORVET has two Rab5-binding subunits (Vps3, Vps8), which act along with the core complex to promote endosome-endosome fusion [153]. On the other hand, HOPS has two Rab7-binding subunits (Vps39, Vps41) that aid in endosome-vacuole fusion along with the core subunits [153].

In the fishing approach with yeast lysates having knockdown in SEC18, three of the four SM family of proteins (Vps45, Sec1, Sly1) co-purified with PrD-GFP transport intermediates (Refer FIGURE 12B). Except for Vps45, which was highly enriched in the transport intermediates of PrD-GFP in SEC18 knockdown strain compared to its negative control (-Auxin) (Refer FIGURE 12B), all others co-purified only in traces. The fourth SM family member, Vps33, did not co-purify with PrD-GFP aggregates in any of the mass spectrometry runs. However, Vps33 was identified as a hit along with other components of HOPS/CORVET (Vps8 and Vps41) in a similar genome-wide screen for genes that are defective in the sequestration of heat-induced Hsp104-GFP aggregates into perivacuolar inclusions, which the authors interpreted as the IPOD [139]. Hence, it was decided to evaluate if deletion of members of SM family of proteins (Vps45, Vps33), which play a key role in SNARE-mediated membrane fusion events, or deletion of components involved in HOPS/CORVET complexes (Vps33, Vps8, Vps41) affect the recruitment of amyloid aggregates to the IPOD. To test this, [*PSI*$^{+}$] strains expressing PrD-GFP under control of a galactose inducible promoter and having a deletion in either of the following genes (*VPS45, VPS33, VPS41,VPS8)* were generated and induced with galactose for

6 hours along with their wild-type (wt) counterparts (no deletion). Post this, cells were fixed with PFA, and the aggregation pattern of PrD-GFP was visualized using fluorescence microscopy. In the control, more than 95% of the cells showed one single large PrD-GFP dot/IPOD (FIGURE 17A-D) as formerly described [59]. In contrast, 55 % and 65% of the cells showed multiple PrD-GFP foci upon deletion of *VPS45* and *VPS33*, respectively (FIGURE 17C). Compared to them, deletion of *VPS41* resulted in mild recruitment defects with only 27% of the cells having multiple PrD-GFP foci compared to the wild-type (wt) control, while *vps8Δ* strains showed no visible recruitment defects, as more than 90% of the cells showed one single large PrD-GFP dot/IPOD (FIGURE 17B,D) similar to the wt (FIGURE 17B, left panel). These results indicate the involvement of Vps45 and Vps33 in the recruitment of PrD-GFP aggregates to the IPOD. Furthermore, they also show that disturbance of components involved either in SNARE-mediated membrane fusion events or different steps in vesicle trafficking via the endosomal pathway to the vacuole affects the recruitment of PrD-GFP to the IPOD. However, it is unclear if these components are directly involved or if their deletion results in an imbalance or collapse of vesicle-mediated transport machinery in the cell in general, resulting in the observed defects.

Just like Mon2, the recruitment defect observed for Vps45 was achieved by a complete knock-out of these non-essential proteins. Therefore, testing the reversibility of VPS45 deletion was technically not possible in the same KO strain, but potentially only in a new strain where Vps45 protein levels can be depleted with the same auxin-aid strategy used for Dop1 depletion. However, like Mon2 (refer FIGURE 15C,F), auxin-based depletion of Vps45 resulted in a milder phenotype with only about 30% of the cells expressing multiple PrD-GFP foci compared to the strong phenotype observed with the full knock out strain (compare FIGURE 17C and 17F). Although the results from western blotting revealed a pretty good degree of depletion of Vps45, the weaker phenotype as compared to the complete KO strain suggests that the depletion was likely not complete, although below the detection level of the antibody (FIGURE 17G).

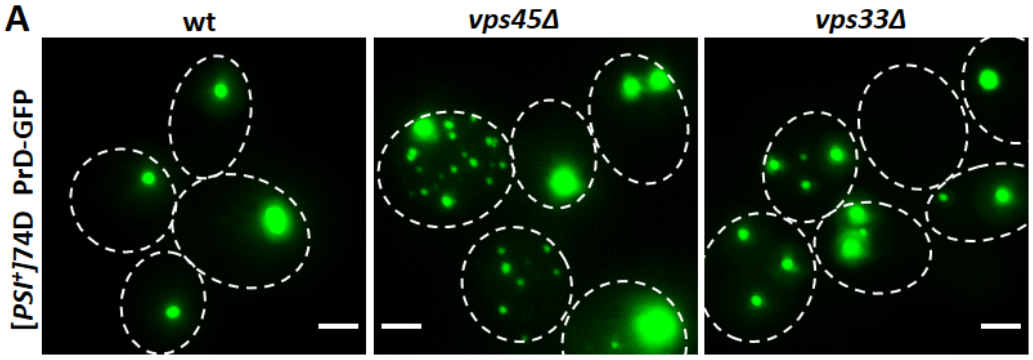
A
wt
vps45Δ
vps33Δ
[PSI+]74D PrD-GFP

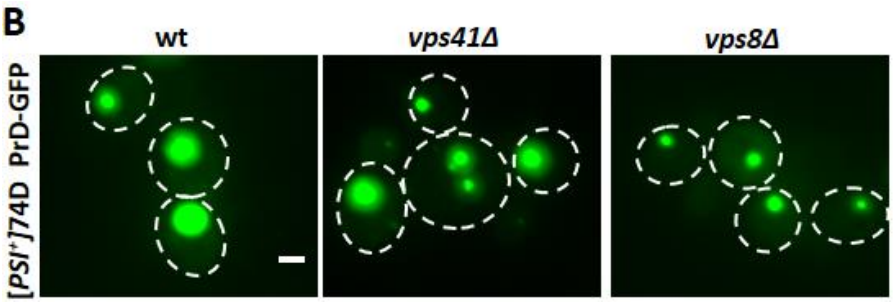
B
wt
vps41Δ
vps8Δ
[PSI+]74D PrD-GFP

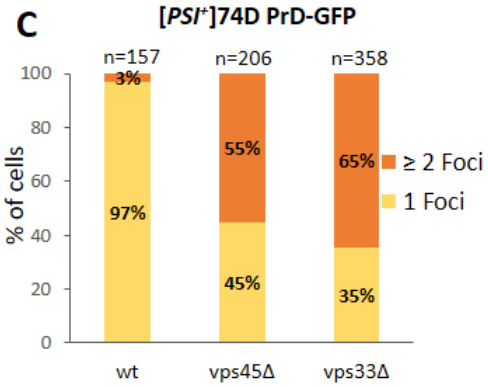
C
[PSI+]74D PrD-GFP
n=157
n=206
n=358
3%
55%
65%
97%
45%
35%
% of cells
≥ 2 Foci
1 Foci
wt
vps45Δ
vps33Δ

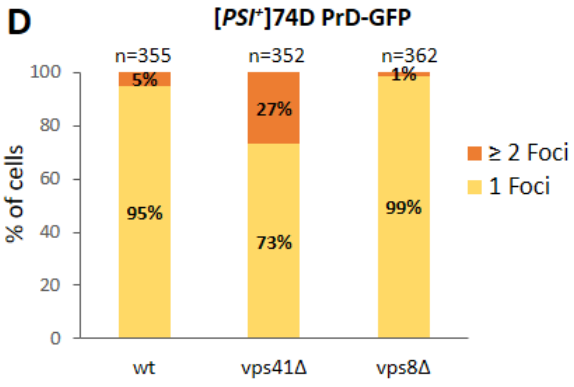
D
[PSI+]74D PrD-GFP
n=355
n=352
n=362
5%
27%
1%
95%
73%
99%
% of cells
≥ 2 Foci
1 Foci
wt
vps41Δ
vps8Δ

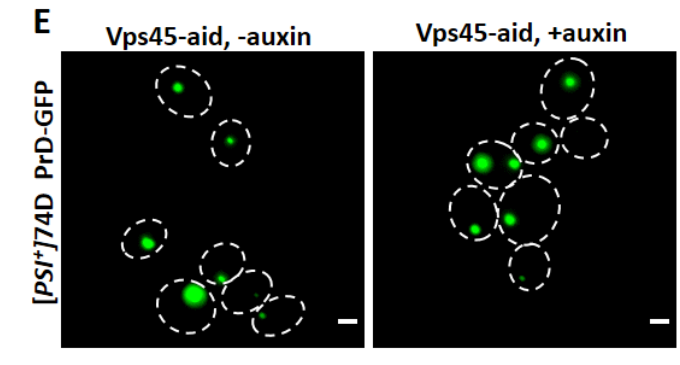
E
Vps45-aid, -auxin
Vps45-aid, +auxin
[PSI+]74D PrD-GFP

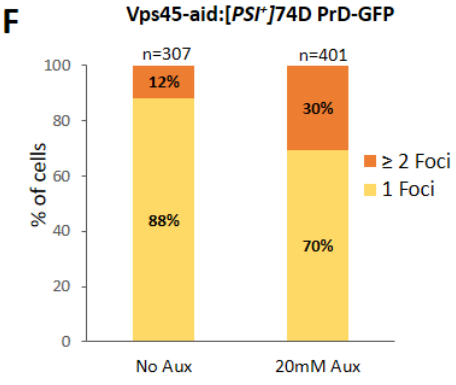
F
Vps45-aid:[PSI+]74D PrD-GFP
n=307
n=401
12%
30%
88%
70%
% of cells
≥ 2 Foci
1 Foci
No Aux
20mM Aux

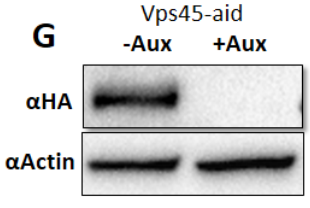
G
Vps45-aid
-Aux
+Aux
αHA
αActin

FIGURE 17: Vps33 and Vps45 are essential for the proper recruitment of PrD-GFP to the IPOD. A) PrD-GFP was integrated into the genome (under control of the Gal1 promoter) and induced with galactose for 6 hours in a [*PSI*$^{+}$] wild-type (wt) strain (left panel) or strains having a deletion in VPS45(middle panel) or VPS33(right panel). Cells were fixed with 4 % PFA and subjected to microscopy analysis. Images were acquired with a 100X objective and Z stacks with a step width of 0.2µm, overlayed as maximum intensity projection and processed using Image J software. B) PrD-GFP was integrated into the genome (under control of the Gal1 promoter) and induced with galactose for 6 hours in a [*PSI*$^{+}$] wild-type (wt) strain (left panel) or strains having a deletion in VPS41 (middle panel) or VPS8 (right panel). Cells were fixed with 4 % PFA and subjected to microscopy analysis. Images were obtained with a 63X objective and Z stacks with a step width of 0.2µm, overlayed as maximum intensity projection and processed using Image J software. C, D) Quantification of PrD-GFP foci upon deletion of VPS45, VPS33 compared to wt control (C) or VPS41, VPS8 compared to their corresponding wt control strain (D). E) PrD-GFP was induced with galactose for 6 hours in a [*PSI*$^{+}$] wild-type strain carrying PrD-GFP (under control of the Gal1 promoter) with a C-terminal aid tag in VPS45 in the absence or presence of 20 mM of auxin as indicated. F) Quantification of PrD-GFP foci upon depletion of Vps45 with 20mM auxin compared to the control, without auxin. G) Western blotting of the Vps45-aid strain after auxin treatment compared to the negative control, without auxin, with an antibody against an HA-tag present in the aid tag. An anti-actin antibody served as loading control. Frequencies of cells with 1 single IPOD focus or ≥2 foci are given in %. The total number of cells counted is denoted by n. Scale bar, 2 µm.

3.8 Vps33 is essential for the proper recruitment of Rnq1 amyloid aggregates at the IPOD

Vps33 is a core subunit of both CORVET (class C core vacuole/endosome tethering) and HOPS (homotypic fusion and vacuole protein sorting) tethering complexes, as well as a member of the Sec1/Munc18 (SM) family of proteins which play a key role in vesicle-mediated processes in the cell [153], [169], [170]. In the current experimental setup, deletion of VPS33 resulted in recruitment defects of model amyloid PrD-GFP to the IPOD (Refer FIGURE 17A,C). In order to evaluate if deletion of VPS33 also results in recruitment defects of other additional bonafide IPOD substrates such as the amyloid-forming protein Rnq1, to the IPOD, a similar experiment was conducted by introducing *vps33Δ* into yeast cells expressing a galactose inducible Rnq1-YFP construct instead of PrD-GFP. In brief, the corresponding IPOD substrate was induced with galactose for 6 hours in a [*PSI*$^{+}$] *vps33Δ* strain or a wild-type (wt) control strain (no VPS33 deletion). Subsequently, these cultures were fixed with 4% PFA and subjected to microscopy analysis. An Rnq1-YFP strain with a deletion in VPS33 displayed multiple foci phenotype in 66% of the cells compared to its wt counterpart (no VPS33 deletion), which displayed one single IPOD in more than 90% of the cells (FIGURE 18A,B). These results were similar to the effects observed with strains expressing PrD-GFP and having

a deletion in VPS33 gene (FIGURE 17A,C), indicating that deletion of VPS33 affected the recruitment of amyloid aggregates in general and is not specific to one particular amyloid substrate.

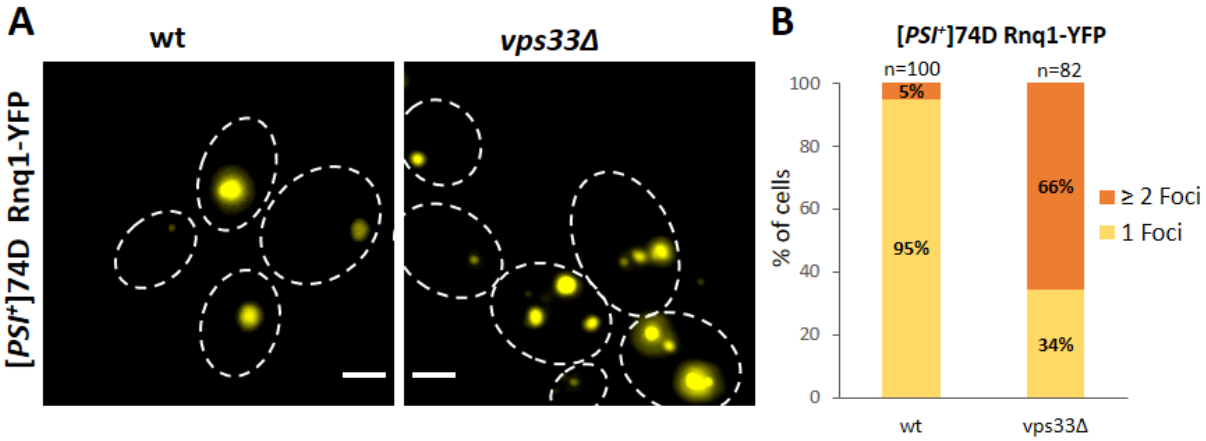

FIGURE 18: Vps33 is also essential for proper accumulation of the amyloid substrate Rnq1 at the IPOD. A) Knockout of VPS33 in a yeast strain expressing Rnq1-YFP (integrated into genome under control of the Gal1 promoter) and induced with galactose for 6 hours (right panel) compared to the wild-type (wt) control strain (left panel). Cultures were fixed with 4 % PFA and subjected to microscopy analysis. Images were acquired with a 100X objective and Z stacks with a step width of 0.2µm, overlayed as maximum intensity projection and processed using Image J software B) Quantification of Rnq1-YFP foci upon deletion of VPS33 compared to wild-type control (wt). Frequencies of cells with 1 single IPOD focus or ≥2 foci are given in %. The total number of cells counted is denoted by n. Scale bar, 2 µm.

3.1 Cop1 is essential for the proper recruitment of PrD-GFP to the IPOD

In the large-scale approach to pull up the transport intermediates of PrD-GFP generated in a *vps1Δ* strain, five of the seven subunits (Cop1, Sec21, Sec27, Sec26, Ret2) required to form the coatomer coat of COPI vesicles co-purified with PrD-GFP aggregates (Refer FIGURE8A). COPI vesicles mediate retrograde transport of proteins from the Golgi to the endoplasmic reticulum (ER) and also intra-Golgi trafficking [150], [171], [172]. Except for Cop1, the alpha subunit of the coatomer complex, all other subunits (Sec21, Sec27, Sec26, Ret2) co-purified in traces and appeared at the bottom of the list (not shown in FIGURE 8A). Subsequently, in the second mass spectrometry run with yeast lysates having knockdown in SEC18, Cop1 along

with another coatomer subunit Sec27, co-purified with the transport intermediates of PrD-GFP, again in traces. Furthermore, Sec21, a previously known confirmed hit of the recruitment pathway, is also a subunit of the COPI vesicle coatomer complex [136], [150], [172]. Hence, it was decided to investigate the possible role of COPI vesicles in the recruitment of PrD-GFP aggregates to the IPOD by depleting some of the subunits of the coatomer complex (Sec28, Sec27, Cop1). Deletion of SEC28 showed no visible recruitment defects of PrD-GFP to the IPOD, as more than 90% of the cells displayed one single focus of PrD-GFP similar to its wild-type (wt) control (no SEC28 deletion) (Ref FIGURE 6A,B). As both Cop1 and Sec27 are essential proteins, their depletion was achieved by the auxin aid method for the degradation of essential proteins, similar to Dop2 protein [162]. In brief, PrD-GFP was induced in galactose-based media for 6 hours in the absence or presence of auxin post which cells were fixed with PFA and visualized by fluorescence microscopy. About 38% of the cells showed a multiple PrD-GFP foci phenotype upon depletion of Cop1 compared to the wild-type (wt) control (no auxin treatment, no Cop1 depletion), where more than 90% of the cells displayed PrD-GFP aggregates with one IPOD like foci (FIGURE 19A,B). However, depletion of Sec27 in the current experimental setup did not show visible recruitment defects as more than 85% of the cells displayed PrD-GFP aggregates with one IPOD like focus similar to the wild-type (wt) control (FIGURE 19C,D). Surprisingly, these results suggested that Cop1, but not Sec28, is involved in the recruitment of PrD-GFP to the IPOD. With respect to Sec27, it can be concluded that either it is not involved in the recruitment process or the depletion levels of this protein by the auxin-aid method were too incomplete to observe any effect (FIGURE 19F).

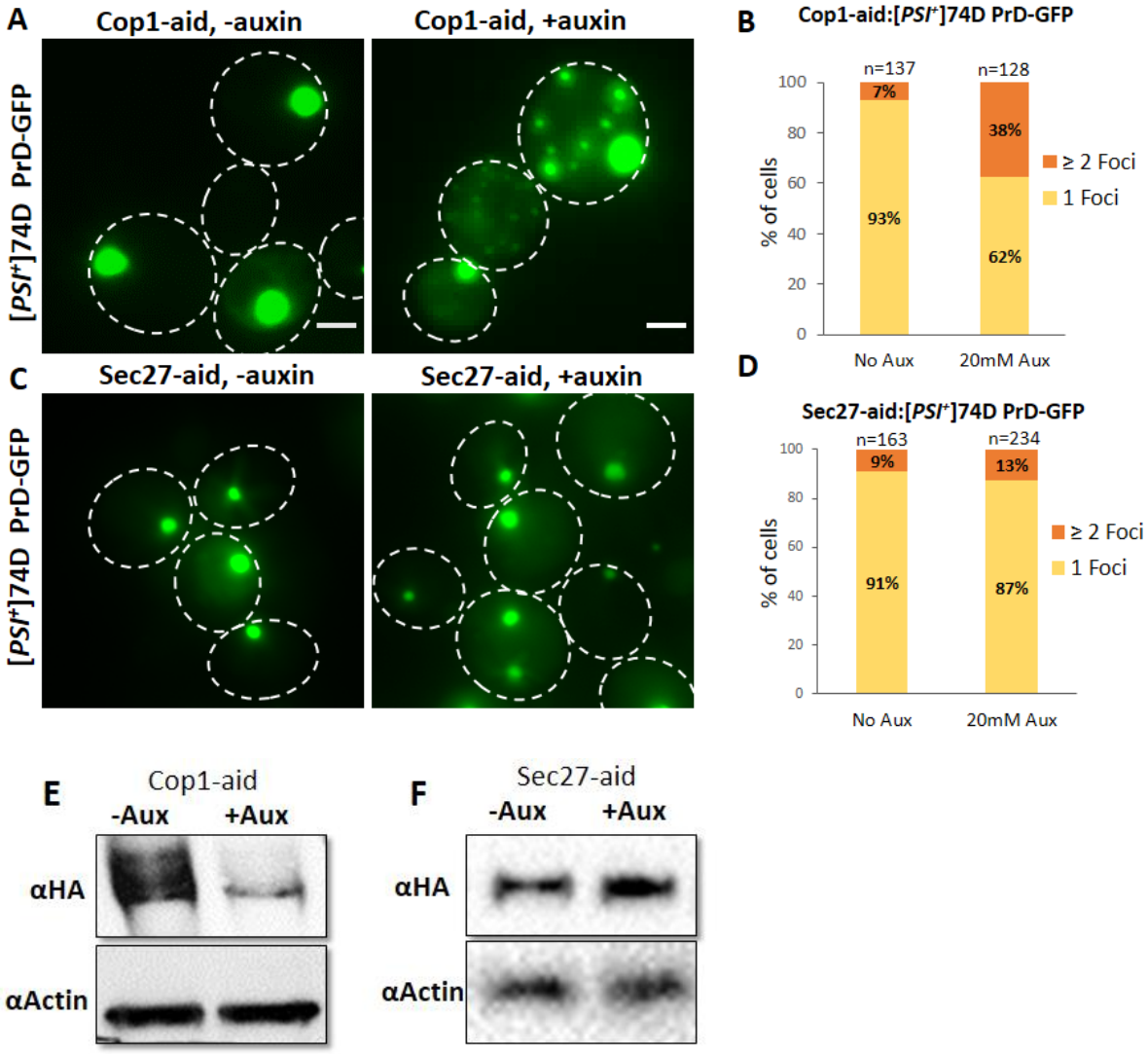

FIGURE 19: Depletion of Cop1 affects the proper recruitment of PrD-GFP to the IPOD. A,C) PrD-GFP was induced with galactose for 6 hours in a [*PSI*$^+$] wild-type strain with a C-terminal aid tag in COP1 (A), or SEC27 (C) in the absence or presence of 20 mM of auxin as indicated. Cells were fixed with 4 % PFA and subjected to microscopy analysis. Images were acquired with a 100X objective and Z stacks with a step width of 0.2µm, overlayed as maximum intensity projection and processed using Image J software. B, D) Quantification of PrD-GFP foci upon depletion of Cop1 (B) or Sec27 (D) with 20mM auxin compared to the control, without auxin. E, F) Western blotting analysis of the Cop1-aid strain (E), Sec27-aid strain (F) treated with/without auxin (+/-Aux) with an antibody against an HA-tag present in the aid-tag. An anti-actin antibody served as loading control. Frequencies of cells with 1 single focus or ≥2 foci are given in %. n refers to the total number of cells counted. Scale bar, 2 µm.

3.2 Co-localization of Cop1 and Vps33 with the transport intermediates of PrD-GFP in *mon2Δ* strain

The results so far indicated that deletion/depletion of Mon2, Dop1, Cop1, Vps33, and Vps45 result in recruitment defects of PrD-GFP to the IPOD. In order to evaluate if these observed recruitment defects are due to direct interaction of these components with PrD-GFP aggregates or due to indirect effects (impairment of the entire vesicular transport machinery in the cell) caused by their deletion/depletion, *in vivo* co-localization experiments were performed. For this, Cop1 and Vps33 were chosen as candidates. This is because Cop1 is one of the main components of COPI vesicles which regulate the transport of cargo between Golgi and the Endoplasmic Reticulum, while Vps33 plays a key role in the late endosomal pathway, especially in vesicle-mediated delivery of substrates to the vacuole [150], [153], [169], [170]. Hence it would be interesting to know if the PrD-GFP utilizes COPI vesicles or/and the endosomal pathway components to reach the IPOD, which is close to the vacuole. To test this, endogenous COP1 and VPS33 were labelled with 3x-mCherry tag and 1x-mcherry tag respectively and introduced into the previously used [*PSI*$^{+}$] *mon2Δ* strain expressing galactose-inducible PrD-GFP and resulting in a multiple dot phenotype. PrD-GFP was induced with galactose for 6 hours post which cells were fixed with PFA and analyzed by fluorescence microscopy in the GFP and mCherry channels. About 20% of the single PrD-GFP IPODs showed co-localization with at least one of the multiple foci representing the pool of Cop1 3x-mCherry (FIGURE 20A, upper panel). Upon *MON2* deletion, multiple foci of PrD-GFP were observed, as expected, which co-localized in 33.6% of the cases with at least one of the multiple foci representing the pool of Cop1 3x-mCherry (FIGURE 20A, lower panel). In the case of Vps33, about 10.6% of the single PrD-GFP IPODs showed co-localization with at least one of the multiple foci of Vps33 1x-mCherry (FIGURE 20B, upper panel). *MON2* deletion in this strain resulted in multiple aggregates of PrD-GFP foci, as expected, which co-localized with at least one of the multiple foci of Vps33 1x-mCherry in about 50.72% of cases (FIGURE 20B, lower panel). The initial results of Vps33 co-localization experiments are positive and need to be validated further.

From these results, it can be concluded that both Cop1, as well as Vps33, are present in the transport intermediates of PrD-GFP as well as play a role in their recruitment to the IPOD

(Refer FIGURES 17A, 17C, 19A, 19B, 20A, 20B). The reason why Cop1 depletion resulted in mild recruitment defects (FIGURE 19A,B), as well as co-localization of Cop1 only in a subset of transport intermediates (FIGURE 20A), generated in a *mon2Δ* strain, is unclear. It's possible that the interaction of Cop1 with the PrD-GFP could be transient in nature, and the observed recruitment defects in Cop1 depletion are more due to indirect effects. On the other hand, deletion of VPS33 showed strong recruitments defects of PrD-GFP to the IPOD, which correlated with strong co-localization of Vps33 with transport intermediates generated in a *mon2Δ* strain (Refer FIGURES 17A, 17C, 20B). Hence, the effects observed by Vps33 are most likely due to its direct interaction with PrD-GFP, although indirect effects can still not be ruled out. In general, the current results clearly hint that disturbing vesicle-based transport pathways in a cell affect the recruitment of PrD-GFP to the IPOD. The evidence so far favours the endosomal pathway to be more likely involved in the recruitment process and have direct interaction with PrD-GFP aggregates compared to COPI vesicles.

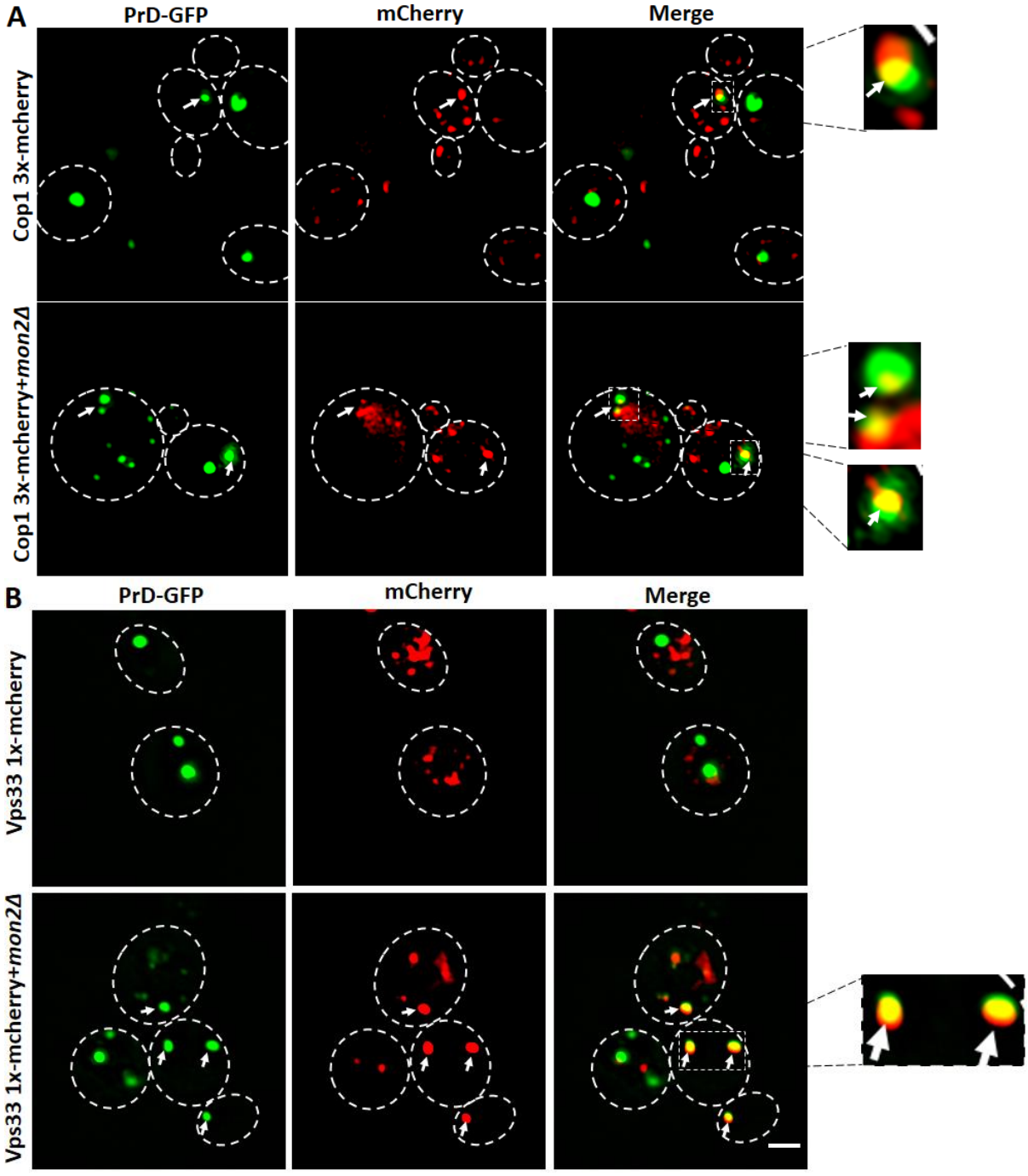

FIGURE 20: Co-localization of Cop1 3x-mcherry and Vps33 1x-mcherry with PrD-GFP foci. A) PrD-GFP was induced with galactose for 6 hours in a [*PSI*$^{+}$] *mon2Δ* strain with a C-terminal 3x-mCherry tag in the endogenous COP1 gene. The same strain in the absence of the *MON2* knockout served as a negative control. Cells were fixed with PFA and analyzed by fluorescence microscopy in the GFP and mCherry channels. Co-localization of existing PrD-GFP foci with at least 1 Cop1 3x-mCherry focus: WT: 20 %, n=224 foci; *+ mon2Δ*: 33.6 %, n=205 foci. B) PrD-GFP was induced with galactose for 6 hours in a [*PSI*$^{+}$] *mon2Δ* strain with a C terminal 1x-mCherry tag in the endogenous VPS33 gene. The same strain in the absence of the *MON2* knockout served as a negative control. Co-localization of existing PrD-GFP foci with at least 1 Vps33 1x-mCherry focus: WT: 10.6 %, n=113 foci; *+ mon2Δ*: 50.72 %, n=416 foci. Scale bar, 2 µm.

4 Discussion and Outlook

In the current study, we show that amyloid aggregates hitchhike to the IPOD by utilizing components of endomembrane trafficking pathways. This is based on the results obtained through *in vivo* depletion of candidates of interest as well as co-localization studies to visualize interactions. Mutants defective for the Golgi to vacuole transport pathway via endosomes (Cop1, Mon2, Dop1, Vps45, Vps33) failed to recruit our model amyloid substrate PrD-GFP to the IPOD but rather accumulated them as multiple aggregates dispersed throughout the cell (Refer FIGURES 14, 17, 19). Furthermore, using one of our candidates, Dop1, as an example we show that these multiple aggregates are indeed transport intermediates of the recruitment pathway, as replenishment of Dop1 in Dop1 depleted cells caused these multiple aggregates to refuse into one central IPOD (Refer FIGURE 15A,G). We also show that the key candidates reported here are not only limited to the recruitment of our model substrate, PrD-GFP, to the IPOD, but are involved in the recruitment of amyloid substrates to the IPOD in general (Refer FIGURES 16,18). Lastly, we conclude that the current results are not only in line with previously reported literature ([130], [136], [139], [140], [142], [144]) on aggregate sorting to the IPOD, but we have also narrowed down the endosomal pathway to be the key vesicular pathway utilized by amyloid aggregates to reach its destination, the IPOD.

4.1 Deletion of Atg9 or components of Atg9 vesicle type did not affect the recruitment of PrD-GFP to the IPOD

Previous results from our lab indicated that the recruitment machinery of amyloid aggregates to the IPOD mirrored with the faithful recruitment of the Cvt pathway substrate, preApe1 to the PAS (Phagophore assembly site) and is dependent on the actin cytoskeleton and vesicle based transport of cargo [112], [136]. As preApe1 is delivered to the PAS via a group of mobile cytoplasmic vesicles called Atg9 vesicles that move along actin cables to reach its destination, it was hypothesized that PrD-GFP aggregates hitchhike on these Atg9 vesicles to reach IPOD, located close to the PAS [104], [112], [136], [140]. In the current study, we tested this

hypothesis by evaluating the effects of depletion of Atg9 or other components crucial for this pathway in the recruitment of PrD-GFP to the IPOD. Surprisingly, deletion of neither Atg9 nor its adaptor protein Atg11 nor other components of Atg9 vesicle (Trs85, Atg23, Atg27) affected the recruitment of our model amyloid substrate to the IPOD (Refer FIGURE 5A,B). In all these mutants, PrD-GFP formed one focus and failed to show visible recruitment defects (Refer FIGURE 5A). On further analysis, we found that this was also the case for Cvt substrate, preApe1, which formed one focus in the null mutants of ATG9, ATG11, TRS85 as well as its receptor ATG19, indicating the successful formation and assembly of the preApe1 complex in these mutants [100]. However, the complex was no longer targeted to the PAS but mislocalized, as revealed by FM464 vacuolar rim staining [100]. As the IPOD is located close to the vacuole, we performed a similar FM464 vacuolar rim staining to evaluate if the single foci of PrD-GFP obtained in the *atg9Δ* and *atg11Δ* strains are mislocalized. In our experiments, we observed mild targeting errors of PrD-GFP from the IPOD in *atg9Δ* and *atg11Δ* strains, which were also in the range of mistargeting reported for preApe1 from the PAS in the literature for null mutants of ATG9 and ATG11 (Refer FIGURE 5C,E). Surprisingly, even our wild-type (wt) control strain (having no mutation in Atg9 or Atg11) showed comparable mislocalization of PrD-GFP from the IPOD (Refer FIGURE 5C,E). As these results were unexpected and the original publication where preApe1 mistargeting experiments were described did not reveal images of their control strain to our knowledge [100], we performed our own experiments to evaluate mistargeting of preApe1 from the PAS in *atg9Δ* strain along with the corresponding wild type control (no deletion). Similar to the results with PrD-GFP, we observed mild mistargeting defects of preApe1 from the PAS in null mutants of ATG9 similar to what was reported in the literature, but also in the wild-type (wt) control strain (Refer FIGURE 5D,F). Based on our results it seems unlikely that Atg9 vesicles are the vesicle type that transport amyloid aggregates to the IPOD. However, the literature providing evidence for the transport of preApe1 to the PAS via Atg9 vesicles is also incomplete and warrants further investigation [87], [100], [102]–[106], [155], [173].

4.2 Potential role of Vid vesicles in the recruitment pathway

Since our results were inconclusive about the involvement of Atg9 vesicles in the recruitment machinery, we focussed on evaluating other vesicular pathways that deliver substrates to the vacuole. Sec21, a previously confirmed positive hit of the recruitment machinery, is a component of the VID (Vacuole Import and Degradation) pathway that delivers FBPase (Fructose 1,6-bisphosphatase) and other gluconeogenic enzymes to the vacuole for degradation via specialized vesicles called 'Vid' vesicles [149], [151], [152], [158]. Therefore, additional components of this pathway were tested next for their possible involvement in PrD-GFP recruitment [149], [151]. Of all the 7 components tested for the Vid pathway in our experiments, only null mutants of UBC1 showed mild recruitment defects of PrD-GFP to the IPOD (Refer FIGURE 6). UBC1 is an E2 Ubiquitin-conjugating enzyme in yeast that plays a role in ubiquitin-mediated protein turnover and degradation. In the Vid pathway, Ubc1 aids in the biogenesis of Vid vesicles by the formation of polyubiquitination chains [152]. As we observed recruitment defects of PrD-GFP to the IPOD only with null mutants of UBC1 and not with the other key components of Vid pathway, we conclude that Vid vesicles are not involved in the transport of amyloid aggregates to the IPOD and the recruitment defects observed by the deletion of UBC1 were either probably due to its function outside of the Vid pathway or due to indirect effects of gene deletion.

4.3 Large Scale approach to identify the vesicular pathways involved in the recruitment of PrD-GFP aggregates to the IPOD

After testing components from two different vesicle-mediated pathways, we realized the need for an unbiased large-scale approach to narrow down the large category of vesicle trafficking related genes to particular molecular pathways that might be involved in the recruitment process. In the current study, we successfully set up and characterized a proteomics-based screen to isolate the transport intermediates of PrD-GFP generated in a yeast strain defective for the dynamin like small GTPase, Vps1 and to identify components co-

purifying with those transport intermediates (Refer FIGURE 7). The aim was to enrich components of the recruitment machinery. The method itself was sufficient to co-purify previously confirmed proteins of the recruitment pathway, known interactors of PrD, as well as interesting candidates involved in actin-based transport of cargo and vesicular transport (Refer FIGURE 8). However, such candidates that are functionally relevant to the recruitment pathway (referred to as “relevant candidates” in the dissertation) co-purified only in traces compared to other proteins that co-purified in much larger quantities, have no plausible relation to the recruitment process, and belong to the functional groups of proteasomal subunits, metabolic enzymes, and ribosomal subunits (referred to as “background” collectively in the dissertation). On the one hand, both proteasomal as well as ribosomal subunits are highly abundant proteins in yeast and are often co-purifying as background in various large-scale studies [130], [139], [174]. On the other hand, it is known that under conditions of carbon exhaustion, proteasomal subunits in a cell can be stored into reversible assemblies termed PSGs (Proteasome storage granules), which transiently co-localize with the IPOD [133], [134]. The IPOD was also reported to be the hub for damaged/dysfunctional proteasomes before they can be degraded by the cell via proteaphagy [134]. This opens the possibility that such proteasomal subunits were en route to the IPOD and accumulated into the same assemblies containing PrD-GFP transport intermediates. However, this possibility needs to be further confirmed to exclude non-specific co-purification with PrD-GFP aggregates. Like proteasomal subunits, even metabolic enzymes in the cell can be stored into reversible complexes which readily assemble/disassemble depending on cellular needs and the presence/absence of various metabolites [175], [176]. Such complexes can be isolated by ultracentrifugation, where they were found to be highly enriched in the pellet fraction [175]. As our sample preparation step also included ultracentrifugation with the objective to enrich the pellet fraction with the transport intermediates of PrD-GFP, its plausible that we also have pelleted other insoluble components such as these assemblies of metabolic enzymes, proteasomes, ribosomes, and other aggregates, and triggered post centrifugation interactions between them, resulting in the observed increased background (Refer FIGURE 10). In general, the isolation of amyloid aggregates may attract a lot of non-specific post-lysis interactions due to their sticky nature. This is one of the major limitations observed while working with aggregates.

In order to further optimize the sample preparation steps and to reduce this kind of possible background, we decided to omit the ultracentrifugation step and use the entire soluble fraction of yeast lysates (S1) for future experiments. As we observed relevant candidates only in traces, we evaluated if we could eliminate the use of detergent in our experiments to ensure the preservation of all *in vivo* interactions. However, in our experimental setup, the absence of detergent resulted in massive non-specific binding to the GFP binder and was counterproductive rather than helpful (Refer FIGURE 9). Therefore, we cross-linked yeast lysates prior to detergent treatment as a final attempt to preserve possible transient or detergent-sensitive *in vivo* interactions (Refer FIGURE 11). Post the above-mentioned optimization of sample preparation steps, we repeated the large scale approach with yeast lysates having a knockdown in SEC18 instead of *vps1Δ* strain for the following reasons:

1) The multiple PrD-GFP aggregates observed in Sec18 knockdown strains were shown to be true transport intermediates as they were still able to fuse with the IPOD when the depletion of Sec18 was eased by the removal of auxin [136]. However, this reversibility of depletion was not possible for the multiple aggregates observed in a strain having a complete knockout of the endogenous VPS1 gene. Although unlikely, it's possible that the multiple PrD-GFP aggregates observed in the *vps1Δ* strain were no true transport intermediates.

2) Auxin based depletion of a protein may cause less non-specific effects to the strains compared to complete knockouts due to the transient and inducible nature of the depletion [162].

Although the second mass spectrometry run with lysates from yeast cells having a knockdown of SEC18 picked up more interesting candidates belonging to vesicle-mediated transport, there was still a lot of background, and the use of cross-linker did not reduce the background or improve the enrichment of functionally relevant candidates (Refer FIGURE 12). Thus, either the chosen cross-linker was unable to cross-link PrD-GFP with putative detergent sensitive interaction partners, or the postulated interactions of PrD-GFP with components of the recruitment machinery were too transient in nature to be captured by this isolation approach.

To conclude, in the current study, we developed and optimized a novel protocol for the isolation of transport intermediates of amyloid aggregates en route to the IPOD. The approach itself was able to pick up candidates involved in the recruitment pathway based on the observation that their depletion disrupted faithful recruitment of PrD-GFP to the IPOD, but their enrichment over possible non-specific/post-lysis interactors was not strong enough to allow for easy identification of possible transport factors. Furthermore, there is an overlay between many of the candidates obtained with both *vps1Δ* strain and SEC18 knockdown strain with identified candidates from other genome-wide screening studies related to aggregate sorting in the literature [130], [139], [142], [144], [177]. However, such an approach had two major limitations: Abundant enrichment of proteins with no plausible relation to the recruitment pathway or transport processes in general (ribosomal genes, glycolysis, cell wall proteins, others) and lower enrichment of relevant candidates (components of the actin cytoskeleton, endosomal transport or vesicle-mediated processes) [130], [136], [139]. Reasons for this could be of technical or biological nature. Technical reasons include post lysis interactions resulting in abundant enrichment of proteins that are not interacting/associating with PrD-GFP *in vivo*, while biological reasons could be that the interactions of PrD-GFP with its molecular partners are too transient in nature or sensitive to the lysis conditions to be captured by this method. Hence, the method is not as straightforward and sensitive as expected but rather warrant further additional testing to differentiate the background from the candidates involved in the recruitment processes.

4.4 Involvement of Cop1 in the recruitment of PrD-GFP aggregates to the IPOD

Vesicle coat proteins such as clathrin, coat protein complex II, and I (COPII and COPI, respectively) enable vesicle formation as well as aid in the selection of cargo to be packaged within them [171]. Cop1 is the alpha subunit of the heptameric coatomer (Sec27, Sec28, Cop1, Sec21, Sec26, Ret2, Ret3) complex, which coats COPI vesicles [150]. COPI vesicles function in the retrograde transport of proteins from the Golgi to the ER and within Golgi cisternae [150], [161], [172]. In the current study, we noticed mild recruitment defects of PrD-GFP to the IPOD upon Cop1 depletion (Refer FIGURE 19A,B). Furthermore, we observed co-purification of 5 of

the 7 coatomer subunits with the PrD-GFP aggregates in the immunoprecipitation experiments. Sec21, a previously characterized putative component of the recruitment machinery, is also a subunit of the coatomer complex of COPI vesicles [136], [150], [171], [178], [179]. Based on these observations, we wondered if COPI vesicles are involved in transporting amyloid aggregates to the IPOD. Hence, in the follow-up experiments, we tested the effect of deletion/depletion of two other subunits of the coatomer complex, Sec27, and Sec28 on amyloid recruitment to the IPOD (Refer FIGURES 19C, 19D, 6A, 6B). Surprisingly, none of the other tested subunits (Sec27, Sec28) showed recruitment defects in our study. The remaining three subunits (Sec26, Ret2, Ret3) were not tested due to time constraints. If COPI vesicles transport amyloid aggregates to the IPOD, then mutants defective for either of the 7 subunits of the coatomer should show recruitment defects, as all the seven subunits are required for COPI vesicle function [150], [179]–[184]. Since we did not observe this, we wondered if there exist other functions for the specific subunits Cop1 and Sec21, outside of COPI vesicle trafficking, and if the impairment of the aforementioned functions of these proteins leads to the observed defects in sequestration of amyloid aggregates at the IPOD. Sec21 is functional in the Vid pathway, which has been tested previously (Refer FIGURE 6). Interestingly, three of the coatomer subunits (Cop1, Sec27, Sec28) have been reported to be functional in the endosomal transport pathway in both mammals as well as in yeast [154], [184]. The endosomal transport pathway delivers substrates to the vacuole via endosomes/MVB (multivesicular bodies) [185]. Mutants of SEC27, SEC28 as well as COP1 were reported to be defective for this pathway and accumulated late endosomes/MVBs [154], [184]. It's possible that the observed recruitment defects of PrD-GFP to the IPOD in Cop1 knockdown strains were due to defects in endosomal protein sorting. If this is indeed the case, then it's still not clear why depletion/deletion of Sec27 and Sec28, also with similar roles in endosomal trafficking, failed to show any visible recruitment defects (Refer FIGURES 6, 19). For Sec27, it can be argued that the degree of depletion of the protein by auxin was maybe insufficient to observe any effects (Refer FIGURE 19F). However, it is surprising why null mutants of SEC28 failed to show any recruitment defects. All these results contradict the involvement of COPI vesicles in the recruitment pathway but rather point to two different interpretations. Either the recruitment defects observed with Cop1 depletion are indirect effects caused by the depletion of an essential protein in the cell and have no relation with sequestration of amyloid aggregates at the IPOD. However, a recent genome-wide screen

identified COPI vesicle components to interact with heat-induced aggregates [130]. The second interpretation is that the Cop1 subunit has other unknown/novel functions distinct from what is described in the literature. The fact that the knowledge on COPI vesicle structure is still quite limited compared to COPII and clathrin-coated vesicles would support this possibility [186].

4.5 PrD-GFP aggregates utilize the components of the endosomal pathway to reach the IPOD

In the current study, we report a novel cellular recruitment machinery that is involved in the recruitment of different amyloid substrates to the IPOD (Insoluble PrOtein Deposit) in *S. cerevisiae*. This machinery is disturbed upon impairment of components involved in various stages of endosomal vacuolar transport such as Mon2, Dop1, Vps45, and Vps33 (Refer FIGURES 14,17). In the endosomal vacuolar pathway, cargo (soluble vacuolar hydrolases, integral membrane proteins, and other substrates) is transported from the trans-Golgi network (TGN) to the vacuole in carrier vesicles via an intermediate sorting compartment called the endosomes/MVB (multivesicular body) [171], [185], [187], [188]. Remarkably, we found that amyloid aggregates use components of the endosomal pathway for their recruitment to the IPOD, located in close vicinity to the vacuole. Null mutants of MON2 are defective in the targeting of carboxypeptidase Y (CPY) to the vacuole [164], [165], [185], [187], [189]. Carboxypeptidase Y (CPY) is a soluble vacuolar hydrolase that is delivered to the vacuole via the endosomal pathway [185], [187]. Interestingly, MON2 null mutants also showed defects in the recruitment of PrD-GFP to the IPOD and accumulated them as multiple aggregates in the cytoplasm (Refer FIGURE 14). Mon2 has been reported to physically interact with Dop1, and the duo together regulates the trafficking of cargo between the Golgi and the endosomes[164], [165], [190], [191]. If Mon2 and Dop1 physically interact with one another and are functional in the same pathway, then depletion of Dop1 should also result in impairment of recruitment of PrD-GFP to the IPOD. We confirmed with our experiments that depletion of Dop1 indeed generated reversible transport intermediates of PrD-GFP aggregates as expected (Refer FIGURE 15A,G).

Fusion of Golgi-derived vesicles with the endosomes is dependent on the interaction between SNARE proteins and the SM proteins [166], [167], [192]. The SM family of proteins (Sly1, Sec1, Vps45, and Vps33) are indispensable for intracellular vesicle trafficking and confer specificity to membrane fusion events [166]–[169], [192]. Both Vps45 and Vps33 are reported to be present in a complex at the endosomes, along with the syntaxin Pep12, to regulate fusion of Golgi-derived vesicles [169], [192], [193]. Sec18, the SNARE disassembly chaperone and one of our previously confirmed positive hit of the recruitment pathway, also interacts with both Vps45 and Pep12 at endosomes [136], [194]. Whether a possible interaction also exists between Sec18 and Vps33 at the endosomes is unclear from the literature. Additionally, Vps33 is also functional at the vacuole where it interacts with syntaxin, Vam3 to promote the fusion of the endosomes with the vacuole, which is the final step in the endosomal pathway [153], [168]–[170], [192]. Similar to the results observed with MON2 deletion, null mutants of both VPS45 and VPS33 were defective in the targeting of carboxypeptidase Y (CPY) to the vacuole as well as our model substrate PrD-GFP to the IPOD (Refer FIGURE 17) [192], [195]. Furthermore, Vps33 co-localized with the multiple aggregates of PrD-GFP generated in MON2 deleted strain (Refer FIGURE 20B). Due to time constraints, the colocalization of the other three candidates (Mon2, Dop1, Vps45) with the transport intermediates of PrD-GFP could not be verified. However, the initial evidence provides proof of concept to hypothesize that amyloid aggregates are trafficked to the IPOD via the endosomal pathway similar to the transport of carboxypeptidase Y (CPY) to the vacuole. As we observe positive candidates to be involved in both early steps of Golgi to endosomal transport and inter-Golgi-transport pathways (Mon2, Dop1) as well as in later steps of endosomal to vacuole transport (Vps33 and Vps45), it's possible that the recruitment of aggregates to the IPOD is a multi-step process.

Recently, Nystrom and co-workers showed that endomembrane components are involved in the sequestration of heat-induced aggregates to a perivacuolar deposition site, the IPOD [130], [139], [144]. According to their model, misfolded proteins were reported to be recruited to the IPOD by utilizing components of the actin cytoskeleton (Myo2, Cmd1) as well as components involved in late endocytosis and endosome to vacuole transport (Vps1, Vps16, Vps39)[130], [139], [144]. In their experiments, it was not tested if amyloid aggregates also utilize this pathway to reach the IPOD. In fact, their results in this regard were inconclusive.

For instance, in the publication Hill *et al.* 2016, Vac17 was reported to be the adaptor protein essential for sequestering heat-induced aggregates to the IPOD. Interestingly, in the same study, deletion of Vac17 failed to affect sequestration of amyloid Huntington (Htt103Q) protein aggregates at the IPOD [130]. Kumar *et al.* 2016 showed that disturbance of actin cytoskeleton based transport components such as Myo2, Cmd1, Tpm1/2 impaired the recruitment of amyloid aggregates to the IPOD. Within the scope of this dissertation, we show that impairment of not only endosome to vacuole transport but also Golgi to endosome transport affects the sequestration of not only our model substrate, PrD-GFP, but amyloid aggregates in general (Refer FIGURES 16,18).

Further evidence for the involvement of the endosomal pathway in aggregate sorting is provided by studies performed with cytoplasmic aggregates of the nuclear RNA-binding protein, TDP43. Clearance of cytoplasmic TDP43 aggregates in yeast was impaired upon inhibition of components of the endolysosomal pathway but not of the autophagic pathway [196]. According to the authors, the autophagic pathway is required for the clearance of aggregates only in the absence of a functional endolysosomal pathway. Similar studies also exist in mammals where it is proposed that the autophagosomes fuse initially with the endosomes to form amphisomes before they merge with the lysosomes [197], [198].

A key question unanswered in all these studies is whether the aggregates are trafficked on the outside of endosomes or are internalized into the endosomes. For TDP43 aggregates, the authors consider both options as a possibility [196]. It's possible that PrD-GFP aggregates traffic on the exterior of these endosomes until they reach the vacuole, which is close to the IPOD, where they may be removed by unknown mechanisms. Alternatively, PrD-GFP aggregates may disrupt the endosomal pathway such that a hybrid endocytic compartment is formed, which may permit aggregate internalization via a novel mechanism. However, in this case, it's not clear how the aggregates would be unloaded from the endosomes and transported further to the IPOD. Further studies are required to understand the role played by the endomembrane systems in trafficking amyloid substrates to IPOD.

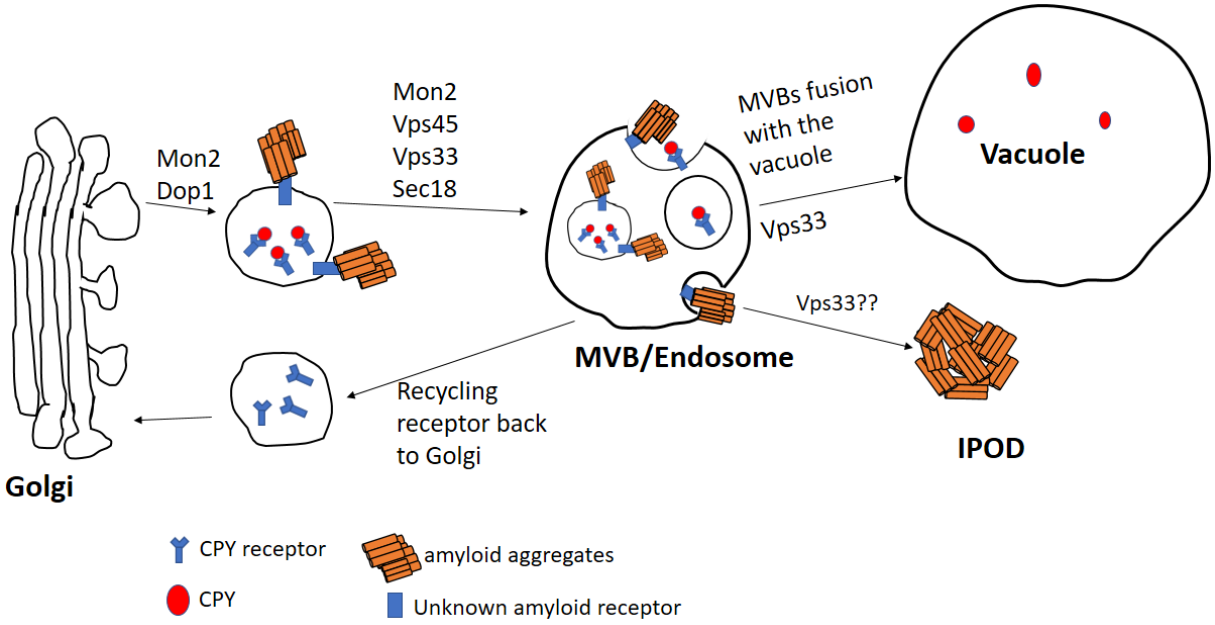

FIGURE 21: A model for the recruitment of PrD-GFP aggregates to the IPOD in yeast. PrD-GFP aggregates are recruited via an unknown receptor to the exterior of these Golgi-derived vesicles, which also transport vacuolar hydrolases such as Carboxypeptidase Y (CPY) from the Golgi network to the vacuole, located near the IPOD [185], [187]. CPY is transported along with its receptor protein Vps10 to the MVB/Endosome, from where the receptor is recycled back to the Golgi, and the CPY is delivered further to the vacuole. PrD-GFP aggregates utilize these carrier vesicles and the MVB to reach the vacuole, vicinity of the IPOD, from where they can integrate with other aggregates deposited there.

Outlook

In summary, we showed that prion aggregates are targeted to the IPOD by utilizing components of the endosomal vacuolar pathway, which transports cargo from the trans-Golgi network (TGN) to the vacuole via endosomes. However, it is not clear how PrD-GFP and other bona fide IPOD substrates are associated with the endosomes. Do they directly bind to the vesicular membrane itself or via specific receptor/adaptor proteins? Finding the linking factor between the endosomes and the aggregates will shed light on whether the interaction is direct or indirect in nature. We still need to verify if the multiple aggregates observed in MON2, VPS33, VPS45 null mutants are actual transport intermediates like those seen with Dop1 depletion by gene complementation studies. Some of the potential experiments that could shed more light on the recruitment machinery include:

1) Testing deletion of other known components of the endosomal transport pathway.

2) Visualizing the colocalization of Mon2, Vps45, and Dop1 as well as prominent markers of TGN and endosomes with transport intermediates of PrD-GFP.

3) Direct visualization of potential interaction of PrD-GFP foci with the endosomes in VPS45/VPS33 null mutants, with Correlative Light and Electron Microscopy (CLEM), would support the current model.

It would be interesting to know if PrD-GFP aggregates are also turned over by endosomal pathway as reported for cytoplasmic TDP43 aggregates in yeast [196]. To test this, we have to perform time-lapse imaging experiments and compare the kinetics of aggregate turnover in mutants defective in endomembrane trafficking with a wild-type strain. Finally, isolation of endosomes with the aggregates and their putative receptor, if possible, will offer the strongest evidence for our claims in the current study.

5 Materials and Methods

5.1 Materials

5.1.1 Software and Equipment

Computer Software

Image J	National Institutes of Health
Office365	Microsoft Corp.
Adobe Acrobat Reader DC	Adobe Systems Inc.
SnapGene Viewer	GSL Biotech
Excellence	Olympus Soft Imaging Solutions
Image Lab	Bio-Rad

Equipment

pH meter	Werner Hassa GmbH
Trans-Blot Turbo™	Bio-Rad
Agarose gel chambers and trays	University Hospital workshop
T-Gradient Thermocycler	Biometra GmbH
Spectrophotometer	Eppendorf
Magnetic stirrer MR 3001 K	Heidolph
SDS gel chambers	Bio-Rad
Vortex mixer	Heidolph
Incubators	Forma Thermo Scientific
Water bath MaxQ 7000	Dinkelberg analytics
Glass ware	Schott
Centrifuges	Heraeus
Weighing Balances	Mettler
Mixer mill MM 400	Retsch
ChemiDoc Imaging Systems	Bio-Rad

Microscopes

- **Olympus CellR-PointFRAP IX81 (ZMBH Imaging Facility)**

Microscope stand	Olympus IX81, inverted microscope, motorized stage
Objectives	PlanC N 10x/0.25 UPlanSApo 20x/0.75 UPlanSApo 40x/0.95 UPlanFL N 60x/0.90 Apo N 60x/1.49 Oil UApo N 100x/1.49 Oil
Fluorescence Lamp	MT 20 illumination system with 150 W Xe or 150 W Hg/Xe arc burner
Excitation Filters	387nm/11 , 427nm/10, 470nm/40, 485nm/20, 504nm/12, 560nm/25, 572nm/35, 650nm/13
Emission Filters	Dualband CFP/YFP sbx HC filter set, Dualband GFP/mCherry sbx ET filter set, Quadband DAPI/FITC/Cy3/Cy5 sbx HC filter set
Camera	EM-CCD C9100-02 (Hamamatsu)
Software	xcellence (Olympus)

- **Nikon Ni-E (Nikon Imaging centre, University Heidelberg)**

Microscope stand	Upright widefield research microscope, motarized stage
Objectives	Nikon Plan Apo λ 2x NA 0.1 Nikon Plan Apo λ 10x NA 0.45 Nikon Plan Apo λ 20x NA 0.75 Nikon Plan Apo λ 40x NA 0.95 Nikon Plan Apo λ 60x NA 1.40 Oil
Fluorescence Lamp	Mercury lamp
Excitation Filters	390nm/18, 472nm/39, 543nm/22, 562nm/40, 632nm/22
Emission Filters	DAPI:460nm/60, EGFP:520nm/35, TRITC:593nm/40, TexasRed:624nm/40, Cy5:692nm/40
Camera	Nikon DS-Ri2 color camera, 24 x 36mm CMSO chip,
Software	NIS-Elements AR 4.30.01

5.1.2 Expendable items

Cover slides	Thermo Scientific Inc.
Cover slips, 20 x 20 mm	Menzel-Gläser (Thermo Scientific Inc.)
Cuvettes	Sarstedt AG & Co.
Falcon tubes 15, 50 ml	Greiner
Petri dishes	Greiner
Microcentrifuge tubes, 1.5 ml, 2 ml	Sarstedt AG & Co.
Low protein binding microcentrifuge tubes, 2 ml	Sigma Aldrich
Low protein binding microcentrifuge tubes, 1.5 ml	Eppendorf
PCR tubes, 200 µl	Kisker Biotech GmbH & Co.
Trans-Blot Turbo RTA Mini Nitrocellulose Transfer Kit	BioRad
Sterile filters, 0.2 µM	GE Healthcare
Whatman paper, 3 mm	Schleicher & Schuell
Costar 96-well plate	Greiner
PolarSafe Label Strips	Sigma Aldrich
PolarSafe Label Dots	Sigma Aldrich
reinforced bead mill tubes 2ml	VWR
Ampule breakers	Thermo Fisher
Disposable SteriStoppers, 20mm, 28mm and 32mm	neolab

5.1.3 Chemicals

If not mentioned differently, all chemicals were purchased from Roth, Sigma Aldrich, Invitrogen, AppliChem or Merck.

Enzymes and protease inhibitors

100X Protease Inhibitor Cocktail (#5871S)	CST
Leupeptin (microbial, >90%) (#L2884)	Sigma Aldrich
Pepstatin A	Pepta Nova GmbH
Aprotinin	AppliChem
Phenylmethylsulfonyl Fluoride (PMSF)	Sigma-Aldrich Co.
OptiTaq DNA Polymerase (#E2600-03)	roboklon
MyTaq Red DNA Polymerase (#21109)	Bioline
Velocity DNA polymerase (#21098)	Bioline

AmpliTaq Gold (#4311806)	Thermo Scientific
Restriction Enzymes	NEB
Zymolyase 100T	Amsbio

Standards and Kits

Proteo Silver silver stain kit (#PRTOSIL1)	Sigma Aldrich
Pierce BCA Protein Assay kit (#23227)	Thermo Fisher
peqGOLD Plasmid Miniprep Kit (#13-6943-02)	PeqLab
QIAquick Gel Extraction Kit	QIAGEN GmbH
GeneRuler 1 kb Plus DNA Ladder (#SM1331)	Thermo Scientific Inc.
PageRuler Prestained Protein Ladder (#26616)	Thermo Scientific Inc

Components for media

Bacto Agar	BD Biosciences
Bacto Peptone	BD Biosciences
Bacto Tryptone	BD Biosciences
Bacto Yeast extract	BD Biosciences
Difco Yeast Nitrogen Base w/o amino acids	BD Biosciences
Complete Supplement Mixture (CSM) (amino acids for drop out media)	MP Biomedicals, LLC

Antibiotics

Only final concentrations are listed here. All stock solutions were filter sterilized.

G418 sulfate (#ALX-380-013-G005)	200 µg/ml	Enzo life sciences
Ampicillin	100 µg/ml	Sigma-Aldrich Co.
ClonNAT (Nourseothricin) powder(#AB-102XL)	200 µg/ml	Jena Bioscience
Hygromycin B	250 µg/ml	Carl Roth

Other Chemicals and Reagents

D(+) Galactose	Roth
D (+) Raffinose (#R0250)	Sigma Aldrich
Bromphenol blue	Sigma Aldrich
Guanidine hydrochloride	Sigma Aldrich

poly(ethylene glycol) (#P4338)	Sigma Aldrich
DSP(dithiobis (succinimidyl propionate)),Lomants Reagent (#22585)	Thermo Scientific
Tween™ 20 Surfact-Amps™ Detergent Solution (#85113)	Thermo Fisher
Lithium Acetate Dihydrate (#L4158)	Sigma Aldrich
DMSO (sterile, cell-culture grade) (#D2650)	Sigma Aldrich
di-Potassium hydrogen phosphate	Sigma Aldrich
Potassium dihydrogen phosphate	Sigma Aldrich
GFP-Trap magnetic agarose beads (#gtma-20)	Chromotek
Amersham ECL Western Blotting Detection Reagent (#RPN2106)	GE Life Sciences
Quick Coomassie Stain (#GEN-QC-STAIN)	ProteinArk
4-20% mini-PROTEAN TGX precast gels, 15µl,30µl and 50µl wells	BioRad
Ponceau S solution (#P7170)	Sigma Aldrich
Gel Red Nucleic Acid Stain (#41003)	Linaris / Biotium
salmon sperm ssDNA (#D9156-5X)	Merck
RT-PCR-grade water (Invitrogen) (#AM9935)	Thermo Fisher
Paraformaldehyde (PFA)	Sigma Aldrich
DH5alpha competent E.coli (20 X 50µl) (#C2987H)	NEB
Indole-3-acetic acid sodium salt (auxin) (#I5148)	Sigma Aldrich
Agarose	Sigma Aldrich
dNTP mix (5mM each) (#AB0196)	Thermo Fisher

5.1.4 Media and Buffers

Growth media were autoclaved prior to usage. For preparation of agar plates, 2% (w/v) autoclaved agar was added to the medium prior to pouring on the plates.

LB (Luria-Bertani) medium	10g/l tryptone, 5 g/l yeast extract, 10 g/l NaCl
YPD/YPGal/YPRaff	20 g/l peptone, 10 g/l yeast extract, 20 g/l D-Glucose /Galactose/Raffinose
SD (Synthetic Dropout) medium	1.7 g/l Yeast Nitrogen Base w/o amino acids and ammonium sulphate, 0.7 g/l CSM mix (according to desired dropout), 5 g/l ammonium sulfate or 1 g/l glutamic acid, 2% (v/v) desired sugar, added post sterilization

PBS	137 mM NaCl, 2.7 mM KCl, 10 mM Na_2HPO_4, 2 mM NaH_2PO_4, pH was adjusted to 7.4 with HCl

5.1.5 Plasmids, Strains, Primers and Antibodies

Plasmids used in this study

Name	Characteristic Features	Source/Reference
pBS34	AmpR; kanMX4	The Yeast Resource Center
pBS35	AmpR; hphNT1	The Yeast Resource Center
pFA6a-kanMX4	AmpR; kanMX4	[199]
pFA6a-hphNT1	AmpR; hphNT1	[199]
pFA6a-natNT2	AmpR; natNT2	[199]
pNHK53	AmpR; URA3	[162]
pMK43_HA	AmpR; kanMX4	[162]
pMaM144 (3X mCherry)	AmpR; hphNT1	[199]
pRS305 Gal RNQ1-YFP::LEU2	AmpR; LEU2	Bernd Bukau lab
pRS305 Gal URE2-YFP::LEU2	AmpR; LEU2	Bernd Bukau lab

Yeast strains used in this study

Name	Genotype	Source/Reference
AB1	74D-694-[PSI+]-Gal-PrD-GFP::LEU2	[59]
AB2	AB1, *atg9Δ*::hphNT1	This study
AB3	AB1, *atg11Δ*::hphNT1	This study
AB4	AB1, *atg27Δ*::hphNT1	This study
AB5	AB1, *atg23Δ*::hphNT1	This study
AB6	AB1, *trs85Δ*::natNT2	This study
AB7	AB1, *ubc1Δ*::natNT2	This study
AB8	AB1, *sec28Δ*::natNT2	This study
AB9	AB1, *vid30Δ*::natNT2	This study
AB10	AB1, *nyv1Δ*::natNT2	This study
AB11	AB1, *vam3Δ*::natNT2	This study
AB12	AB1, *vam7Δ*::natNT2	This study
AB13	AB1, *ypt7Δ*::hphNT1	This study
AB14	AB1, *mon2Δ*::natNT2	This study
AB15	AB1, *mon2Δ*::hphNT1	This study
AB16	AB1, *vps45Δ*::hphNT1	This study

AB17	AB1, *vps33Δ*::hphNT1	This study
AB18	AB1, *vps41Δ*::natNT2	This study
AB19	AB1, *arl1Δ*::hphNT1	This study
AB20	AB1, *vps8Δ*::natNT2	This study
AB21	AB1,OsTIR1::URA3	This study
AB22	AB21, DOP1-AID ::kanMX4	This study
AB23	AB21, COP1-AID ::kanMX4	This study
AB24	AB21, SEC27-AID ::kanMX4	This study
AB25	AB21, SEC7-AID ::kanMX4	This study
AB26	74D-305 Gal RNQ1-YFP::LEU2	This study
AB27	74D-305 Gal URE2-YFP::LEU2	This study
AB28	AB26, *mon2Δ*::hphNT1	This study
AB29	AB27, *mon2Δ*::hphNT1	This study
AB30	AB1,COP1-3xmCh::hph NT1	This study
AB31	AB26, *vps33Δ*::hphNT1	This study
AB32	AB30,*mon2Δ*::natNT2	This study
AB33	AB1,VPS33-1xmCh::kanMX4	This study
AB34	AB33, *mon2Δ*::hphNT1	This study
AB35	AB21, SEC18-AID ::kanMX4	[136]
AB36	AB21, MON2-AID ::kanMX4	This study
AB37	AB21, VPS45-AID ::kanMX4	This study
AB38	AB1, *vps1Δ*::hphNT1	[136]

Primers used in this study

Name	**Sequence**
Atg23_S1	CCTCGTTGTTCTATAAGGTAACAAAATAAAGTGAAGAAGTAAATATGCGTACGCTGCAGGTCGA
Atg23_S2	CAATGTTTAAATTTACATTATCCTCATGGCTACTCTAGCTATTTGCATTTCAATCGATGAATTCGAGCTCG
Atg9_S3	GGGTGGTGTCTTAGGACTTGTTAAAGAGTATTACAAGAAGTCTGACGTCGGAAGACGTACGCTGCAGGTC GAC
Atg9_S2	CAGTTATATATATAGTTATATTGGATGATGTACACGACACAGTCTGCCTTAATCGATGAATTCGAGCTCG
Sec28_S1	GAACGGATTGTGAAGAACTCGGTGGAGAACATAGAAACAGACAAAAAATCATGCGTACGCTGCAGGTCGA C
Sec28_S2	CTTTTTCTAAAAAACCTACATGTTTAATGTGAGATATTACGTAAATCAATCGATGAATTCGAGCTCG
Sec28_check	GCGTATGCAGCGTCTTCAATGGG
Ubc1_S1	CAAGTGGTATATATATAAGTAGTAGTAGTAAGAAGTAAGCGATGCGTACGCTGCAGGTCGAC
Ubc1_S2	CTTTATTTACTTACTTACTTGGTGCGTTTTTTTTTTATCTATTCAATCGATGAATTCGAGCTCG
Ubc1_check	CAATGAGATGACAGTTGAATGC
Vam3_S1	GGATCAGCATTAACAAATTGGCCAACTAATATCCACTGCAGAAAGTTGAGATTATGCGTACGCTGCAGGTC GAC
Vam3_S2	GATTGGGTCTACCAGAAAGTCTGTGCTCAATGCGCGTTTAAGGAGATTACTAATCGATGAATTCGAGCTCG
Vam3_check	GCCTCATATTCGAGTTTCACATC
Vam7_S1	GCCAACAAAAACAAAAACAATAAAGTCATATAAGGGTTGATAATTGATATTGATGCGTACGCTGCAGGTCG AC

Vam7_S2	GTACAAATATACTCTCAGGATTTGTAACCCGGATAGTAACTCATTAATTCAATCGATGAATTCGAGCTCG
Vam7_check	CCAATACTTGATTAACCTC
Ypt7_S1	CCACTTCTTATCCATATAGAAACCCCTTCTGTATCAATTCAAATTAAGTGATGCGTACGCTGCAGGTCGAC
Ypt7_S2	GGATACGCTATAAAGGATTACATAATAGAAGATACAATTAAGTAGTACAGCTCAATCGATGAATTCGAGCTCG
Ypt7_check	CGCGGATTAACTTTTCGC
Nyv1_S1	GCGACAATTTATTAAGCTGTTAGAGCATTGGACTTTTATATTTTTACCAAATGCGTACGCTGCAGGTCGAC
Nyv1_S2	CCGTTATTAATGTTATTGTCGTGGGACAGCTCCCCTTTTTTTTTATTTACTTAATCGATGAATTCGAGCTCG
Nyv1_check	CGCATTACCACCAAGCGCCCGG
Vid30_S1	GTAGTACGTTAAAGCCAAGCGTCGAATTTCAGCATAATTAAGAGGAAATGCGTACGCTGCAGGTCGAC
Vid30_S2	GACTGATATCACATGGCTTTGTTGTTTGAAGGTGCTTGTTTTATGCTCAATCGATGAATTCGAGCTCG
Vid30_check	CAGGGGAGGGAACTGATGAATC
Vid28_S1	CCTGTATCATTGCCCTCGTGTTAGATTGGTGATATATTACAGTTACACTATGCGTACGCTGCAGGTCGAC
Vid28_S2	CTATAGCATAAATTAATTGTAGGAAATACTACGAGTTCTGTGCATTCAATCGATGAATTCGAGCTCG
Vid28_check	GACTGAAGGGGCGCGAAC
Dnm1_S1	CATTAAGTAGCTACCAGCGAATCTAAATACGACGGATAAAGAATGCGTACGCTGCAGGTCGAC
Dnm1_S2	CGCCCGCAATGTTGAAGTAAGATCAAAAATGAGATGAATTATGCAATTAATCGATGAATTCGAGCTCG
Trs85_S1	CGGTACCTCTTTATTCAGTCGGCTTTACAGATACTGAGGTAACTTATAATGCGTACGCTGCAGGTCGAC
Trs85_S2	CGTACGTATAATTTATACTCAAAACATGAATTTTCCATAAAGTCAATCGATGAATTCGAGCTCG
Vps1_S2	CTCAAAACCAAGCTTGAGTCGACCGGTATAGATGAGGAAAACCTA
Vps1_S1	AAGGACCGTACGAAAACTGCACATTTTATATTATCAGATATCATG
Vps1_check	GCTCGAGGGTAAACCACTTG
Dnm1_check	GTTAGTACCTTGATCGCCACC
Atg23_check	CCGATATCCTAGCCCTAGG
Atg27_check	GCGAAAGAGCTTCACTTCC
Trs85_check	CATCGCCTGAGTGATATG
Hse1_S1	GGGCCATGCCAGAGGCAATGCGTAAATCTATCTAAGGAAACCGTTGACAAAAATGCGTACGCTGCAGGTCGAC
Hse1_S2	GCTCTTCGTAAAAATTAAAGATATGTAAAGGTGCTATATAAGTTGAAGGGCTAATCGATGAATTCGAGCTCG
Vps13_S1	GTGACTACCAAAAGGGAAAAGGCAGAAAAAAGGAAAATTAAGAACAGTTAAATGCGTACGCTGCAGGTCGAC
Vps13_S2	GAATTATAGCTACATAGTGTACAAAAGCGGGTATATACTTTCATATGTGATCAATCGATGAATTCGAGCTCG
Vid27_S1	CTTTCTTTACGTATCCAGTCCAATAATATCTGCAGTAGTTATAGTGACTGATGCGTACGCTGCAGGTCGAC
Vid27_S2	CAACTATATAATACACTCGGAATACAACTTTAAAACCTTGAAAATAAGAATTAATCGATGAATTCGAGCTCG
Vid27_check	GCTTACCGTGATATGAAC
Hse1_check	GCCGCAGAACTTCGGTAGC
Vps13_check	CGCGAAGCCGGGTAATAC
Bni5_S1	GATTTACTGTTATGGTGATGCTATGTTAGTGTGAAATAGAACAACAGAAACGATGCGTACGCTGCAGGTCGAC
Bni5_S2	CTGTCTTAATTTATAAATATTTATAACAACCCTTGGCGTAATGTAATCAATCGATGAATTCGAGCTCG
Bni5_check	CATGCGGATCTTTGGCAAATG
Mix23_S1	GATATAGTTAGAAAAAAAACTTCTCATTTATACACGTAGACAAAAAGACGGTATGCGTACGCTGCAGGTCGAC
Mix23_S2	CAAGAATCTTTAAGTGATATAATCTTTCAGCGGACTAGAAGAATAGGGCGTTCAATCGATGAATTCGAGCTCG
Mix23_check	CTAAGATAGGAGGCTTGAAG
Cis3_S1	GTAAATCAAGACACATAAAACTATTTCACTCGCTAAACTTACATCTAAAATGCGTACGCTGCAGGTCGAC
Cis3_S2	CTTTTCCCTTATAAAAGGTAGAACATTAGTACTTTGATGTAGCTATTTAATCGATGAATTCGAGCTCG
Cis3_check	CCAAAAGAAACGGGTCAG

Syn8_S1	GCATAGAGACAGATCTCACGACAGCAAATAGATGCGTAAGCACACACGGTATGCGTACGCTGCAGGTCGAC
Syn8_S2	GATCAAAACCAAACTTCGTATTCGAGCCTAAAAAACAGAATATAATGTTAATCGATGAATTCGAGCTCG
Syn8_check	GTGCTTCCTTCCCTTGTAC
Vps33_S1	GGAAGAAAAAGCTGATATTGCCCATCTCCAACTTTATCAAATCATTTCACGATGCGTACGCTGCAGGTCGAC
Vps33_S2	GCACATTTGCATATACAAAAAATTAACAAATCTATCATATAATAATTAATCGATGAATTCGAGCTCG
Vps33_KO_check	GCGGTTCATCTTCGTAAGC
Apl1_S1	GAAGGGAATACAGCAAGAACATTCACTTCATTAATAGGACGTATTTCGCTTATGCGTACGCTGCAGGTCGAC
Apl1_S2	CGTTAAATATGAGTATATTTAAATACAGGAATTAGTATCATTTGCAGTCAATCGATGAATTCGAGCTCG
Apl1_check	GATCTCTTTAGTGCCATCAG
Cos3_S1	GTTACTATCTCGAATAAAAAACCCCTCGAACTGCCATCTCACTACCGAAAATGCGTACGCTGCAGGTCGAC
Cos3_S2	CGCAGCTGACAAACTACAAAATATATAAATTGAAAAAGTTGTATTTATCTCTAATCGATGAATTCGAGCTCG
Cos3_check	CCGGAAATGTAATGGATGCC
Mon2_s3	GGCCTCCAAGATAAAGTTTTGGAATTATCACTTGGATTTACGAAACTAGACCGTACGCTGCAGGTCGAC
Mon2_Fusion_check	GCCCTTGCTCTTAGAAG
Arl1_S1	GAAAGATCTAAGAAGAAAGTTCCAGTAAAGTGAGTTATAGATCAAGATGCGTACGCTGCAGGTCGAC
Arl1_S2	GCCATTTAAAAAGTATGCATCTACACTTTTTTTTTGCAAATCTTTATCGCTAATCGATGAATTCGAGCTCG
Arl1_KO check	CAGGACGGGTAACAGAGC
Bud21_S1	CGAATTGATACCCTGAACTGTTACTACCCGTATACACGTATTAAGTAAGACAATGCGTACGCTGCAGGTCGAC
Bud21_S2	GATTAATTTTGTGATTGTACTATTATTTTATTATGTTGTATGCTATATATTAATCGATGAATTCGAGCTCG
Bud21_KO check	CAACCAGAGATGAAATCGG
Tom7_S1	CCCTCTTATCTCTCAATATTTGCCAAAATTAGCTTTTAACAAATAAACCATGCGTACGCTGCAGGTCGAC
Tom7_S2	GGAAATATGGGCTTCCTCTCTCACCCAAGTTGTATCGAACTGATGTTTTTAATCGATGAATTCGAGCTCG
Tom7_KO Check	CACGTCAAACGGTGCGTC
Bna1_S1	CAGTCTACAAGTAACTGAAATAGCATACATTTACCAAAAAAATCGAAAAAAATGCGTACGCTGCAGGTCGAC
Bna1_S2	CTTACGTAACAAGAGAGCTATAAAAGTACAACTAACAACTCTTCTAATACTTAATCGATGAATTCGAGCTCG
Bna1_KO check	CGGCATTTAGAACGCTGCC
Vps29_s1	GCTGTAACTAGTGGCGAAAAGGTCATAGAATTATTCGCCTAAATTATGCGTACGCTGCAGGTCGAC
Vps29_s2	GCATCTAATGTTTAGACATCATAGAAATGCATAAAAATGAAAATGGCTACCCTAATCGATGAATTCGAGCTCG
Vps29_KO check	GGGCATAACGTTGTATCG
Vps45_S1	CAGTGACTTGGTTTTGAGTTAAGGCCATCTTTTACTGTATAGAACAAAGAAATGCGTACGCTGCAGGTCGAC
Vps45_S2	GATTTATGCCTCATATATAAAATAGAATTTTAGAATAAGATAATCCTTATTTAATCGATGAATTCGAGCTCG
Vps45_KO check	GACTGTATGGCGAAAAGTTG
Vps45_S3	GGCACCTCTATACTTTCAACTAAAGAATATATGGATTCTATTAGATCTGCAAAACGTACGCTGCAGGTCGAC
Vps45_Fusion_check	GATACTCAAGGCCATAGAG
Rav1_s1	CCGCAAACAATTGAGAAAGTAAACAAACGTGCACACGCAAAGGTAGTTCTCATGCGTACGCTGCAGGTCGAC
Rav1_s2	GATGTAATTATTTTTATTTATAAATCCATTTATTTGATAAAAAATATGATATCAATCGATGAATTCGAGCTCG
Rav1_KO check	GCGACAGCCTTCTTCTGATC
Pdr16_S1	CCAACAAATAATACAAAACCACTTTATATAAAAAAAATTACAAAAGCAAAAAATGCGTACGCTGCAGGTCGAC
Pdr16_S2	CTTTTATTTATTATATATTATAGTGCATTATCATTATCTATCTAAATTTGCCTTTAATCGATGAATTCGAGCTCG
Pdr16_KO check	CCACCCGACTCTATTTGAG
Cop1_S3	GCTATGATTTCTAAGATCGGTGCACCTGCATCCGGATTAAGAATACGTGTACGTACGCTGCAGGTCGAC
Cop1_S2	GGTCGAGCAGAATACAATCCCGAGAAAATCAATAGGCAAAATAGCAT ATCGATGAATTCGAGCTCG

Cop1_Fusion_check	CCTCGTGCAGAACAAGCACG
Sec26_S3	GAGTGGCATTGATTGCTAAGAAGACCAATAAACTTGCTCTCACTCATGTTCGTACGCTGCAGGTCGAC
Sec26_S2	CTTATCTCCTTTGACATTATAACTTACATTGCATCAGCTCAGGGTGGTATCGATGAATTCGAGCTCG
Sec26_Fusion_check	CACCATCAGAGTCGTTGGG
Sec23_S3	CCTTACAAAATTTCATGACTCACTTACAACAAGTAGCCGTCTCTGGTCAGGCACGTACGCTGCAGGTCGAC
Sec23_S2	CAAAAAGCCTAATAACGATCAAATAAAACAAAAGAAAGCCGTTGCTCATCGATGAATTCGAGCTCG
Sec23_Fusion_check	CCAAGACGATCCACAGTACGC
Sec24_S3	CGAAAGTTACAGAGAATTCTTACAAATCATGAAAGCCAGAATTAGCAAACGTACGCTGCAGGTCGAC
Sec24_S2	GCAACCAACAAAAATATACAGTTTCTTTTTATCATTGATTCCCTTTTAGCCATCGATGAATTCGAGCTCG
Sec24_Fusion_check	CTGAATTCAATCAAAGAGTAAG
Sec27_S3	GAACAACAGCCGGAGCAAGGAGAGGCAGTGCCGGAGCCTGTGGAAGAAGAGAGTCGTACGCTGCAGGTCGAC
Sec27_S2	GATGTTTTCTCATTCGTTGATTAGTTCTTTATTTGTCTTTCTATGAGGTGGATCGATGAATTCGAGCTCG
Sec27_ Fusion_check	CCACTCCAGCCCCAGAAC
Sec7_S3	CATGCTATAAAACAATTTCTAAGCAGAGTTGGTGAATTATACCTTTCTACTGATCGTACGCTGCAGGTCGAC
Sec7_S2	CTGTGTTCTACAACTAAGCATATTTTAATCTGCTGGACCATTCAACAAAGCCATCGATGAATTCGAGCTCG
Sec7_Fusion_check	CAATGCCTGGCGTTCAGTG
Vps35_S1	CGATAAAAGGAGGAGGACGAGAAAGAAGAAGCTGAAAAACACAATGCGTACGCTGCAGGTCGAC
Vps35_S2	GTGTAGTTTTTTTTTATCTTGGGCATGTACGAAGAGCAAGTACGTTATTTAACTAATCGATGAATTCGAGCTCG
Vps35_check	CACTTCGTCTTAAAGGGGCG
Ypt7_S1	CCACTTCTTATCCATATAGAAACCCCTTCTGTATCAATTCAAATTAAGTGATGCGTACGCTGCAGGTCGAC
Ypt7_S2	GGATACGCTATAAAGGATTACATAATAGAAGATACAATTAAGTAGTACAGCTCAATCGATGAATTCGAGCTCG
Ypt7_check	CGGGTAACGTTTGTATCTCGCGG
Mon2_S1	CAAGTGATTTTCAAAGAAAGTAAACCAACTTGACCTGTTACACACCATTCATATGCGTACGCTGCAGGTCGAC
Mon2_S2	CTATTTATCCTACGTGATTTTTAAAAATATTCGTCCATGCTTCAGCTTCTAATCGATGAATTCGAGCTCG
Mon2_check	CATTGCGAAGTCTTCATTATCC
Slt2_S1	GCTATCAAAATAGTAGAAATAATTGAAGGGCGTGTATAACAATTCTGGGAGATGCGTACGCTGCAGGTCGAC
Slt2_S2	GCTTACATCTATGGTGATTCTATACTTCCCCGGTTACTTATAGTTTTTTGTCCTAATCGATGAATTCGAGCTCG
Slt2_check	GAAGACTGCGAAATGTTGGC
Vma5_S1	GTTTTCTTACCTAATTCTAGATCAATTCTTTTTTCTGAAAAAAAAAAAATGCGTACGCTGCAGGTCGAC
Vma5_S2	CTAAAAAAAAAACAGAAATATATATTAATCTAAGTTAGTATTATAAATCGATTAATCGATGAATTCGAGCTCG
Vma5_check	CCGTAAAGAGAAGCGTCAG
Dop1_S2	CTCAAAGCGTATAACTATATTTCGGTTTATAAAGAAAAATTCATAGCTATGCATCGATGAATTCGAGCTCG
Dop1_S3	GGGTCAGTTGATTTATATGGTTGTGGTGAAGATCTCAAAAAAGATATTCTGTCACGTACGCTGCAGGTCGAC
Dop1_Fusion_check	CATTCGTCGCGCTGGTAG
REVCompTIR1	GACTTGAACGGATCCACTAGC
5' in URA	GTCATGCAAGGGCTCCCTATC
Kan B	CAATTCAACGCGTCTGTGAG
Rev_mCherry	CTTCAAGTAGTCGGGGATGTC
Vps33_S3	CATCATCGCCGATGGCTTGATCAATGGCACAAGGATCATGAACTCTATATCTCGTACGCTGCAGGTCGAC
Vps33_Fusion_check	CGAAGAGAGTATATGGGTCC
Vps41_S1	GCAAAATAAAAAAGCATTTTAACGAAGAGTATATACCTACTATTAGACATTAATGCGTACGCTGCAGGTCGAC

Vps41_S2	GTACATTCCTGAAGTGTACACTTGCCTTGTGTATTAAATGATGATTCGATATTAATCGATGAATTCGAGCTC G

Antibodies used in this study

anti-GFP (mouse) clones 7.1 and 13.1 (#11814460001)	1:1000	Roche
anti-actin (mouse) clone C4 (#MAB1501)	1:1000	Millipore
anti-HA (mouse) clone 16B12 (#901514)	1:3000	BioLegend
anti-mouse IgG, HRP-linked Antibody (#7076)	1:5000	Cell Signaling

5.2 Molecular Biology Methods

5.2.1 Agarose Gel Electrophoresis

DNA fragments were separated and analyzed using one-dimensional agarose gel electrophoresis. 1% (w/v) agarose gels were prepared by melting agarose in 0.5X TBE buffer. To visualize DNA fragments under UV light, Gel Red at a final concentration of 1X was added to the molten agarose and poured into agarose tray with gel combs. DNA samples in loading buffer were applied to the gels. Gels were run in 0.5X TBE buffer at 80-120mV constant voltage, depending on the size of the gel. The DNA was detected using UV light and the size of the DNA fragments was determined using GeneRuler 1kb Plus DNA Ladder as standard.

5X TBE	54g/l Tris, 27.5g/l Boric acid 20ml/l 0.5M EDTA (pH 8.0)
6x DNA loading dye	30 % (v/v) Glycerol, 0.25 % (w/v) Bromophenol blue

5.2.2 Restriction digestion of DNA

For genomic integration, plasmids were linearized by restriction digestion experiments. About 5–10 units of enzyme per µg DNA, and 10–20 units for genomic DNA was used to digest the plasmid in a total 50 µl reaction volume. The enzymes were purchased from NEB. The reaction

was set up as shown below and incubated at 37°C for 5-15 minutes or as stated in the manufacture's protocol.

DNA	1 µg
10X reaction Buffer	5 µl (1X)
Restriction Enzyme	1.0 µl (10 units)
Nuclease-free Water	to 50 µl

5.2.3 Purification of DNA fragments

The linearized DNA or PCR products was separated by agarose gel electrophoresis, specific bands of interest were excised using a scalpel and the DNA was extracted using QIAquick Gel Extraction Kit (Qiagen) by following the manufacturer's protocol.

5.2.4 Polymerase Chain Reaction (PCR)

PCR was used to amplify a fusion cassette for yeast genomic integration or to check the correct insertion/integration or deletion of gene of interest. For amplification of a fusion cassette, OptiTaq polymerase was used and the reactions were set up as shown below. To check the correct insertion/integration or deletion of gene of interest by colony PCR, MyTaq DNA polymerase was used and the reactions were set up as shown below.

OptiTaq PCR reaction mix:

10X Buffer B	10 µl
dNTP mix (5mM each)	3 µl
Forward primer (Eurofins) 100 uMol/ µl	0.4 µl
Reverse primer (Eurofins) 100 uMol/ µl	0.4 µl
Template DNA	20-50 ng
OptiTaq DNA Polymerase, 5 U/µl	1 µl

ddH_2O	adj 50 µl

PCR cycling conditions

PCR steps	Temperature	Time	Cycles
Initial denaturation	95 °C	3 min	1
Denaturation Annealing Extension	95 °C 55 °C 72 °C	30 s 30 s 1 min/1 kb	33
Final Extension	72 °C	7 min	1

Colony PCR reaction mix

5X MyTaq red reaction buffer	10 µl
Forward primer (Eurofins) 100 uMol/ µl	0.2 µl
Reverse primer (Eurofins) 100 uMol/ µl	0.2 µl
MyTaq red DNA polymerase	0.3 µl
ddH_2O	adj 50 µl

Colony PCR cycling conditions

PCR steps	Temperature	Time	Cycles
Initial denaturation	95 °C	1 min	1
Denaturation Annealing Extension	95 °C 55 °C 72 °C	20 s 20 s 30 s/1 kb	33
Final Extension	72 °C	7 min	1

Bacterial Methods

5.2.5 Transformation of E. coli

For the bacterial transformation, 1-5 µl (~100 ng) of DNA was added to 20-50µl of E.coli DH5α competent cells and the mixture was incubated on ice for 20 min. After a 45-second heat

shock at 42°C, the samples were incubated on ice for 2 min. Then, 250µl LB Medium was added and the transformed bacteria were incubated at 37°C for 1hr with constant agitation (400rpm) and then plated on LB-agar plates with respective antibiotics. To ensure the growth of bacterial colonies, plates were incubated over night at 37°C.

5.2.6 Plasmid isolation

Plasmids were isolated from *E. coli* using standard peqGOLD Plasmid Miniprep Kit (PEQLAB) according to the manufacturers' instruction.

Yeast Methods

5.2.7 Genetic manipulation in yeast

Genetic modification in yeast was performed by homologous recombination techniques. The primers for both N/C terminal tagging as well as for generation of deletion constructs were designed with flanking sequences homologous to the target genomic loci as described in the literature [199]. These PCR products were then transformed into yeast cells and the transformants were selected based on growth in the corresponding antibiotic resistance or auxotrophic marker plate. Correct genomic integration of PCR products in transformed yeast cells were verified by colony PCR using primer pairs that anneal within the amplicon and upstream of the target locus. Tagging of essential genes with the N terminal “aid degron” tag for auxin aid experiments was done similar to the N terminal tagging of fusion proteins [162].

5.2.8 FM464 Vacuolar staining

Yeast cultures grown to logarithmic phase to an OD600 0.6-0.9 were pelleted by centrifugation (3000RPM, 5 min, RT). FM464 was added to the cell pellet to a final concentration of 8µM and the cells were incubated for 30 minutes at 30°C on a shaker in a dark room. Cells were pelleted and washed twice with YPD medium post which they were

allowed to recover for 1 hour in YPD at 30°C to chase FM4-64 to the vacuole. The cells were again spun down, resuspended in 1X PBS and visualized by fluorescence microscopy.

FM464 Stock solution	8mM (5µg/µl) in DMSO

5.2.9 Transformation of Yeast cultures

The yeast cultures to be transformed were allowed to grow to logarithmic growth phase (OD600-0.6-0.8) and pelleted by centrifugation (3000 RPM, 4 min, RT). The cell pellet was washed with 10 ml sterile distilled water. The cells were again harvested by centrifugation (3000 RPM, 4 min, RT) and the cell pellet was resuspended in 100 µl of 0.1M Lithium Acetate solution and transferred to a 1.5 ml Eppendorf tube. The cell/LiOAc suspension mix was incubated for 15 min at 30°C and then transferred to a 1.5 ml Eppendorf tube containing the transformation mix. The transformation mix was vortexed for 30s to thoroughly mix all the components and were heat shocked for 22 min at 42°C. Transformed cells were harvested again by centrifugation (13000 RPM, 30s, RT). For transformation with an antibiotic resistance cassette, transformed cells were resuspended in 2.5ml YPD and incubated overnight at RT on a rotator prior to plating them on the respective antibiotic plate. For transformation with auxotrophic markers, transformed cells were resuspended in sterile distilled water and directly plated on the respective drop out plate without any overnight incubation. Cells were allowed to grow for four days at 30°C post which positive clones were confirmed by colony PCR, microscopy and /or by Western Blotting.

Transformation Mix	10 µl PCR product 300 µl PEG-LiOAc mix 10 µl Single stranded carrier DNA (salmon sperm DNA) 22.5 µl DMSO
PEG-LiOAc Mix	50% (w/v) PEG 4000 0.1 M LiOAc

5.2.10 Preparation of yeast protein extracts for Western Blotting

Yeast cells grown to mid-log phase were pelleted by centrifugation (3000 RPM, 10 min, RT). The cell pellet was then resuspended in 500 µl of 1M LiOAc and incubated on ice for 5 min. Cells were again pelleted (13000 RPM, 2 min, RT), resuspended in 600 µl of 0.4M NaOH and incubated on ice for 5 min. Cells were pelleted once more (13000 RPM, 2 min, RT) and the pellet was resuspended in 100µl of 2X SDS sample buffer. Samples were boiled at 98°C for 20-30 min and analysed by SDS-PAGE and Western Blot.

5.2.11 Preparation of yeast cell lysate by mixer mill for Large scale approach

50-100ml of yeast cells grown to mid-log phase (OD600 0.6-0.8) were pelleted by centrifugation (3500 RPM, 10 min, 4°C) and the cell pellet was resuspended in 100 µl of lysis buffer. Post this, they were transferred to an Eppendorf tube and snap frozen in liquid nitrogen for several minutes. Meanwhile, the adaptors for mixer mill lysis were prepared, fresh reinforced 2 ml bead mill tubes (from VWR) containing a 7mm stainless steel ball were placed on them. The whole setup was submerged in liquid nitrogen. Snap frozen yeast samples were thawed on ice and dripped as small drops into the 2 ml bead mill tubes containing liquid nitrogen. Post this, the liquid nitrogen is boiled out, tubes are closed and placed into their adapters of the Retsch Mixer Mill MM400 and agitated for three times for 2 min at 30Hz. Samples were cooled in liquid nitrogen between different agitation rounds. The resulting powder from lysed cells was resuspended in 200-300 µl of lysis buffer and centrifuged (4500RPM, 5 min, 4°C) to remove cell debris. The entire soluble fraction was used for Immunoprecipitation and further processing.

Lysis Buffer (100X protease Inhibitor cocktail directly added before use to a final concentration of 1X)	0.5 mM EDTA (pH 8)
	150 mM NaCl
	10 mM Tris
	0.1 % NP40 adj to 50ml ddH_20

5.2.12 Crosslinking of yeast cell lysates with DSP (dithiobis (succinimidyl propionate))

To generate yeast cell lysates for crosslinking with DSP, the same Retsch Mixer Mill MM400 method as described above was used. However instead of lysis buffer, another buffer called crosslinking buffer (having no detergent) was used for the cell lysis process. Post cell lysis, the resulting cell lysate was first cross-linked with DSP (4mM conc, 2 hrs on ice) and then treated with 40 mM Tris buffer (pH 7.5-8, 15 min on ice) to quench the reaction. Then, the detergent NP40 at a final concentration of 0.1% is added and the mixture is vortexed vigorously for 30-50s. Clearing the cell debris by centrifugation (4500 RPM, 5min, 4°C) generated the soluble fraction of lysates which were used for immunoprecipitation and further processing.

Crosslinking buffer(100X protease inhibitor cocktail directly added before use to a final concentration of 1X)	0.5 mM EDTA (pH 8)
	150 mM NaCl
	50 mM HEPES
	700 mM Sorbitol
	100 mM KH_2PO_4 (pH 7.5)
	adj to 50ml ddH20
DSP(50mM Stock)	10 mg DSP in 495 µl DMSO

5.2.13 Immunoprecipitation with yeast lysates

Yeast cell lysates obtained by cryolysis as mentioned above, were cleared of debris by centrifugation, and the entire soluble fraction was used for immunoprecipitation experiments. Immunoprecipitation was carried out using the GFP-Trap_MA beads from ChromoTek (gtma#20) to isolate the model amyloid substrate PrD-GFP along with all its interaction partners *in vivo* in specific yeast mutant cultures. 25 µL of bead slurry was used per reaction. Beads were washed once with ice cold lysis buffer and magnetically separated until a clear supernatant was obtained, which was discarded. The washing step was repeated

two more times. Yeast cell lysates equivalent to 2-3µg of total protein extract (post debris clearing) were mixed with equilibrated GFP-Trap_MA beads and the total volume was normalized to 300µl with the lysis buffer. The reaction was incubated for 2 hours at 4°C in a end-over-end tumbling tube. Beads were magnetically separated, washed with 300ul lysis buffer and again magnetically separated till a clear supernatant was obtained. The supernatant was discarded and the wash step was repeated two more times. Post this, the beads were resuspended in 50µl 2X SDS sample buffer and boiled for 30 min at 98°C to dissociate immunocomplexes from the beads. The eluted fraction was further analysed by SDS-PAGE and Western blotting using anti-GFP antibodies.

Lysis Buffer (100X protease inhibitor cocktail directly added before use to a final concentration of 1X)	0.5 mM EDTA (pH 8)
	150 mM NaCl
	10 mM Tris
	0.2 % NP40 adj to 50ml ddH_20

5.3 Biochemical Methods

5.3.1 BCA protein assay to determine protein concentration

Protein concentration was determined using the Pierce™ BCA Protein Assay Kit from Thermo Scientific by following manufacturer's instructions.

5.3.2 SDS-polyacrylamide gel electrophoresis (SDS-PAGE)

Separation of proteins by molecular weight was achieved by employing SDS-PAGE under denaturing conditions. Protein samples were solubilized in SDS sample buffer and incubated at 98°C for 20-30 min and were then run in 4-20% mini-PROTEAN TGX precast gels from Bio-Rad. Electrophoresis was performed at 150-200V till the blue dye reaches the bottom of the gel. These gels were then used for Western Blotting.

5X SDS Loading buffer	0.25% (w/v) Bromophenol Blue, 50% (w/v) Glycerol,10% (w/v) SDS, 0.25 M Tris HCl pH 6.8
10X SDS Buffer	30.3 g Tris,144 g Glycine,10 g SDS

5.3.3 Western Blotting

Samples separated by SDS-PAGE gels were transferred to nitrocellulose membranes using semidry transfer method by Trans-Blot®Turbo™system, Bio-Rad. The membranes were blocked with 2% milk powder for 1 hour at room temperature and then incubated overnight at 4°C with primary antibodies. After three times of extensive TBST washing each lasting 10 min, horseradish peroxidase (HRP)-conjugated secondary antibodies were applied for 1.5-2 hour. After TBST washing, the membrane was incubated with Amersham ECL Western Blotting Detection Reagent (#RPN2106) for 1 min before developing the blot with the Bio-Rad ChemiDoc Imaging Systems.

1X Transfer buffer	200 ml of 5X Transfer buffer(Bio-Rad) + 600 ml of nanopure water + 200 ml of ethanol
10X TBS	0.2 M Tris-HCl, 1.5 M NaCl, pH 7.5
TBST	100 ml of 10X TBS+ 900 ml ddH20+0.5 ml Tween 20
Blocking solution	TBST with 2% milk powder
Primary antibody solution	TBST with 2% milk powder
Secondary antibody solution	TBST with 2% milk powder
Western blotting Substrate	Amersham ECL Western Blotting Detection Reagent (#RPN2106)

5.4 Microscopy

5.4.1 Fixation of yeast cells for microscopy

5 ml of yeast cultures of were mixed with 5ml of 8% PFA (paraformaldehyde) and incubated for 10min at RT. Cells were centrifuged (3500 RPM,7min, RT) and the pellet was washed with 10ml of 0.1M potassium phosphate buffer(pH 6.5). Cells were pelleted again (3500 RPM, 7min, RT), resuspended in 1ml PBS and transferred to an Eppendorf tube. Post another short centrifugation (13000 RPM, 2 min, RT) cells were resuspended in 20-30µl of PBS and analyzed by fluorescence microscopy.

5.4.2 Standard image acquisition, processing and data analysis

Fixed cells were imaged as stacks of optical sections with 0.2µm width using widefield microscopes (Refer section “Microscopes” in 5.1.1). For imaging with the Olympus CellR-Point FRAP IX81, UApo N 100x/1.49 Oil immersion objective was used and images with the Nikon Ni-E were acquired using the Plan Apo λ 60x NA 1.40 Oil immersion objective. Images were deconvolved with xcellence software (Olympus) using the Wiener filter. ImageJ software was used for further processing of the images.

5.4.3 Time-lapse microscopy

Ultrapure Agarose (1% w/v) in SD-Ura media were prepared and poured to create agarose pads of 20 x 20 x 1 mm which were used in time-lapse microscopy. Cells (10µl) were added to the agarose pads and later covered with coverslip and sealed with melted VLAP wax (1:1:1 Vaseline:lanolin:paraffin). The samples were imaged at the NiE microscope using the Plan Apo λ 60x NA 1.40 Oil immersion objective, by acquiring a stack of 10 optical sections spaced 0.3 µm apart in every 5 min for 1 hour.

5.4.4 Quantification of amyloid aggregates and substrates for colocalization experiments

In general, PrD-GFP aggregates were quantified manually. More than 100 cells were counted and classified into either of the two groups: cells having one focus, cells having two or more foci and the results were plotted as percentile chart. Quantification of co-localization of PrD-GFP with other proteins was done by first counting the number of clear and distinguishable PrD-GFP fluorescent foci formed within the cells and next by determining how many of those PrD-GFP foci co-localized at least partially with the corresponding other protein.

Abbreviations

IPOD	Insoluble PrOtein Deposit
JUNQ	JUxtaNuclear Quality control
INQ	IntraNuclear Quality control
CVT	Cytoplasm-to-Vacuole Targeting
PAS	Phagophore Assembly Site
SM	Sec1/Munc18
HOPS	Homotypic fusion and vacuole protein sorting
CORVET	class C core vacuole/endosome tethering
MVB	Multivesicular bodies
UPS	Ubiquitin Proteasome System
ALS	Amyotrophic lateral sclerosis
ATP	Adenosine triphosphate
GFP	Green fluorescent protein
PrD	Prion domain
VID	Vacuole Import and Degradation
DNA	deoxyribonucleic acid
E.coli	*Escherichia coli*
Hsp	heat shock protein
kDa	kilo Dalton
LB	Luria Bertani
OD	optical density
S. cerevisiae	*Saccharomyces cerevisiae*
sHsp	small heat shock protein
DUBs	Deubiquitinating Enzymes
IMiQ	intramitochondrial protein quality control
VHL	Von Hippel-Lindau tumor suppressor
MTOC	microtubule-organizing center
PAGE	polyacrylamide gel electrophoresis
PFA	p-formaldehyde
LC3	Light Chain 3
polyQ	polyglutamine
PrP	Prion protein
RPM	revolutions per minute
PSGs	Proteasome Storage Granules
PBS	Phosphate-buffered saline
UV	Ultraviolet
FM464	N-(3-Triethylammoniumpropyl)-4-(6-(4-(Diethylamino) Phenyl) Hexatrienyl) Pyridinium Dibromide
RT	Room temperature
PCR	polymerase chain reaction

SNARE	Soluble NSF (N-Ethylmaleimide-Sensitive Factor) Attachment Protein Receptor
SD	synthetic dropout
YPD	Yeast Extract–Peptone–Dextrose
TBE	Tris/Borate/EDTA
Tris	tris(hydroxymethyl)aminomethane
FBPase	Fructose 1,6-bisphosphatase
MS	Mass Spectrometry
IP	Immunoprecipitation
LFQ	label-free quantitation
DSP	dithiobis (succinimidyl propionate)
wt	Wild-type
KO	Knock out
CPY	carboxypeptidase Y
TGN	trans-Golgi network
ER	Endoplasmic reticulum
TDP43	TAR DNA-binding protein 43
BCA	bicinchoninic acid assay
ECL	Enhanced chemiluminescence

References

[1] M. Karplus, C. M. Dobson, and S. Andrej, “Protein Folding : A Perspective from Theory and Experiment.”

[2] P. G. Wolynes, J. N. Onuchic, and D. Thirumalai, “Navigating the Folding Routes,” vol. 267, no. March, 1995.

[3] A. R. Dinner, S. Andrej, L. J. Smith, C. M. Dobson, and M. Karplus, “Understanding protein folding via free-energy surfaces from theory and experiment,” vol. 0004, no. July, pp. 331–339, 2000.

[4] K. A. Dill, “From Levinthal to pathways to funnels [J],” no. June, 1997.

[5] J. Tyedmers, A. Mogk, and B. Bukau, “Cellular strategies for controlling protein aggregation,” *Nat. Publ. Gr.*, vol. 11, no. 11, pp. 777–788, 2010.

[6] C. M. Dobson, “Protein folding and misfolding,” vol. 426, no. December, 2003.

[7] F. U. Hartl and M. Hayer-Hartl, “Converging concepts of protein folding in vitro and in vivo,” *Nat. Struct. Mol. Biol.*, vol. 16, no. March, pp. 574–581, Jun. 2014.

[8] Bs. Claudio Soto, PhD; Lisbell D. Estrada and A, “Protein Misfolding and Neurodegeneration,” vol. 65, no. 2, pp. 184–189, 2008.

[9] F. Chiti and C. M. Dobson, “Protein Misfolding , Amyloid Formation , and Human Disease : A Summary of Progress Over the Last Decade,” no. February 2006, 2017.

[10] K. Trzeœniewska, M. Brzyska, and D. Elbaum, “Neurodegenerative aspects of protein aggregation,” no. January, 2004.

[11] F. U. Hartl, “Protein Misfolding Diseases,” 2017.

[12] T. Shamsi, “A Review on Protein Misfolding, Aggregation and Strategies to Prevent Related Ailments,” no. July, 2017.

[13] T. P. J. Knowles, M. Vendruscolo, and C. M. Dobson, “The amyloid state and its association with protein misfolding diseases,” *Nature Reviews Molecular Cell Biology*. 2014.

[14] C. A. Ross and M. A. Poirier, “Protein aggregation and neurodegenerative disease,” no. July, pp. 10–17, 2004.

[15] Y. M. & N. S. Tohru Kitada*†, Shuichi Asakawa†, Nobutaka Hattori*, Hiroto Matsumine*, Yasuhiro Yamamura‡, Shinsei Minoshima†, Masayuki Yokochi§, “Mutations in the parkin gene causeautosomal recessive juvenile parkinsonism,” vol. 169, no. 1993, pp. 166–169, 1998.

[16] J. A. Olzmann, L. Li, M. V Chudaev, J. Chen, F. A. Perez, and R. D. Palmiter, “Parkin-mediated K63-linked polyubiquitination targets misfolded DJ-1 to aggresomes via binding to HDAC6,” vol. 178, no. 6, pp. 1025–1038, 2007.

[17] and L. L. Lih-Shen Chin1, James A. Olzmann, “Parkin-mediated ubiquitin signalling in aggresome formation and autophagy,” vol. 38, no. Pt 1, pp. 144–149, 2011.

[18] D. A. Drummond and C. O. Wilke, “Theory Mistranslation-Induced Protein Misfolding as a Dominant Constraint on Coding-Sequence Evolution,” pp. 341–352, 2008.

[19] J. Rochet, “Errors in Translation Cause Selective Neurodegeneration,” vol. 1, no. 9.

[20] M. A. S. & S. L. Dawn A. Parsell, Anthony S. Kowalt, “Protein disaggregation mediated by heat-shock protein Hsp104,” pp. 475–478.

[21] E. R. Stadtman and R. L. Levine, “Protein Oxidation,” pp. 191–208.

[22] T. Nystro, “Role of oxidative carbonylation in protein quality control and senescence,” vol. 24, no. 7, pp. 1311–1317, 2005.

[23] Y. J. Suzuki, M. Carini, and D. A. Butterfield, “Protein Carbonylation,” vol. 12, no. 3, pp. 2–5, 2010.

[24] A. Höhn and T. Grune, “Lipofuscin: Formation, effects and role of macroautophagy,” *Redox Biol.*, vol. 1, no. 1, pp. 140–144, 2013.

[25] T. Reinheckel, N. Sitte, O. Ullrich, U. Kuckelkorn, K. J. A. Davies, and T. Grune, “Comparative resistance of the 20 S and 26 S proteasome to oxidative stress,” *Biochem. J.*, vol. 335, no. 3, pp. 637–642, 1998.

[26] E. R. Stadtman, “Protein Oxidation and Aging,” vol. 257, no. August, 1992.

[27] N. Erjavec, L. Larsson, J. Grantham, and T. Nyström, “Accelerated aging and failure to segregate damaged proteins in Sir2 mutants can be suppressed by overproducing the protein aggregation-remodeling factor Hsp104p,” pp. 2410–2421, 2007.

[28] R. C. T. and A. D. Howard, “Aging as an Event of Proteostasis Collapse,” vol. 1, pp. 1–17, 2011.

[29] L. Wanga, K. Sharmab, and and R. P. R. Gabriella Grisottia, “The effect of mutant SOD1 dismutase activity on non-cell autonomous degeneration in familial amyotrophic lateral sclerosis,” vol. 35, no. 2, pp. 234–240, 2010.

[30] and R. I. M. Elise A. Kikis*, Tali Gidalevitz*, “Protein homeostasis in models of aging and age-related conformational disease,” no. 13, pp. 138–159, 2010.

[31] M. S. Hipp, S. Park, and F. U. Hartl, “Proteostasis impairment in protein- misfolding and -aggregation diseases,” *Trends Cell Biol.*, vol. 24, no. 9, pp. 506–514, 2014.

[32] A. L. Fink, “Protein aggregation : folding aggregates , inclusion bodies and amyloid,” pp. 9–23, 1998.

[33] N. S. De Groot, R. Sabate, and S. Ventura, “Amyloids in bacterial inclusion bodies,” 2009.

[34] M. Morell *et al.*, “Inclusion bodies : Specificity in their aggregation process and amyloid-like structure,” vol. 1783, pp. 1815–1825, 2008.

[35] S. B. PRUSINER†, “Prions STANLEY,” vol. 95, no. November, pp. 13363–13383, 1998.

[36] S. B. P. and F. E. C. Paul M Harrison , Paul Bamborough , Valerie Daggett *, “The prion folding problem,” pp. 53–59.

[37] S. A. Priolat, B. Chesebrot, G. J. Raymondt, P. T. Lansbury, and B. Caugheytt, “Cell-free formation of protease-resistant prion protein,” pp. 471–474, 1994.

[38] P. T. Lansbury and B. Caughey, “The double life of the prion protein How are prion protein diseases transmitted ?,” vol. 6, no. 8, pp. 914–916, 1996.

[39] R. B. Wickner *et al.*, “Amyloids and yeast prion biology Reed,” vol. 52, no. 9, pp. 1514–1527, 2020.

[40] S. W. Liebman and Y. O. Chernoff, “Prions in Yeast,” vol. 191, no. August, pp. 1041–1072, 2012.

[41] 6 Simon Alberti1, 5, Randal Halfmann1, 3, 5, Oliver King1, 4, Atul Kapila1, 3, and Susan Lindquist1, 2, 3, “A systematic survey identifies prions and illuminates sequence features of prionogenic proteins,” *Cell*, vol. 137, no. 1, pp. 146–158, 2009.

[42] S. Alberti, R. Halfmann, and S. Lindquist, *Biochemical , Cell Biological , and Genetic Assays to Analyze Amyloid and Prion Aggregation in Yeast*, 2nd ed., vol. 470, no. 10. Elsevier Inc.

[43] R. B. Wickner, “[URE3] as an Altered URE2 Protein : Evidence for a Prion Analog in Saccharomyces cerevisiae,” vol. 264, no. April, pp. 566–570, 1994.

[44] G. Suzuki, N. Shimazu, and M. Tanaka, “A Yeast Prion, Mod5, Promotes Acquired Drug Resistance and Cell Survival Under Environmental Stress,” vol. 336, no. April, pp. 355–360, 2012.

[45] S. J. Saupe, “The [Het-s] prion of Podospora anserina and its role in heterokaryon incompatibility,” *Semin. Cell Dev. Biol.*, vol. 22, no. 5, pp. 460–468, 2011.

[46] B. . COX, “[PSI] A CYTOPLASMIC SUPPRESSOR OF SUPER-SUPPRESSOR IN YEAST,” 1964.

[47] J. R. Glover, A. S. Kowal, E. C. Schirmer, M. M. Patino, J. Liu, and S. Lindquist, “Self-Seeded Fibers Formed by Sup35 , the Protein Determinant of [PSI ⁒], a Heritable Prion-like Factor of S . cerevisiae,” vol. 89, pp. 811–819, 1997.

[48] R. Protein-only and R. Diaz-avalos, “Protein-only transmission of three yeast prion strains Chih-Yen King ; Ruben Diaz-Avalos,” no. April 2004, pp. 319–323, 2004.

[49] S. V Paushkin, V. V Kushnirov, V. N. Smirnov, and M. D. Ter-avanesyan, “Interaction between Yeast Sup45p (eRF1) and Sup35p (eRF3) Polypeptide Chain Release Factors : Implications for Prion-Dependent Regulation,” vol. 17, no. 5, pp. 2798–2805, 1997.

[50] M. Tanaka, P. Chien, N. Naber, and R. Cooke, “Conformational variations in an infectious protein determine prion strain differences,” vol. 428, no. March, pp. 323–328, 2004.

[51] M. Reidy and D. C. Masison, “Modulation and elimination of yeast prions by protein chaperones and co-chaperones,” no. December, pp. 245–249, 2011.

[52] Z. Zhou and G. Xiao, “Conformational conversion of prion protein in prion diseases,” *Acta Biochim. Biophys. Sin. (Shanghai).*, vol. 45, no. 6, pp. 465–476, 2013.

[53] S. Alberti, “Molecular mechanisms of spatial protein quality control,” *Prion*, vol. 6, no. 5, pp. 437–442, 2012.

[54] N. Sondheimer and S. Lindquist, “Rnq1 : An Epigenetic Modifier of Protein Function in Yeast,” vol. 5, pp. 163–172, 2000.

[55] I. L. Derkatch *et al.*, “Dependence and independence of [PSI +] and [PIN +] : a two-prion system in yeast ?,” vol. 19, no. 9, 2000.

[56] C. W. Helsen and J. R. Glover, “Insight into Molecular Basis of Curing of [PSI ⁜] Prion by Overexpression of 104-kDa Heat Shock Protein (Hsp104) * □,” vol. 287, no. 1, pp. 542–556, 2012.

[57] J. Liu, N. Sondheimer, and S. L. Lindquist, “Changes in the middle region of Sup35 profoundly alter the nature of epigenetic inheritance for the yeast prion [PSI ⁜],” 2002.

[58] B. Deuticke, B. B. Acta, M. Adachi, K. H. Iwasa, L. Li, and S. Lindquist, “Creating a Protein-Based Element of Inheritance,” vol. 287, no. January, pp. 661–665, 2000.

[59] J. Tyedmers, S. Treusch, J. Dong, J. M. Mccaffery, B. Bevis, and S. Lindquist, “Prion induction involves an ancient system for the sequestration of aggregated proteins and heritable changes in prion fragmentation,” *Proc. Natl. Acad. Sci.*, 2010.

[60] B. Bukau, J. Weissman, and A. Horwich, “Review Molecular Chaperones and Protein Quality Control,” *Cell*, vol. 125, no. 3, pp. 443–451, May 2006.

[61] M. P. Mayer and B. Bukau, “Cellular and Molecular Life Sciences Hsp70 chaperones : Cellular functions and molecular mechanism,” vol. 62, pp. 670–684, 2005.

[62] S. Escusa-Toret, W. I. M. Vonk, and J. Frydman, “Spatial sequestration of misfolded proteins by a dynamic chaperone pathway enhances cellular fitness during stress,” *Nat. Cell Biol.*, 2013.

[63] S. B. M. M. Miller, A. Mogk, and B. Bukau, “Spatially Organized Aggregation of Misfolded Proteins as Cellular Stress Defense Strategy,” *J. Mol. Biol.*, vol. 427, no. 7, pp. 1564–1574, 2015.

[64] J. R. Glover and S. Lindquist, “Hsp104 , Hsp70 , and Hsp40 : A Novel Chaperone System that Rescues Previously Aggregated Proteins,” vol. 94, pp. 73–82, 1998.

[65] A. Mogk, T. Tomoyasu, P. Goloubinoff, S. Ru, and H. Langen, “Identification of thermolabile Escherichia coli proteins : prevention and reversion of aggregation by DnaK and ClpB,” vol. 18, no. 24, pp. 6934–6949, 1999.

[66] J. Winkler, J. Tyedmers, B. Bukau, and A. Mogk, “Hsp70 targets Hsp100 chaperones to substrates for protein disaggregation and prion fragmentation,” vol. 198, no. 3, 2012.

[67] A. Mogk, B. Bukau, and H. H. Kampinga, “Review Cellular Handling of Protein Aggregates by Disaggregation Machines,” *Mol. Cell*, vol. 69, no. 2, pp. 214–226, 2018.

[68] F. den Brave *et al.*, “Chaperone-Mediated Protein Disaggregation Triggers Proteolytic Clearance of Intra-nuclear Protein Inclusions,” *Cell Rep.*, vol. 31, no. 9, p. 107680, 2020.

[69] R. Hjerpe *et al.*, “UBQLN2 Mediates Autophagy-Independent Protein Aggregate Clearance by the Proteasome,” *Cell*, vol. 166, no. 4, pp. 935–949, 2016.

[70] D. Voges, P. Zwickl, and W. Baumeister, “THE 26S PROTEASOME:A MOLECULAR MACHINE DESIGNED FOR CONTROLLED PROTEOLYSIS,” pp. 1015–1068, 1999.

[71] I. Jariel-encontre, G. Bossis, and M. Piechaczyk, “Ubiquitin-independent degradation of proteins by the proteasome,” *BBA - Rev. Cancer*, vol. 1786, no. 2, pp. 153–177, 2008.

[72] N. B. Nillegoda *et al.*, “Ubr1 and Ubr2 Function in a Quality Control Pathway for Degradation of Unfolded Cytosolic Proteins,” vol. 21, pp. 2102–2116, 2010.

[73] J. W. Heck, S. K. Cheung, and R. Y. Hampton, “Cytoplasmic protein quality control degradation mediated by parallel actions of the E3 ubiquitin ligases Ubr1 and San1,” vol. 107, no. 3, pp. 1106–1111, 2010.

[74] D. Kaganovich, R. Kopito, and J. Frydman, “Misfolded proteins partition between two distinct quality control compartments,” *Nature*, 2008.

[75] L. Bedford *et al.*, “Depletion of 26S Proteasomes in Mouse Brain Neurons Causes Neurodegeneration and Lewy-Like Inclusions Resembling Human Pale Bodies,” vol. 28, no. 33, pp. 8189–8198, 2008.

[76] 1 and Jose´ J. Lucas Ester Martı´n-Aparicio, 1 Ai Yamamoto, 2 Fe´ lix Herna´ndez, 1 Rene´ Hen, 2 Jesu´s Avila, “Proteasomal-Dependent Aggregate Reversal and Absence of Cell Death in a Conditional Mouse Model of Huntington ’ s Disease,” vol. 21, no. 22, pp. 8772–8781, 2001.

[77] N. F. Bence, R. M. Sampat, and R. R. Kopito, “Impairment of the ubiquitin-proteasome system by protein aggregation,” *Science (80-.).*, vol. 292, no. 5521, pp. 1552–1555, 2001.

[78] J. A. Johnston, C. L. Ward, and R. R. Kopito, “Aggresomes: A Cellular Response to Misfolded Proteins,” vol. 143, no. 7, pp. 1883–1898, 1998.

[79] J. M. T. Hyttinen, M. Amadio, J. Viiri, A. Pascale, A. Salminen, and K. Kaarniranta, “Clearance of misfolded and aggregated proteins by aggrephagy and implications for aggregation diseases,” *Ageing Res. Rev.*, vol. 18, pp. 16–28, 2014.

[80] C. I. Holmberg, K. E. Staniszewski, K. N. Mensah, A. Matouschek, and R. I. Morimoto, “Inefficient degradation of truncated polyglutamine proteins by the proteasome,” *EMBO J.*, vol. 23, no. 21, pp. 4307–4318, 2004.

[81] P. Venkatraman, R. Wetzel, M. Tanaka, N. Nukina, and A. L. Goldberg, “Eukaryotic proteasomes cannot digest polyglutamine sequences and release them during degradation of polyglutamine-containing proteins,” *Mol. Cell*, vol. 14, no. 1, pp. 95–104, 2004.

[82] S. Schipper-Krom, K. Juenemann, and E. A. J. Reits, “The ubiquitin-proteasome system in huntington’s disease: Are proteasomes impaired, initiators of disease, or coming to the rescue?,” *Biochem. Res. Int.*, vol. 2012, 2012.

[83] D. Glick, S. Barth, and K. F. Macleod, “Autophagy : cellular and molecular mechanisms,” vol. 221, no. 1, pp. 3–12, 2010.

[84] T. Lamark and T. Johansen, “Aggrephagy : Selective Disposal of Protein Aggregates by Macroautophagy,” vol. 2012, 2012.

[85] Z. Y. and D. J. Klionsky, “Mammalian autophagy: core molecular machinery and signaling regulation,” vol. 22, no. 2, pp. 124–131, 2011.

[86] T. Yorimitsu and D. J. Klionsky, “Autophagy : molecular machinery for self-eating,” pp. 1542–1552, 2005.

[87] U. Nair and D. J. Klionsky, “Molecular Mechanisms and Nonspecific Autophagy Pathways in Yeast *,” *J. Biol. Chem.*, vol. 280, no. 51, pp. 41785–41788, 2006.

[88] H. Nakatogawa, K. Suzuki, Y. Kamada, and Y. Ohsumi, “Dynamics and diversity in autophagy mechanisms : lessons from yeast,” vol. 10, no. julY, 2009.

[89] A. Lilienbaum, “Relationship between the proteasomal system and autophagy,” vol. 4, no. 1, pp. 1–26, 2013.

[90] S. Pankiv‡, A. B. , Terje Høyvarde Clausen‡, Trond Lamark‡, A. Ø. , Jack-Ansgar Bruun‡ , Heidi Outzen‡, G. Bjørkøy‡, and and Terje Johansen, “p62 / SQSTM1 Binds Directly to Atg8 / LC3 to Facilitate Degradation of Ubiquitinated Protein Aggregates,” vol. 282, no. 33, pp. 24131–24145, 2007.

[91] V. Kirkin *et al.*, “A Role for NBR1 in Autophagosomal Degradation of Ubiquitinated Substrates,” *Mol. Cell*, vol. 33, no. 4, pp. 505–516, 2009.

[92] K. Lu, I. Psakhye, and S. Jentsch, “Autophagic Clearance of PolyQ Proteins Mediated by Ubiquitin-Atg8 Adaptors of the Conserved CUET Protein Family,” *Cell*, vol. 158, no. 3, pp. 549–563, 2014.

[93] S. V Scorr *et al.*, “Cytoplasm-to-vacuole targeting and autophagy employ the same machinery to deliver proteins to the yeast vacuole,” vol. 93, no. October, pp. 12304–12308, 1996.

[94] T. M. Harding, A. Hefner-Gravink, M. Thumm, and D. J. Klionsky, “Genetic and phenotypic overlap between

autophagy and the cytoplasm to vacuole protein targeting pathway," *J. Biol. Chem.*, vol. 271, no. 30, pp. 17621–17624, 1996.

[95] and De Daniel J. Klionsky, Rosario Cueva and bbie S. Yaver, "Aminopeptidase I of Saccharomyces cerevisiae Is Localized to the Vacuole Independent of the Secretory Pathway," vol. 119, no. 2, pp. 287–299, 1992.

[96] M. U. H. and D. J. Klionsky‡, "Vacuolar Localization of Oligomeric α-Mannosidase Requires the Cytoplasm to Vacuole Targeting and Autophagy Pathway Components in Saccharomyces cerevisiae*," vol. 276, no. 23, pp. 20491–20498, 2001.

[97] J. Kim, S. V Scott, M. N. Oda, and D. J. Klionsky, "Transport of a Large Oligomeric Protein by the Cytoplasm to Vacuole Protein Targeting Pathway," vol. 137, no. 3, pp. 609–618, 1997.

[98] S. V Scott, J. Guan, M. U. Hutchins, J. Kim, and D. J. Klionsky, "Cvt19 Is a Receptor for the Cytoplasm-to-Vacuole Targeting Pathway," vol. 7, no. 6, pp. 1131–1141, 2001.

[99] R. Leber, E. Silles, I. V Sandoval, and J. Mazo, "Yol082p , a Novel CVT Protein Involved in the Selective Targeting of Aminopeptidase I to the Yeast Vacuole *," vol. 276, no. 31, pp. 29210–29217, 2001.

[100] C.-Y. C. and W.-P. Huang, "Atg19 Mediates a Dual Interaction Cargo Sorting Mechanism in Selective Autophagy," *Int. J. Biol. Sci.*, vol. 6, no. 6, pp. 569–583, 2010.

[101] and D. J. K. Takahiro Shintani, Wei-Pang Huang, Per E. Stromhaug, "Mechanism of Cargo Selection in the Cytoplasm to Vacuole Targeting Pathway," vol. 3, no. 6, pp. 825–837, 2002.

[102] T. Lang, S. Reiche, M. Straub, M. Bredschneider, and M. Thumm, "Autophagy and the cvt pathway both depend on AUT9," *J. Bacteriol.*, vol. 182, no. 8, pp. 2125–2133, 2000.

[103] T. Noda *et al.*, "Apg9p/Cvt7p is an integral membrane protein required for transport vesicle formation in the Cvt and autophagy pathways," *J. Cell Biol.*, vol. 148, no. 3, pp. 465–479, 2000.

[104] H. Yamamoto *et al.*, "Atg9 vesicles are an important membrane source during early steps of autophagosome formation," *J. Cell Biol.*, vol. 198, no. 2, pp. 219–233, 2012.

[105] M. Baba, M. Osumi, S. V Scott, D. J. Klionsky, and Y. Ohsumi, "Two Distinct Pathways for Targeting Proteins from the Cytoplasm to the Vacuole/Lysosome," vol. 139, no. 7, pp. 1687–1695, 1997.

[106] and D. J. K. Fulvio Reggiori, Takahiro Shintani, Usha Nair, "Atg9 Cycles between Mitochondria and the Pre-Autophagosomal Structure in Yeasts," vol. 1, no. 2, pp. 101–109, 2005.

[107] J. Geng and D. J. Klionsky, "The Atg8 and Atg12 ubiquitin-like conjugation systems in macroautophagy," no. August, pp. 1–6, 2008.

[108] M. A. L.-D. and D. J. Klionsky, "The Cvt pathway as a model for selective autophagy," vol. 584, no. 7, pp. 1359–1366, 2011.

[109] and M. D. Ilija Melentijevic1, Marton L. Toth1,*, Meghan L. Arnold1,*, Ryan J. Guasp1, Girish Harinath1, Ken C. Nguyen2, Daniel Taub3,4, J. Alex Parker5, Christian Neri6, Christopher Gabel3,4, David H. Hall2, "C. elegans Neurons Jettison Protein Aggregates and Mitochondria Under Neurotoxic Stress," *Physiol. Behav.*, vol. 176, no. 1, pp. 100–106, 2016.

[110] K. Bagola and T. Sommer, "Protein Quality Control : On IPODs and Other JUNQ," *Curr. Biol.*, vol. 18, no. 21, pp. 1019–1021, 2007.

[111] R. Spokoini, O. Moldavski, Y. Nahmias, J. L. England, M. Schuldiner, and D. Kaganovich, "Report Confinement to Organelle-Associated Inclusion Structures Mediates Asymmetric Inheritance of Aggregated Protein in Budding Yeast," *CellReports*, vol. 2, no. 4, pp. 738–747, 2012.

[112] S. Rothe, A. Prakash, and J. Tyedmers, "The Insoluble Protein Deposit (IPOD) in Yeast," vol. 11, no. July, pp. 1–9, 2018.

[113] A. I. Gragerov, "in Escherichia coli rpaH mutant defective in heat shock protein induction and inclusion body formation," vol. 291, no. 2, pp. 222–224, 1991.

[114] E. Laskowska *et al.*, "Aggregation of heat-shock-denatured , endogenous proteins and distribution of the IbpA / B and Fda marker-proteins in Escherichia coli WT and grpE 280 cells," pp. 247–259, 2004.

[115] S. Ventura and A. Villaverde, "Protein quality in bacterial inclusion bodies," vol. 24, no. 4, 2006.

[116] Ron R. Kopito, “Aggresomes, inclusion bodies and protein aggregation,” 2000.

[117] A. B. Lindner, R. Madden, A. Demarez, and E. J. Stewart, “Asymmetric segregation of protein aggregates is associated with cellular aging and rejuvenation,” vol. 105, no. 8, 2008.

[118] R. Garcia-mata, Y. Gao, and E. Sztul, “Hassles with Taking Out the Garbage : Aggravating Aggresomes,” no. 11, pp. 388–396, 2002.

[119] Y. Kawaguchi *et al.*, “The Deacetylase HDAC6 Regulates Aggresome Formation and Cell Viability in Response to Misfolded Protein Stress,” vol. 115, pp. 727–738, 2003.

[120] M. Bruderek *et al.*, “IMiQ: A novel protein quality control compartment protecting mitochondrial functional integrity,” *Mol. Biol. Cell*, vol. 29, no. 3, pp. 256–269, 2018.

[121] S. Specht, S. B. M. Miller, A. Mogk, and B. Bukau, “Hsp42 is required for sequestration of protein aggregates into deposition sites in Saccharomyces cerevisiae,” *J. Cell Biol.*, vol. 195, no. 4, pp. 617–629, 2011.

[122] I. Gallina *et al.*, “Cmr1/WDR76 defines a nuclear genotoxic stress body linking genome integrity and protein quality control,” *Nat. Commun.*, vol. 6, pp. 1–16, 2015.

[123] S. B. B. Miller *et al.*, “Compartment-specific aggregases direct distinct nuclear and cytoplasmic aggregate deposition,” *EMBO J.*, vol. 34, no. 6, pp. 778–797, 2015.

[124] E. M. Sontag, R. S. Samant, and J. Frydman, “Mechanisms and Functions of Spatial Protein Quality Control,” 2017.

[125] L. Malinovska, S. Kroschwald, M. C. Munder, D. Richter, and S. Alberti, “Molecular chaperones and stress-inducible protein-sorting factors coordinate the spatiotemporal distribution of protein aggregates,” *Mol. Biol. Cell*, vol. 23, no. 16, pp. 3041–3056, 2012.

[126] S. J. Weisberg, R. Lyakhovetsky, A. C. Werdiger, A. D. Gitler, Y. Soen, and D. Kaganovich, “Compartmentalization of superoxide dismutase 1 (SOD1G93A) aggregates determines their toxicity,” *Proc. Natl. Acad. Sci. U. S. A.*, vol. 109, no. 39, pp. 15811–15816, 2012.

[127] M. Ogrodnik *et al.*, “Dynamic JUNQ inclusion bodies are asymmetrically inherited in mammalian cell lines through the asymmetric partitioning of vimentin,” *Proc. Natl. Acad. Sci. U. S. A.*, vol. 111, no. 22, pp. 8049–8054, 2014.

[128] A. Shiber, M. Brandeis, and T. Ravid, “Ubiquitin conjugation triggers misfolded protein sequestration into quality control foci when Hsp70 chaperone levels are limiting,” no. May, 2013.

[129] J. M. Chalovich and E. Eisenberg, “Sorting out the trash: the spatial nature of eukaryotic protein quality control,” *Biophys. Chem.*, vol. 257, no. 5, pp. 2432–2437, 2014.

[130] S. M. Hill, X. Hao, D. Kaganovich, S. Spikings-nordby, P. O. Widlund, and T. Amen, “Asymmetric Inheritance of Aggregated Proteins and Age Reset in Yeast Are Regulated by Vac17- Dependent Vacuolar Functions Article Asymmetric Inheritance of Aggregated Proteins and Age Reset in Yeast Are Regulated by Vac17-Dependent Vacuolar Functions,” pp. 826–838, 2016.

[131] D. Kryndushkin, G. Ihrke, T. C. Piermartiri, and F. Shewmaker, “A yeast model of optineurin proteinopathy reveals a unique aggregation pattern associated with cellular toxicity,” *Mol. Microbiol.*, vol. 86, no. 6, pp. 1531–1547, 2012.

[132] H. R. Saibil *et al.*, “Heritable yeast prions have a highly organized three-dimensional architecture with interfiber structures,” *Proc. Natl. Acad. Sci. U. S. A.*, vol. 109, no. 37, pp. 14906–14911, 2012.

[133] L. Z. Peters, O. Karmon, S. Miodownik, and S. Ben-Aroya, “Proteasome storage granules are transiently associated with the insoluble protein deposit in Saccharomyces cerevisiae,” *J. Cell Sci.*, 2016.

[134] L. Z. Peters *et al.*, “The Protein Quality Control Machinery Regulates Its Misassembled Proteasome Subunits,” *PLoS Genet.*, 2015.

[135] R. S. Marshall, F. Mcloughlin, and R. D. Vierstra, “Autophagic Turnover of Inactive 26S Proteasomes in Yeast Is Directed by the Ubiquitin Receptor Cue5 and the Hsp42 Chaperone Article Autophagic Turnover of Inactive 26S Proteasomes in Yeast Is Directed by the Ubiquitin Receptor Cue5 and the Hsp42 Chaperone,” *CellReports*, vol. 16, no. 6, pp. 1717–1732, 2016.

[136] R. Kumar, P. P. Nawroth, and J. Tyedmers, “Prion Aggregates Are Recruited to the Insoluble Protein Deposit (IPOD) via Myosin 2-Based Vesicular Transport,” *PLoS Genet.*, vol. 12, no. 9, pp. 1–31, 2016.

[137] D. Kryndushkin, R. B. Wickner, and F. Shewmaker, “FUS / TLS forms cytoplasmic aggregates , inhibits cell growth

and interacts with TDP-43 in a yeast model of amyotrophic lateral sclerosis," vol. 2, no. 3, pp. 223–236, 2011.

[138] C. Lagier-Tourenne, M. Polymenidou, and D. W. Cleveland, "TDP-43 and FUS/TLS: Emerging roles in RNA processing and neurodegeneration," *Hum. Mol. Genet.*, vol. 19, no. R1, pp. 46–64, 2010.

[139] R. Babazadeh *et al.*, "Syntaxin 5 Is Required for the Formation and Clearance of Protein Inclusions during Proteostatic Article Syntaxin 5 Is Required for the Formation and Clearance of Protein Inclusions during Proteostatic Stress," *CellReports*, vol. 28, no. 8, pp. 2096-2110.e8, 2019.

[140] R. Kumar, N. Neuser, and J. Tyedmers, "Hitchhiking vesicular transport routes to the vacuole: Amyloid recruitment to the Insoluble Protein Deposit (IPOD)," *Prion*, vol. 11, no. 2, pp. 71–81, 2017.

[141] and H.-J. L. Seung-Jae Leea, c,*, Hee-Sun Lima, c, Eliezer Masliahd, "Protein aggregate spreading in neurodegenerative diseases: Problems and perspectives," vol. 70, no. 4, pp. 339–348, 2014.

[142] L. L. Berglund, X. Hao, B. Liu, J. Grantham, and T. Nyström, "Differential effects of soluble and aggregating polyQ proteins on cytotoxicity and type-1 myosin-dependent endocytosis in yeast," *Sci. Rep.*, vol. 7, no. 1, pp. 1–13, 2017.

[143] P. Tim and 3 Thomas Nystro¨m1 Hugo Aguilaniu, 1, 2, 3 Lena Gustafsson, 2 Michel Rigoulet, "Asymmetric Inheritance of Oxidatively Damaged Proteins During Cytokinesis," vol. 299, no. March, pp. 1751–1754, 2003.

[144] J. Song *et al.*, "Essential Genetic Interactors of SIR2 Required for Spatial Sequestration and Asymmetrical Inheritance of Protein Aggregates," *PLoS Genet.*, vol. 10, no. 7, pp. 17–19, 2014.

[145] P. Tessarz, M. Schwarz, A. Mogk, and B. Bukau, "The Yeast AAA ɛ Chaperone Hsp104 Is Part of a Network That Links the Actin Cytoskeleton with the Inheritance of Damaged Proteins ,," vol. 29, no. 13, pp. 3738–3745, 2009.

[146] N. L. Nuckolls *et al.*, "The wtf4 meiotic driver utilizes controlled protein aggregation to generate selective cell death," pp. 1–35, 2020.

[147] K. Wang, Z. Yang, X. Liu, K. Mao, U. Nair, and D. J. Klionsky, "Phosphatidylinositol 4-kinases are required for autophagic membrane trafficking," *J. Biol. Chem.*, vol. 287, no. 45, pp. 37964–37972, 2012.

[148] Y. Takahashi *et al.*, "The Bif-1-Dynamin 2 membrane fission machinery regulates Atg9-containing vesicle generation at the Rab11-positive reservoirs," *Oncotarget*, vol. 7, no. 15, pp. 20855–20868, 2016.

[149] P. H. Huang and H. L. Chiang, "Identification of novel vesicles in the cytosol to vacuole protein degradation pathway," *J. Cell Biol.*, vol. 136, no. 4, pp. 803–810, 1997.

[150] M. G. Waters, T. Serafini, and J. E. Rothman, "'Coatomer': A cytosolic protein complex containing subunits of non-clathrin-coated Golgi transport vesicles," *Nature*, 1991.

[151] C. R. Brown, D. Dunton, and H. L. Chiang, "The vacuole import and degradation pathway utilizes early steps of endocytosis and actin polymerization to deliver cargo proteins to the vacuole for degradation," *J. Biol. Chem.*, vol. 285, no. 2, pp. 1516–1528, 2010.

[152] H. L. Shieh, Y. Chen, C. R. Brown, and H. L. Chiang, "Biochemical Analysis of Fructose-1,6-bisphosphatase Import into Vacuole Import and Degradation Vesicles Reveals a Role for UBC1 in Vesicle Biogenesis," *J. Biol. Chem.*, vol. 276, no. 13, pp. 10398–10406, 2001.

[153] H. J. Balderhaar and C. Ungermann, "CORVET and HOPS tethering complexes – coordinators of endosome and lysosome fusion," 2013.

[154] J. A. Whitney, M. Gomez, D. Sheff, T. E. Kreis, and I. Mellman, "Cytoplasmic Coat Proteins Involved in Endosome Function," 1995.

[155] S. Kakuta, H. Yamamoto, L. Negishi, C. Kondo-Kakuta, N. Hayashi, and Y. Ohsumi, "Atg9 vesicles recruit vesicle-tethering proteins Trs85 and Ypt1 to the autophagosome formation site," *J. Biol. Chem.*, vol. 287, no. 53, pp. 44261–44269, 2012.

[156] S. K. Backues, D. P. Orban, A. Bernard, K. Singh, Y. Cao, and D. J. Klionsky, "Atg23 and Atg27 Act at the Early Stages of Atg9 Trafficking in S. cerevisiae," *Traffic*, vol. 16, no. 2, pp. 172–190, 2015.

[157] C. He *et al.*, "Recruitment of Atg9 to the preautophagosomal structure by Atg11 is essential for selective autophagy in budding yeast," *J. Cell Biol.*, vol. 175, no. 6, pp. 925–935, 2006.

[158] A. A. Alibhoy, "Vacuole import and degradation pathway: Insights into a specialized autophagy pathway," *World J. Biol. Chem.*, vol. 2, no. 11, p. 239, 2011.

[159] B. Cosson *et al.*, “Poly(A)-Binding Protein Acts in Translation Termination via Eukaryotic Release Factor 3 Interaction and Does Not Influence [PSI+] Propagation,” *Mol. Cell. Biol.*, vol. 22, no. 10, pp. 3301–3315, 2002.

[160] D. A. Kiktev, J. C. Patterson, S. Muller, B. Bariar, T. Pan, and Y. O. Chernoff, “Regulation of Chaperone Effects on a Yeast Prion by Cochaperone Sgt2,” *Mol. Cell. Biol.*, vol. 32, no. 24, pp. 4960–4970, 2012.

[161] T. Serafini, M. Amherdt, M. Brunner, J. E. Rothman, L. Orci, and R. A. Kahn, “ADP-ribosylation factor is a subunit of the coat of Golgi-derived COP-coated vesicles: A novel role for a GTP-binding protein,” *Cell*, vol. 67, no. 2, pp. 239–253, 1991.

[162] K. Nishimura, T. Fukagawa, H. Takisawa, T. Kakimoto, and M. Kanemaki, “An auxin-based degron system for the rapid depletion of proteins in nonplant cells,” *Nat. Methods*, vol. 6, no. 12, pp. 917–922, 2009.

[163] D. Mahajan *et al.*, “Mammalian Mon2/Ysl2 regulates endosome-to-Golgi trafficking but possesses no guanine nucleotide exchange activity toward Arl1 GTPase,” *Sci. Rep.*, vol. 3, 2013.

[164] A. K. Gillingham, J. R. C. Whyte, B. Panic, and S. Munro, “Mon2, a relative of large Arf exchange factors, recruits Dop1 to the Golgi apparatus,” *J. Biol. Chem.*, vol. 281, no. 4, pp. 2273–2280, 2006.

[165] J. A. Efe, F. Plattner, N. Hulo, D. Kressler, S. D. Emr, and O. Deloche, “Yeast Mon2p is a highly conserved protein that functions in the cytoplasm-to-vacuole transport pathway and is required for Golgi homeostasis,” *J. Cell Sci.*, vol. 118, no. 20, pp. 4751–4764, 2005.

[166] R. F. G. Toonen and M. Verhage, “Vesicle trafficking: Pleasure and pain from SM genes,” *Trends Cell Biol.*, vol. 13, no. 4, pp. 177–186, 2003.

[167] D. Gallwitz and R. Jahn, “The riddle of the Sec1/Munc-18 proteins - New twists added to their interactions with SNAREs,” *Trends Biochem. Sci.*, vol. 28, no. 3, pp. 113–116, 2003.

[168] B. T. Lobingier, D. P. Nickerson, S. Y. Lo, and A. J. Merz, “SM proteins Sly1 and Vps33 co-assemble with Sec17 and SNARE complexes to oppose SNARE disassembly by Sec18,” *Elife*, vol. 2014, no. 3, pp. 1–22, 2014.

[169] C. R. Cowles, S. D. Emr, and B. F. Horazdovsky, “Mutations in the VPS45 gene, a SEC1 homologue, result in vacuolar protein sorting defects and accumulation of membrane vesicles,” *J. Cell Sci.*, vol. 107, no. 12, pp. 3449–3459, 1994.

[170] J. A. Solinger and A. Spang, “Tethering complexes in the endocytic pathway : CORVET and HOPS,” vol. 280, pp. 2743–2757, 2013.

[171] C. G. A. and A. J. Merz, “New links between vesicle coats and Rab-mediated vesicle targeting,” *Bone*, vol. 23, no. 1, pp. 1–7, 2011.

[172] R. Duden, G. Griffiths, R. Frank, P. Argos, and T. E. Kreis, “β-COP, a 110 kd protein associated with non-clathrin-coated vesicles and the golgi complex, shows homology to β-adaptin,” *Cell*, vol. 64, no. 3, pp. 649–665, Feb. 1991.

[173] I. Monastyrska, E. Rieter, D. J. Klionsky, and F. Reggiori, “Multiple roles of the cytoskeleton in autophagy - Monastyrska - 2009 - Biological Reviews - Wiley Online Library,” *Biol. Rev. Camb. Philos. Soc.*, vol. 84, no. 3, pp. 431–48, 2009.

[174] H. G. Budayeva and I. M. Cristea, “A mass spectrometry view of stable and transient protein interactions,” *Adv. Exp. Med. Biol.*, vol. 806, pp. 263–282, 2014.

[175] R. Narayanaswamy *et al.*, “Widespread reorganization of metabolic enzymes into reversible assemblies upon nutrient starvation,” *Proc. Natl. Acad. Sci.*, 2009.

[176] E. W. J. Wallace *et al.*, “Reversible, Specific, Active Aggregates of Endogenous Proteins Assemble upon Heat Stress,” *Cell*, vol. 162, no. 6, pp. 1286–1298, 2015.

[177] D. Ahmadpour, R. Babazadeh, and T. Nystrom, “Hitchhiking on vesicles: a way to harness age-related proteopathies?,” *FEBS J.*, vol. 287, no. 23, pp. 5068–5079, 2020.

[178] P. Novick, S. Ferro, and R. Schekman, “Order of events in the yeast secretory pathway,” *Cell*, vol. 25, no. 2, pp. 461–469, 1981.

[179] J. Kappler, N. Roehm, P. Marrack, U. Staerz, J. White, and H. R. Macdonald, “13. White,” 1987.

[180] S. Hara-Kuge *et al.*, “En bloc incorporation of coatomer subunits during the assembly of COP- coated vesicles,” *J. Cell Biol.*, vol. 124, no. 6, pp. 883–892, 1994.

[181] E. C. Arakel and B. Schwappach, “Correction: Formation of COPI-coated vesicles at a glance [J. Cell Sci, 131, (jcs209890)] doi:10.1242/jcs.209890,” *J. Cell Sci.*, vol. 131, no. 7, 2018.

[182] L. Orci *et al.*, “Bidirectional transport by distinct populations of COPI-coated vesicles,” *Cell*, vol. 90, no. 2, pp. 335–349, 1997.

[183] S. Zink, D. Wenzel, C. A. Wurm, and H. D. Schmitt, “A Link between ER Tethering and COP-I Vesicle Uncoating,” *Dev. Cell*, vol. 17, no. 3, pp. 403–416, 2009.

[184] G. Gabriely, R. Kama, and J. E. Gerst, “Involvement of Specific COPI Subunits in Protein Sorting from the Late Endosome to the Vacuole in Yeast,” *Mol. Cell. Biol.*, vol. 27, no. 2, pp. 526–540, 2007.

[185] K. J. Day, J. C. Casler, and B. S. Glick, “Budding Yeast Has a Minimal Endomembrane System,” *Dev. Cell*, vol. 44, no. 1, pp. 56-72.e4, 2018.

[186] E. C. Gaynor, T. R. Graham, and S. D. Emr, “COPI in ER/Golgi and intra-Golgi transport: Do yeast COPI mutants point the way?,” *Biochim. Biophys. Acta - Mol. Cell Res.*, vol. 1404, no. 1–2, pp. 33–51, 1998.

[187] S. K. Lemmon and L. M. Traub, “Sorting in the endosomal system in yeast and animal cells,” pp. 457–466, 2000.

[188] K. A. Hecht, A. F. O’Donnell, and J. L. Brodsky, “The proteolytic landscape of the yeast vacuole,” *Cell. Logist.*, vol. 4, no. 1, p. e28023, 2014.

[189] and J. S. B. Cecilia J. Bonangelino, Edna M. Chavez, “Genomic Screen for Vacuolar Protein Sorting Genes in Saccharomyces cerevisiae,” *Mol. Biol. Cell*, vol. 13, no. June, pp. 1977–2000, 2002.

[190] S. Barbosa, D. Pratte, H. Schwarz, R. Pipkorn, and B. Singer-Krüger, “Oligomeric Dop1p is part of the endosomal Neo1p-Ysl2p-Arl1p membrane remodeling complex,” *Traffic*, vol. 11, no. 8, pp. 1092–1106, 2010.

[191] D. Mahajan, H. C. Tie, B. Chen, and L. Lu, “Dopey1-Mon2 complex binds to dual-lipids and recruits kinesin-1 for membrane trafficking,” *Nat. Commun.*, vol. 10, no. 1, pp. 1–19, 2019.

[192] and E. W. J. Shoba Subramanian,* Carol A. Woolford, “The Sec1/Munc18 Protein, Vps33p, Functions at the Endosome and the Vacuole of Saccharomyces cerevisiae,” *Mol. Biol. Cell*, vol. 14, no. December, pp. 5069–5081, 2003.

[193] K. Bowers and T. H. Stevens, “Protein transport from the late Golgi to the vacuole in the yeast Saccharomyces cerevisiae,” *Biochim. Biophys. Acta - Mol. Cell Res.*, vol. 1744, no. 3 SPEC. ISS., pp. 438–454, 2005.

[194] C. G. Burd, M. Peterson, C. R. Cowles, and S. D. Emr, “A novel sec18p/NSF-dependent complex required for golgi-to-endosome transport in yeast,” *Mol. Biol. Cell*, vol. 8, no. 6, pp. 1089–1104, 1997.

[195] N. J. Bryant, R. C. Piper, S. R. Gerrard, and T. H. Stevens, “Traffic into the prevacuolar/endosomal compartment of saccharomyces cerevisiae: A VPS45-dependent intracellular route and a VPS45-independent endocytic route,” *Eur. J. Cell Biol.*, vol. 76, no. 1, pp. 43–52, 1998.

[196] C. Leibiger *et al.*, “TDP-43 controls lysosomal pathways thereby determining its own clearance and cytotoxicity,” *Hum. Mol. Genet.*, vol. 27, no. 9, pp. 1593–1607, 2018.

[197] M. Filimonenko *et al.*, “Functional multivesicular bodies are required for autophagic clearance of protein aggregates associated with neurodegenerative disease,” *J. Cell Biol.*, vol. 179, no. 3, pp. 485–500, 2007.

[198] G. Liu *et al.*, “Endocytosis regulates TDP-43 toxicity and turnover,” *Nat. Commun.*, vol. 8, no. 1, 2017.

[199] C. Janke *et al.*, “A versatile toolbox for PCR-based tagging of yeast genes: New fluorescent proteins, more markers and promoter substitution cassettes,” *Yeast*, vol. 21, no. 11, pp. 947–962, 2004.

Acknowledgements

First of all, I would like to thank Dr. Jens Tyedmers for giving me the opportunity and the resources to work on such an exciting topic. Without his constant guidance, supervision, fruitful discussions, and feedback, this thesis would have been impossible. It has been a pleasure working with you.

I would like to extend my gratitude to my two TAC members, Prof. Dr. Bernd Bukau and Prof. Dr. Matthias Mayer, for their valuable suggestions and constructive discussions during my TAC meetings. Thanks to Prof. Bukau and his lab members for allowing me to use their lab equipment and facilities to carry out my research successfully.

I also thank Prof. Dr. Rüdiger Hell and Prof. Dr. Tobias P. Dick for agreeing to be a member of my defense committee.

I also especially thank PD Dr. Axel Mogk for allowing me to participate in his lab meetings and for letting me present my research data on a regular basis. Thanks Axel, for taking the time out to discuss my project and to inspire new ideas in every meeting.

My hearty thanks to my colleagues Steffi, Claus, Johanna, Annika, Bilgen, Elisabeth, Han, Varun and Mina. I had a great time working and discussing together with you all and sharing the fun ups and downs in the lab.

My thanks also go to Dr. Holger Lorenz of the Imaging Facility at the ZMBH for invaluable support and expertise on all microscopy-related topic.

A special thanks to Dr. Thomas Fleming for offering his constant support and guidance with proteomics studies conducted in this thesis.

I thank the Hartmut Hoffmann-Berling International Graduate School of Molecular and Cellular Biology (HBIGS) for letting me participate in various interesting courses throughout my Ph.D. which helped me a lot with writing my dissertation as well as contributed to my personal growth.

I thank all my friends Frauke, Jidnyasa, Siddhi, for making my experience in Heidelberg enjoyable.

I am indebted to my husband, parents, my brother, and my German parents (Carola and Frank) for always being there for me and providing me the necessary emotional support through all the hardships I faced.